REFLECTED-LIGHT IMAGE ANALYSIS OF CONIFER TREE RINGS FOR DENDROCHRONOLOGICAL RESEARCH

by

Paul Ray Sheppard

A Dissertation Submitted to the Faculty of the

DEPARTMENT OF GEOSCIENCES

In Partial Fulfillment of the Requirements
For the Degree of

DOCTOR OF PHILOSOPHY

In the Graduate College

THE UNIVERSITY OF ARIZONA

1995

INFORMATION TO USERS

This manuscript has been reproduced from the microfilm master. UMI films the text directly from the original or copy submitted. Thus, some thesis and dissertation copies are in typewriter face, while others may be from any type of computer printer.

The quality of this reproduction is dependent upon the quality of the copy submitted. Broken or indistinct print, colored or poor quality illustrations and photographs, print bleedthrough, substandard margins, and improper alignment can adversely affect reproduction.

In the unlikely event that the author did not send UMI a complete manuscript and there are missing pages, these will be noted. Also, if unauthorized copyright material had to be removed, a note will indicate the deletion.

Oversize materials (e.g., maps, drawings, charts) are reproduced by sectioning the original, beginning at the upper left-hand corner and continuing from left to right in equal sections with small overlaps. Each original is also photographed in one exposure and is included in reduced form at the back of the book.

Photographs included in the original manuscript have been reproduced xerographically in this copy. Higher quality 6" x 9" black and white photographic prints are available for any photographs or illustrations appearing in this copy for an additional charge. Contact UMI directly to order.

UMI

A Bell & Howell Information Company
300 North Zeeb Road, Ann Arbor MI 48106-1346 USA
313/761-4700 800/521-0600

REFLECTED-LIGHT IMAGE ANALYSIS OF CONIFER TREE RINGS FOR DENDROCHRONOLOGICAL RESEARCH

by

Paul Ray Sheppard

A Dissertation Submitted to the Faculty of the

DEPARTMENT OF GEOSCIENCES

In Partial Fulfillment of the Requirements
For the Degree of

DOCTOR OF PHILOSOPHY

In the Graduate College

THE UNIVERSITY OF ARIZONA

1995

THE UNIVERSITY OF ARIZONA
GRADUATE COLLEGE

As members of the Final Examination Committee, we certify that we have read the dissertation prepared by Paul Ray Sheppard entitled REFLECTED-LIGHT IMAGE ANALYSIS OF CONIFER TREE RINGS FOR DENDROCHRONOLOGICAL RESEARCH

and recommend that it be accepted as fulfilling the dissertation requirement for the Degree of Doctor of Philosophy

Lisa J. Graumlich	11/29/95 Date
Owen K. Davis	11/29/95 Date
Judith T. Parrish	8/25/95 Date
Donald F. Post	Date
David M. Hendricks	8-25-95 Date

Final approval and acceptance of this dissertation is contingent upon the candidate's submission of the final copy of the dissertation to the Graduate College.

I hereby certify that I have read this dissertation prepared under my direction and recommend that it be accepted as fulfilling the dissertation requirement.

Dissertation Director Lisa J. Graumlich — 11/29/95 Date

STATEMENT BY AUTHOR

This dissertation has been submitted in partial fulfillment of requirements for an advanced degree at The University of Arizona and is deposited in the University Library to be made available to borrowers under rules of the Library.

Brief quotations from this dissertation are allowable without special permission, provided that accurate acknowledgment of source is made. Requests for permission for extended quotation from or reproduction of this manuscript in whole or in part may be granted by the copyright holder.

SIGNED: 

ACKNOWLEDGMENTS

This dissertation research was funded in part by Grant #ATM-9203944 from the U.S. National Science Foundation, the A.E. Douglass Award from the Laboratory of Tree-Ring Research of The University of Arizona, and a Student Research Grant from the Graduate College of The University of Arizona. I gratefully acknowledge the following people for their assistance and advice on specific parts of this dissertation research:

1. Developing the reflected-light image-analysis system: Rene Aragon, Peter Brown, James Burns, Brian Craze, Robert Gore, Henri Grissino-Mayer, Richard Holmes, Andi Lloyd, Ron Lynch, George McNamara, Martin Munro, James Palmer, Won-Kyu Park, Robin Strickland, Frank Telewski, Chaz Tompkins, and Ken Zeiler.
2. Studying past climate of western Maine: Laura Conkey, Gregg Garfin, Henri Grissino-Mayer, Andi Lloyd, Dave Meko, Robin Strickland, Frank Telewski, Chaz Tompkins, and Tom Yanosky.
3. Studying past climate of southeastern Arizona: James Burns, Steve Leavitt, James Miller, Chaz Tompkins, and Meg Weesner and other staff members of Saguaro National Park East.
4. Studying geomorphic processes of the Modoc Plateau, northeastern California: Malcolm Cleaveland, Gordon Jacoby, Alex McCord, Judith Totman Parrish, and Lester White.
5. Studying low-frequency tree-ring variation: Franco Biondi, Ed Cook, Lisa Graumlich, Richard Holmes, Dave Meko, and Jean Weber.

I thank Owen Davis, Bill Bull, and Judith Totman Parrish of the Department of Geosciences for serving as major members of my academic committee, and I thank

Don Post and Dave Hendricks of the Department of Soil and Water Science for serving as minor members of my academic committee. I especially acknowledge Lisa Graumlich for fulfilling the many facets of her role as my major academic advisor; with intellectual challenges throughout, I thank Lisa for having me along from the kettles of Wisconsin to the Sierra Nevada and from the meandering Kobuk to the Tibetan Plateau.

I acknowledge the Laboratory of Tree-Ring Research as an outstanding institute for studying all facets of dendrochronology. All students, staff, administrators, and faculty of the Lab contributed to my academic and professional advancement, and I especially thank Dr. Bryant Bannister, who shared with me his unique perspective of tree-ring science; Chaz Tompkins, with whom I have much in common; Henri Grissino-Mayer, with whom I most closely shared the graduate experience; and Richard Holmes, whose talents and contributions in dendrochronology are staggering and whose friendship I value highly.

From off campus, I acknowledge and appreciate the support of friends and family, especially Greer, Jerry, Chris, and Grandma Vi. Daughter Katherine's arrival in 1994 inspired me to actually finish this academic pursuit. Most importantly, I am grateful for the support, friendship, and love of my wife, Irene; I could not have preferred earning a Ph.D. degree anywhere else, at any other time, or with any other person, than here, now, and with Irene.

DEDICATION

I dedicate this work to my parents, John and Joanne Sheppard, who instilled in me my appreciation for learning and desire to excel.

TABLE OF CONTENTS

TABLE OF CONTENTS – *Continued*

TABLE OF CONTENTS – *Continued*

TABLE OF CONTENTS – *Continued*

LIST OF FIGURES

LIST OF FIGURES – *Continued*

LIST OF TABLES

3. ABSTRACT

The primary objective of this dissertation research is to use reflected-light image analysis to measure brightness of standard samples of conifer rings and then use brightness in dendrochronological research as a substitute for density. I developed an imaging system that ensures identical configuration of all components and measuring steps for all rings of a sample so that subsequent comparison of brightness between rings would be valid. From a mesic New England tree-ring site, I measured ring brightness of cores that had been previously measured using X-ray densitometry. Latewood brightness and density both correlate with April–May temperature such that they reconstruct that climate variable equally well. From a semiarid Southwest tree-ring site, I measured ring brightness of cores with severe extraneous color—mostly due to heartwood-sapwood color differences. Bleaching and organic extraction of cores did not overcome the problem of extraneous color, but autoregressively modeling brightness index series did. Various brightness and width variables combined to model July–October precipitation, a climate variable not usually reconstructed by Southwest tree-ring sites. From a stand of trees affected by a past earthquake, I measured ring brightness of one tree that responded to surface deformation with an apparent change in latewood density. Absolute latewood brightness did not change *per se* after the earthquake, but the amount of latewood relative to the total ring increased dramatically. Although technical and paleoenvironmental issues remain for future research, this study indicates that reflected-light image analysis is an excellent tool in dendrochronological research for increasing our understanding paleoenvironmental processes of the latest Holocene.

The secondary objective of this dissertation research is to demonstrate a method for identifying low-frequency variation of tree-ring chronologies and/or past

climate as reconstructed using tree-rings. This method provides confidence intervals with which to judge the significance or importance of low-frequency departures in tree-ring data as well as a visual basis for determining whether or not low-frequency variation is robustly estimated. This method is a re-ordering of the individual steps commonly used in constructing tree-ring chronologies or reconstructions.

4. GENERAL INTRODUCTION

Characterizing natural behavior of climatic and geologic systems is critically important as humans seek to assess hazards posed by climatic variability or by geomorphic events. In research presented here, I contribute in two ways to the overall question of how best to characterize environmental variability. First, I describe how reflected-light image analysis of conifers can quantify multiple variables of tree growth, including ring width, ring brightness, and other derived variables, all of which potentially relate to environmental variability. Second, I develop and apply a method for assessing the significance of low-frequency variation in paleoenvironmental series. To demonstrate these innovations, I apply them to characterize (1) spring temperature of western Maine, (2) summer precipitation in southeastern Arizona, and (3) tree-ring responses to an earthquake in northeastern California.

Reflected-Light Image Analysis of Conifers

Ring density has been used with ring width in past dendrochronological studies of conifer tree rings to reconstruct and analyze climate of the latest Holocene. Density has been critical in some studies where ring width exhibited little variation and therefore was not useful by itself for reconstructing past climate (Parker and Henoch 1971; Parker 1976). Density has been used to reconstruct growing-season temperature at cool, moist sites (Conkey 1986; Briffa et al. 1988a, 1988b, 1990, 1992a, 1992b, and 1995; Jacoby et al. 1988) or precipitation at drier sites (Hughes et al. 1984; Cleaveland 1986).

Unfortunately, measuring ring density using X-ray densitometry is time consuming and expensive (Parker and Meleskie 1970; Telewski and Jacoby 1987; Schweingruber 1990). Tree-ring samples must be thin-sectioned to a uniform thickness, a task that is difficult to do well. This step also limits the usefulness of X-ray

densitometry because it is difficult to thin-section cross-sections or increment cores that are broken into many pieces. Additionally, samples must be X-ray imaged. This step requires an X-ray source, careful projection of X rays onto samples, and a shielded chamber to protect workers from exposure to high-energy radiation.

The cost of a new densitometry system, including a sliding microtome for thin-sectioning (Telewski et al. 1987), X-ray source and chamber, and optical densitometer to analyze the X-ray images, can be as high as US$100,000. This cost is prohibitively high for many tree-ring research facilities, and consequently many researchers are not able to measure ring density, even when experience indicates that density might significantly improve reconstructions of climate of the latest Holocene.

The field of computerized video image analysis (Inoué 1989) has evolved quickly during the last decade and is now revolutionizing measurement and analysis in many scientific disciplines (e.g., see recent issues of the journal Advanced Imaging). Within dendrochronology, several studies have applied video image-analysis techniques to hardwood species (Amparado et al. 1990; Sass and Eckstein 1992; Dustin et al. 1994; Vollenweider et al. 1994; Sass and Eckstein 1995) and to conifer species (Yanosky and Robinove 1986; Yanosky et al. 1987; Jagels and Telewski 1990; Thetford et al. 1991; Guay et al. 1992a and 1992b; Ebding et al. 1995).

Dendrochronologists have experimented with image analysis of conifer tree rings as an alternative to X-ray densitometry for measuring ring-growth variables (Jagels and Telewski 1990). Past approaches include analyzing light transmitted through micro-thin sections of wood (Park and Telewski 1993) or through X-ray images of wood (Thetford et al. 1991). Unfortunately, these approaches still require thin-sectioning and/or X-ray imaging of tree-ring samples.

Another approach is to analyze light reflected off the surface of tree-ring

samples (Yanosky et al. 1987). This approach has three attractive features. One, no special preparation of tree-ring samples is required above and beyond mounting and sanding, which are commonly done in tree-ring studies. Because of this feature, cross-sections and broken increment cores can be analyzed. Two, X-ray imaging of the sample is not necessary. Three, the current cost of a new reflected-light image-analysis system, including a microscope, video camera and monitor, light source, and commercially available software, is no more than US$30,000.

In conifer wood, surface brightness is directly related to the lumen:wall ratio of tracheid cells (Yanosky and Robinove 1986) and the lumen:wall ratio is inversely related to density (Park and Telewski 1993). Thus, surface brightness should logically be inversely related to wood density, as is required in this application of image analysis (Clauson and Wilson 1991). This relationship is certainly true within rings: Latewood is dense, dark-colored and low in brightness, and earlywood is less dense, light-colored and high in brightness (Fig. 4.1). Density also covaries with brightness between rings: Latewood in a dense ring is low in brightness (Fig. 4.1, Ring 1) relative to latewood in a less-dense ring (Fig. 4.1, Ring 2). Brightness often differs between rings strongly enough to aid in dating tree-ring collections (Filion et al. 1986; Delwaide et al. 1991; Yamaguchi et al. 1993).

To take advantage of video image-analysis technology and the covariation of density and brightness in conifer rings, I measure and analyze brightness in place of density (Parker 1987). If reflected-light image analysis can be used to measure brightness variables that correspond to tree-ring structure, then image analyzing tree-ring samples could substitute for X-ray densitometry (Yanosky et al. 1987). Because a complete video image-analysis system is less expensive and potentially easier to operate than an X-ray densitometry system, tree-ring researchers should be

able to improve paleoenvironmental analyses by measuring brightness.

The primary objective for this dissertation research is to use reflected-light image analysis to measure brightness of conifer rings and then use brightness in dendrochronological research as a substitute for density (Chapter 5 of this dissertation; Sheppard and Graumlich 1996). I use brightness to reconstruct past climate, first with a New England site where density was used to reconstruct past temperature and then with a Southwest site where density was used to model tree growth with precipitation. I also use brightness to demonstrate a tree-ring response to an earthquake in northeastern California.

Paleoclimatology: Elephant Mountain, Western Maine

To demonstrate that conifer ring brightness can be used to reconstruct climate just as if density were used, I image analyzed cores from red spruce (*Picea rubens* Sarg.) growing at Elephant Mountain, Maine, (44° 46' N, 70° 46' W, 930 m elevation; Fig. 6.1). Conkey (1986) originally measured these cores densitometrically and reconstructed April–May temperature of western Maine. I compared statistical characteristics of density and brightness and climate-tree growth models using density or brightness (Chapter 6 of this dissertation; Sheppard et al. 1996).

Paleoclimatology: Mica Mountain, Southeastern Arizona

Some conifer species exhibit extraneous color, i.e., color variation of wood that occurs after rings are formed and therefore has no relationship to environmental conditions at the time of ring formation. The most notable type of extraneous color is the heartwood-sapwood color change commonly seen in many conifer species. Extraneous color variation can also arise from fungal staining (Kreber and Byrne 1994) and/or compartmentalization of wounds (Shigo 1985). A reflected-light imaging system that can detect environmentally relevant brightness variation be-

tween rings can certainly detect extraneous color (Fig. 4.2), which would be statistical noise in later analyses. In species with extraneous color, the relationship between density and brightness is not constant throughout a sample and thus a primary requirement for applying reflected-light image analysis to approximate density is not met (Telewski and Jacoby 1987, Yanosky et al. 1987).

Tree species that exhibit highly pronounced heartwood-sapwood and other extraneous color include pines (*Pinus* L.) and Douglas-firs (*Pseudotsuga* Carr.), which comprise the majority of collections of the International Tree-Ring Data Bank (Grissino-Mayer 1995). To be widely applicable to dendrochronology, reflected-light image analysis must overcome the problem of extraneous color, either by chemically removing it from wood using organic extraction or bleaching, or by mathematically removing its effects from measured data (Yanosky et al. 1987).

Furthermore, given that ring density of pines and Douglas-firs has been used for reconstructing climate of the latest Holocene in semiarid Southwestern North America (Cleaveland 1986), it is logical to attempt image analysis of these species. Park (1990) image analyzed ponderosa pines (*Pinus Ponderosa* Dougl. ex Laws.) growing at Mica Mountain, Arizona (32° 12' N, 110° 33', 2400 m elevation; Fig. 7.1), and he modeled the lumen area:total cell area ratio to July–October precipitation. However, Park's image analysis method used very high magnification, light transmitted through thin sections of core samples, and binary object analysis of black cell walls versus white lumina. Consequently, while extraneous color was not a concern for Park, his image analysis method was time consuming such that he limited his climate-tree growth modeling to the period 1910–1930.

To investigate various strategies for overcoming extraneous color and to attempt low-magnification reflected-light image analysis on a semiarid Southwest

tree-ring site, I image analyzed cores from ponderosa pine growing at Mica Mountain. I compared precipitation-tree growth models using brightness from various combinations of sample preparation, chronology type, and data strategies to overcome extraneous color (Chapter 7 of this dissertation).

Paleoseismology: Stephens Pass, Northeastern California

Among published studies using tree-ring techniques to the study of past earthquakes (e.g., see references in Sheppard and White 1995), only one study has noted a change in ring density due to an earthquake. Following the 1811–1812 earthquake at New Madrid, Missouri, baldcypresses (*Taxodium distichum* (L.) Rich.) growing in Tennessee responded with decreased latewood density in addition to increased ring-width (Stahle et al. 1992).

An opportunity arose to investigate an additional latewood brightness response to a past earthquake when, during the first half of August, 1978, a swarm of 200+ earthquakes occurred at Stephens Pass, California (41° 27' N, 121° 52' W, 1510 m elevation; Fig. 8.1). Although none of the earthquakes was large–the maximum magnitude was 4.6–they dropped a series of grabens that average 4.5 m in width, extend up to 3 m in depth, and occur intermittently along a 2-km-long rupture zone (Bennett et al. 1979). The formation of this graben series killed or otherwise affected many trees growing in or immediately adjacent to the rupture zone (e.g., see photos 2, 3, and 4 of Bennett et al. 1979). In addition to ring-width responses to this earthquake, one sampled red fir (*Abies magnifica* A. Murr.) responded with an apparent change in latewood brightness. To quantify this brightness response, I image analyzed the core samples from this tree (Chapter 8 of this dissertation; Sheppard and White 1995).

IDENTIFYING LOW-FREQUENCY TREE-RING VARIATION

Dendrochronological research is replete with studies that, in part, identify and interpret low-frequency variation (period length > 10 years) in tree-ring chronologies (LaMarche 1974; Jacoby et al. 1985; Norton et al. 1989; Briffa et al. 1990). A common approach to identifying low-frequency tree-ring variation is (1) to construct a standard chronology using several samples from a homogeneous stand of trees (Fritts 1976), (2) to generate a smoothed index series from that standard chronology, e.g., with a cubic smoothing spline (Cook and Peters 1981), and (3) to overlay the standard chronology with its smoothed index series. Trends in low-frequency variation, i.e., departures from a reference line, are commonly interpreted as responses to biological or physical events.

As stated, this approach has two inadequacies that arise from the fact that the smoothed index series is generated from only a single time series. First, the smoothed index series does not have accompanying confidence intervals with which trends might be evaluated as being significant or important. Second, the smoothed index series does not reflect changing sample depth through time, even though sample depths of tree-ring chronologies range from as low as a single sample at the beginning year to a maximum value, commonly >20 trees, sometime before the ending year. While it is tempting to interpret low-frequency trends for the full length of a chronology, there should be some distinction between well-replicated portions of a chronology, where low-frequency variation is robustly estimated, and poorly replicated portions of a chronology, where low-frequency variation is weakly estimated (Shiyatov et al. 1990).

To overcome these two inadequacies, I propose a method of re-ordering the individual steps commonly used in constructing tree-ring chronologies. This method

provides approximate 95% confidence intervals for a chronology of low-frequency variation so that a level of significance or importance for trends may be inferred, and it visually reveals the portions of a chronology where sample depth is so poor that low-frequency variation is not robustly estimated, i.e., when the mean value is significantly affected by the addition or deletion of a single sample. Because this method is merely a re-ordering of the individual steps commonly used in constructing tree-ring chronologies. Consequently, this method is computationally simple for researchers who already routinely construct standard tree-ring chronologies, especially for those who have access to the library of data-reduction programs compiled under the auspices of the International Tree-Ring Data Bank, of the National Geophysical Data Center. The secondary objective for this dissertation research is to demonstrate this method for identifying low-frequency variation of tree-ring chronologies and/or past climate as reconstructed using tree-rings.

Chronologies: Coddington Lake, Northern Minnesota

To illustrate this method of identifying low-frequency tree-ring variation, I applied it to a tree-ring collection of ring-width series from white oak (*Quercus alba* L.) growing at Coddington Lake, Minnesota (47° 44' N, 94° 03' W, 128 m). The standard chronology from this site exhibits strong low-frequency variation, which makes it useful for illustrating this method (Chapter 9 of this dissertation; Sheppard 1991).

Reconstructions: Mica Mountain, Southeastern Arizona

Analyzing variation in tree-ring chronologies is not usually the ultimate goal of dendrochronological research. Rather, researchers seek to analyze and understand variation in environmental factors that cause tree growth to vary. Accordingly, I applied this method of identifying low-frequency variation to past July–October

precipitation as reconstructed using tree-ring chronologies of brightness and width variables from ponderosa pines growing on Mica Mountain (Chapter 9 of this dissertation).

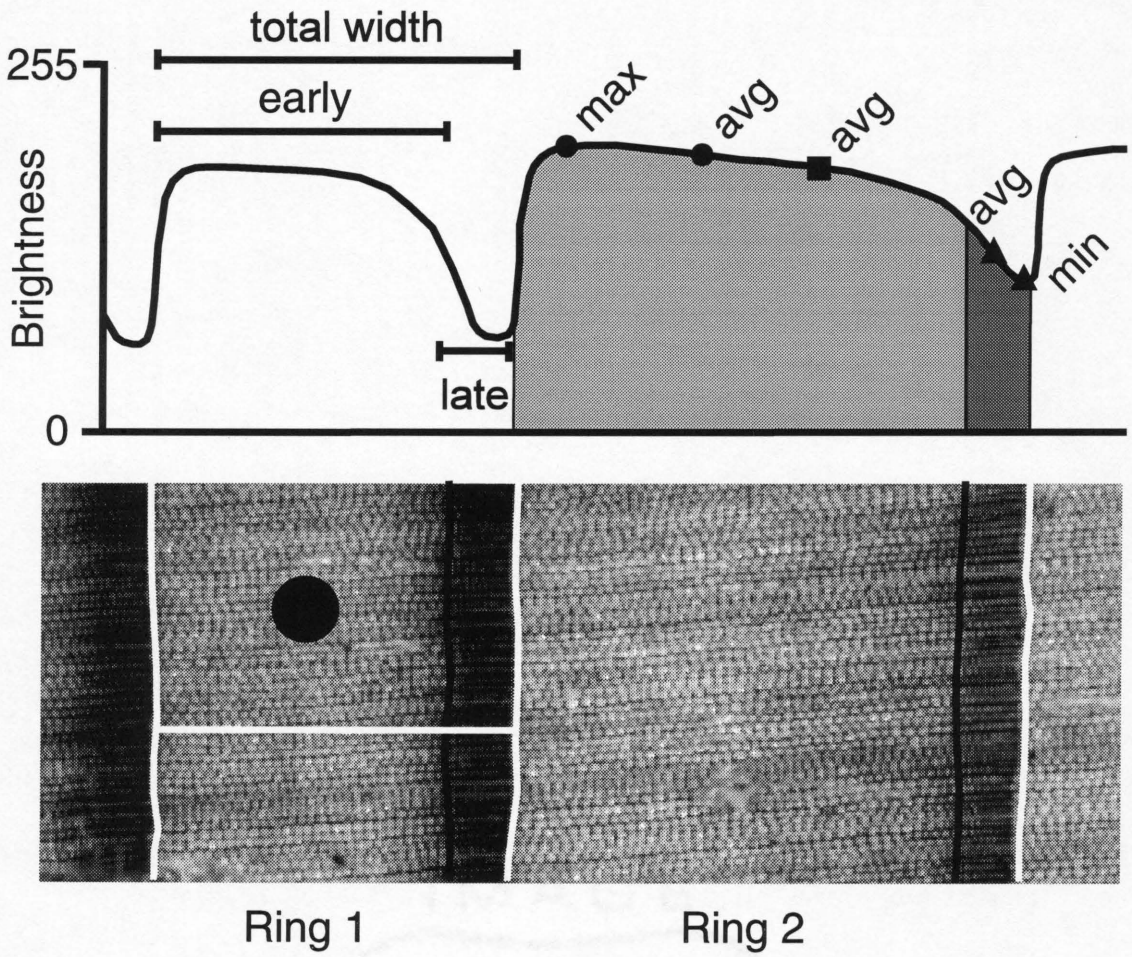

Fig. 4.1. Tree-Ring Image and Brightness Scan: An image of two full rings (bottom) and their associated brightness scan (top). On the image, vertical white lines mark ring boundaries and vertical black lines mark earlywood-latewood transitions, the horizontal white line marks a representative radial file for Ring 1, and the black spot in Ring 1 covers up a resin duct that is excluded from the analysis. On the brightness scan, total ring, earlywood, and latewood widths are marked for Ring 1, and maximum and average earlywood brightness (circles), average and minimum latewood brightness (triangles), total ring average brightness (square), and areas beneath the earlywood scan (light stippled area) and latewood scan (dark stippled area) are marked for Ring 2.

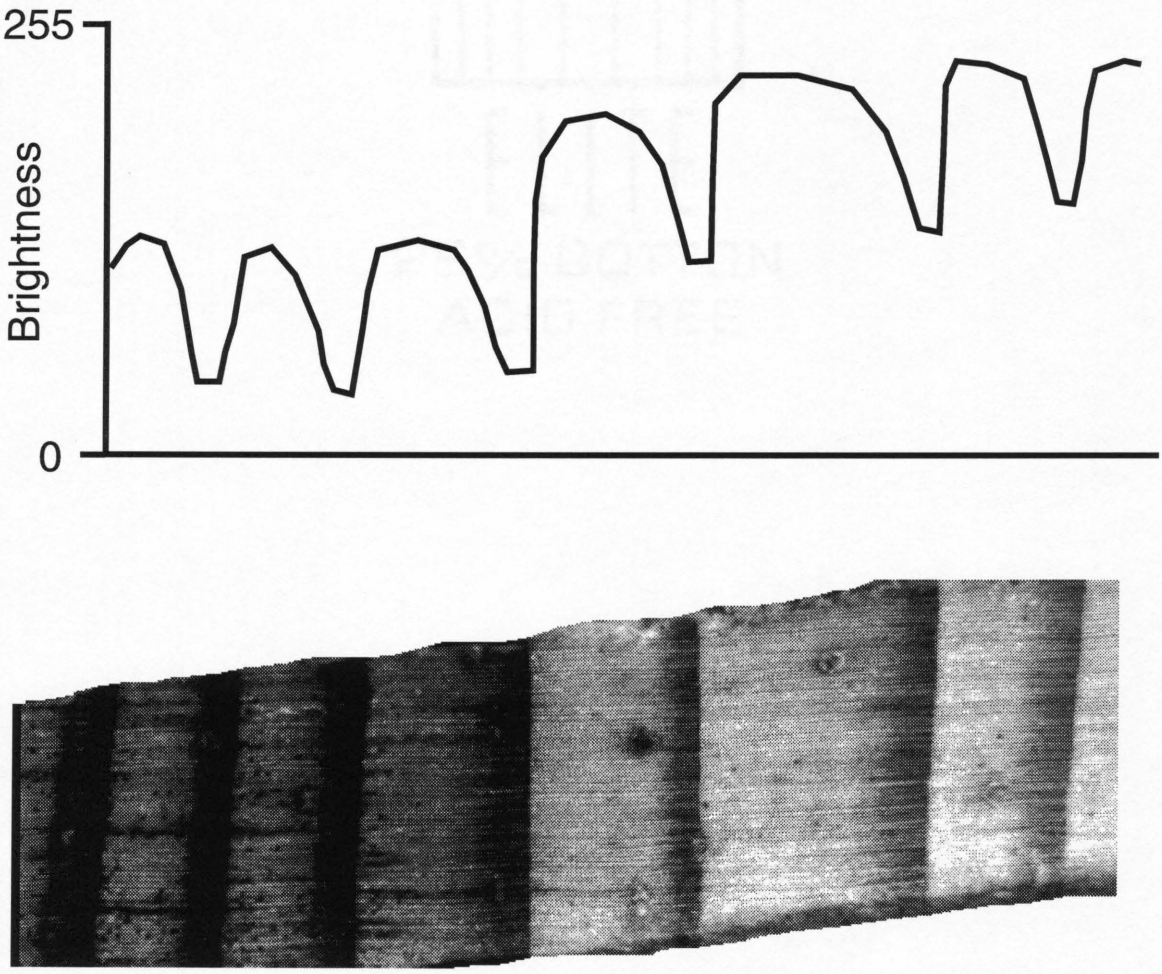

Fig. 4.2. Heartwood-Sapwood Rings and Brightness Scan: An image of three rings before and after the heartwood-sapwood boundary (bottom) and their associated brightness scan (top).

5. REFLECTED-LIGHT IMAGE ANALYSIS SYSTEM FOR DENDROCHRONOLOGICAL RESEARCH OF CONIFER TREE RINGS

INTRODUCTION

In this application of reflected-light video image analysis, the imaging system must be configured identically for all rings of a sample. If the imaging system varies from ring to ring, then subsequent comparisons of brightness between rings is invalid. This system, which resembles Yanosky's et al. (1987), was developed to ensure constancy while measuring. Most of the individual components are standard equipment within the imaging industry, though I added some custom components to enhance control of the system's configuration. For purposes of documentation, I include product names of the commercially available components that I purchased without implying any recommendation for, or endorsement of, those products.

HARDWARE COMPONENTS

Tree-Ring Sample

In contrast to X-ray densitometry and other imaging approaches that analyze X-ray film (Thetford et al. 1991), reflected-light image analysis does not require that tree-ring samples be thin-sectioned, a preparation technique that is difficult to consistently perform well (Park et al. 1992). Reflected-light image analysis uses increment cores—or even cross-sections—that have been mounted and sanded just as for most other typical tree-ring analysis (Fig. 5.1). Not only is this sample preparation easy, but it also allows image analysis of core samples that are broken into many pieces and are therefore not suitable for densitometry (Thetford et al. 1991).

Nonetheless, surfaces of tree-ring samples must be of high quality for image analysis to be effective (Saß and Eckstein 1994). Samples must be mounted with

tracheids aligned vertically and sanded so that all rings are clearly visible in transverse sectional view (Swetnam et al. 1985). A side effect of sanding is that tracheid lumina are packed with sawdust, which is light-colored and enhances the contrast between cell lumina and walls.

Video Camera

A charged-couple device black-and-white video camera (Dage-MTI, Inc., model CCD-72) generates images of the sample (Fig. 5.1). Equipped with an image-capturing board and an 8-bit analog-to-digital converter, the camera has an image output of 512 columns by 480 rows and a video capture rate of 33 msec frame^{-1}. The camera discerns 256 shades of gray, ranging from pure black (gray value = 0) to pure white (gray value = 255), and it has a linear output gray-value response to variation in light input within the typical range of input. The maximum spectral sensitivity of the camera is at 550 nm, and its spectral response is limited to visible light by an infrared filter.

The amplitude of the video signal can be manually controlled with black-level and gain (white) settings. With manual control, which is not a feature of all video cameras, black-and-white image contrast is maximized over the entire core. If, for each image of rings, the black-level and gain settings were to automatically adjust—a typical mode of operation for video cameras—then brightness would not be comparable between rings within a core.

Video Monitor

A video monitor (Sony® Trinitron®) displays images of rings (Fig. 5.1). The monitor has a display resolution of 512 columns and 480 rows, which matches the usable image resolution of the video camera. Other than displaying images, the video monitor plays no important role in video image analysis; various monitor set-

tings can be adjusted for operator convenience, but doing so has no effect on the stored digital images.

Microscope

A compound stereo zoom microscope (Nikon Inc. SMZ-U) magnifies and focuses images of rings onto the video camera (Fig. 5.1). The microscope has a common main objective lens and a trinocular head with binocular eyepieces and a monocular tube for the video camera. Together, the microscope and video camera take the place of line-scanning cameras or image scanners of other dendrochronological image-analysis systems (Guay et al. 1992a, 1992b) .

All lenses of the microscope are coated for anti-reflection, and the objective lens is corrected for plano distortion so that it transmits a flat image without edge distortion (Richardson 1991). The objective lens has a 1x magnifying power and the zoom magnification ranges continuously from 0.75x to 7.5x. This magnification, low enough to include several rings in the field of view, is considerably lower than that used in image-analysis studies that measure rings at the cellular level (Park and Telewski 1993, Munro et al. 1995). This magnification range provides ample flexibility for image analysis (Yanosky et al. 1987): At the lowest magnification the field of view extends 11 mm radially, which is wider than any tree ring usually encountered, while at the highest magnification a single pixel represents 2.1 μm radially, which is easily small enough to resolve rings that are only a few tracheids wide.

Ideally, images should be in focus, i.e., the sample surface should be at the focal distance of the objective lens (84 mm in our case). However, a continuous-focus range of 0.4 mm above or below the focal distance results in images that appear to be in focus when displayed on the video monitor. Unfortunately, images yield different brightness across this depth of focus (Fig. 5.2A) because the light

source and video camera are attached to the microscope (Fig. 5.1). If the sample is <84 mm from the objective lens, then the sample is too close to the light source and the video camera and the resultant brightness is too high. Conversely, if the sample is >84 mm from the objective lens, then the sample is too far from the light source and the video camera and the resultant brightness is too low.

To ensure accurate and repeatable focus, I project a beam of light onto the sample from a laser penlight attached to the microscope (Fig. 5.2B). When the surface of the sample is at the focal distance (B), then the projected beam hits the sample such that a spot overlays a crosshair reference on the video monitor (B'). If the microscope and sample are too close together (A), then the spot is offset to the left of center (A'); if the microscope and sample are too far apart (C), then the spot is offset to the right of center (C'). Using this focusing aid ensures that the sample surface is always at the focal distance.

Lighting System

Non-coherent white light is generated from a tungsten halogen bulb (Dolan-Jenner Industries, Inc. Fiber-Lite A-240L), transmitted through a fiber-optic bundle, and emitted from a ring illuminator attached to the objective lens of the microscope (Abramovitz 1989) (Fig. 5.1). Light is projected onto the sample and then diffusely backscattered by the opaque surface of the sample. This lighting system is classified as symmetrical, incident dark-field illumination (Rochow and Rochow 1978).

For valid comparison of brightness of different rings, the intensity of the incident light must not vary between rings of a core because this imaging system has no calibration standard such as the cellophane wedges used in densitometry (Park and Telewski 1992). Unfortunately, a constant, stable light intensity cannot be assumed. High-frequency, high-amplitude light variation results from spikes and drops in the

alternating current electrical source (Fig. 5.3A). This electrical variation is not removed by the surge protectors or battery-powered units that are commonly used to protect computers. Additionally, low-frequency, low-amplitude light variation results from filament resistance changes, long-term bulb decay, or some combination of these or other causes (Fig. 5.3B).

I eliminated light variation in two steps with a regulated light controller (Mercron, Inc. model TXC150-20). First, alternating current is converted to direct current (Green and Worrall 1964). Second, direct current and amperage are regulated to the bulb to compensate for variation in bulb output as measured using a photo-resistor sensor. Using these steps, light variation is held to ±0.25% of the bulb output every 30 msec.

SOFTWARE CONCEPTS

General

There are many commercial and public-domain image-analysis software packages with similar sets of capabilities in digital image analysis and enhancement (Inoué and Inoué 1989). In selecting an imaging software package (Image-1® from Universal Imaging Corporation, installed on a personal computer), I specifically looked for features that would enhance the precision and control of the system and ease of data capture. For example, I acquire images by averaging multiple video frames in real time. I store multiple images in local memory buffers that provide quick access to images, a desirable capability because of commonly manipulating images during measuring. I conveniently save and load images to and from various storage devices. I combine frequently repeated operations into customized modules to ease repetitive use of selected functions. I transparently interact with the operating system of the computer to execute external, customized programs that perform

functions not included in the commercial software.

Initializing the System

When initializing the imaging system to measure a tree-ring samples, I obtain the best possible analog image, i.e., one that is in focus and has maximum contrast, and thereby reduce the need for digital image enhancements (Inoué 1986; Commare 1988; Dustin et al. 1994; Vollenweider et al. 1994). After determining the appropriate magnification and focusing the image of the core, I adjust the black-level and gain settings of the video camera so that the darkest part of the core has a gray value just above 0 while the lightest part has a gray value just below 255. Once the system is initialized, I hold all components constant while acquiring images and measuring rings of that core. As with Thetford et al. (1991), I maintain a constant magnification while measuring a core.

Acquiring and Enhancing Images

I acquire up to 10 rings per image, depending on widths of the rings and the magnification of the microscope. Each image is an average of many separate video frames of the field of view. Spatially random noise, which is inherent in the video signal, is eliminated by frame averaging (Russ 1990). The effect of frame averaging increases as the square root of the number of frames, and averaging 16 frames is usually adequate.

Frame averaging does not rid images of systematic, non-random defects, which result from dust particles in the optical system, lens imperfections, video detector faults, and uneven illumination (McMillin 1982; Richardson 1991). I eliminate these defects by using a blank background image to correct images of rings (Arkin et al. 1990). I use the following ratio correction process, which is evaluated for all picture elements of a particular image of a ring:

$$\text{corrected image}_{(x,y)} = \text{raw image}_{(x,y)} \cdot \frac{128}{\text{background image}_{(x,y)}}$$

where x and y denote the horizontal and vertical position of each picture element of the image. The background image is of a reference gray card such as is commonly used in black-and-white photography (Adams 1981). I hold the gray card 10 mm above the focal plane, where it is considerably out of focus, so that details of the card, e.g., scratches, are blurred. This digital correction process does not change the average brightness of the image of the tree rings if the blank background image has an average gray value of 128.

I computationally distinguish individual rings on an image by differencing each 1-pixel-high radial brightness scan and then locating all maximum differences that correspond to known ring boundaries (Fig. 4.1). Based on the visible change from light to dark picture elements, I manually mark the earlywood-latewood transition on one radial scan within each ring in the image, and I assume a constant earlywood-latewood width ratio within a ring (Fig. 4.1). This process of identifying individual rings within an image is accomplished easily and quickly with customized software that is executed from within the commercial imaging software (Appendix I). I visually check the results of this program on the video monitor, and I correct the image as necessary if rings are improperly identified, e.g., due to intra-annual bands or absent rings.

This image-analysis approach requires that the tree rings be dated prior to measuring (Yanosky et al. 1987). Thus, this approach conforms to standard procedures of dendrochronology, i.e., collecting and preparing samples, dating and measuring rings, checking for errors in dating and measuring, analyzing data and interpreting results (Stokes and Smiley 1968).

Once a ring is identified in an image, I average all available radial scans in that ring (Fig. 4.1, one representative scan marked for Ring 1) into a single brightness scan. Specifically, I average picture elements across radial scans according to their relative positions in a ring—not within an absolute vertical column, which would be inappropriate in rings with wavy boundaries. I exclude blemishes, e.g., resin ducts or breaks, from analysis by painting their picture elements black on the image (Fig. 4.1, Ring 1) and then ignoring black picture elements in subsequent analysis. I obtain an average brightness scan that incorporates all pertinent information from the entire ring using customized software (Appendix II) and thus avoid choosing a single radial slit as representative of the entire ring (Moschler and Winistorfer 1990).

I obtain several tree-growth variables from the average scan, including earlywood, latewood, and total ring widths, which are calculated from the number of picture elements multiplied by the calibrated size of each picture element; maximum and average earlywood brightness; minimum and average latewood brightness; average brightness for the entire ring; and integrated areas beneath earlywood and latewood curves (Fig. 4.1). Partial-ring variables, which are measured using densitometry as well as using image analysis, may be useful for studying environmental factors within segments of tree growing seasons (Smith 1977).

I also derive other tree-growth variables from these measured variables, notably latewood width as a percentage of total ring width. This variable has been useful in dendrochronological studies of conifers (Schulman 1942). Data for all variables are written to files (Appendix II) for further analysis with standard programs used in dendrochronology (Grissino-Mayer et al. 1992; Holmes 1994). Measuring takes approximately 30 seconds per ring.

Repeatability Testing and Results

The first goal of this work was to develop an imaging system with which precisely repeatable data can be obtained. As a test of repeatability of this imaging system, I measured a 50-year segment of rings twice, carefully controlling the imaging system so that its components were configured identically between, and held constant within, each measurement session.

For total ring width, earlywood maximum brightness, and latewood minimum brightness, measured values did not differ significantly between the two measurement sessions (Fig. 5.4). This implies that the precision of the reflected-light imaging system and measuring process is sufficient to justify their use in dendrochronological research.

Total ring widths measured using reflected-light image analysis correlate nearly perfectly with those measured using a computer-based incremental measuring system (Robinson and Evans 1980). The average difference between total ring widths as measured by each system is 0.006 mm (standard error = 0.002), which is within the ± 0.01 mm level of precision of both systems.

Discussion

For measuring intra-ring brightness of standard increment cores of conifer species, this reflected-light video imaging system, composed of commercially available components plus customized modifications, is easy to operate and designed to yield data that are repeatable. The repeatability tests were satisfactory (Fig. 5.4) only after taking great care to control all settings of the imaging system and to hold them constant while measuring a sample. Eliminating incident light variation (Fig. 5.3) was particularly vexing, and ensuring correct focus of the microscope (Fig. 5.2) was also challenging.

Although some commercially available image-analysis software is specifically oriented to tree-ring applications (Guay et al. 1992a), data from most general-purpose image-analysis software will not automatically be in formats commonly used in dendrochronological research. When using general imaging software, tree-ring researchers must efficiently convert useful information of an image of rings into tree-ring data, a task that inevitably requires customized software (Appendices I and II).

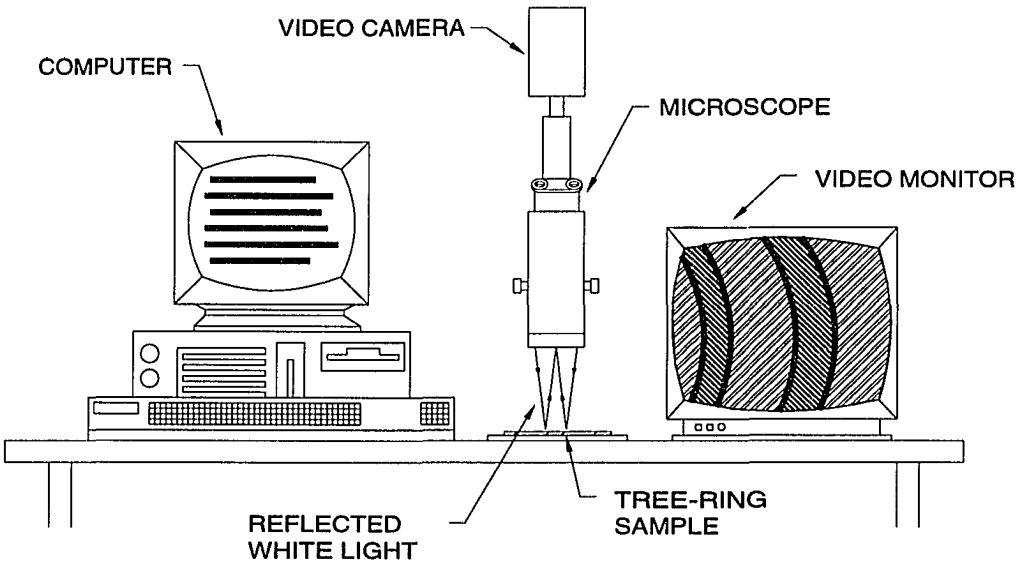

Fig. 5.1. Reflected-Light Image-Analysis System: Standard components of the system used in this research.

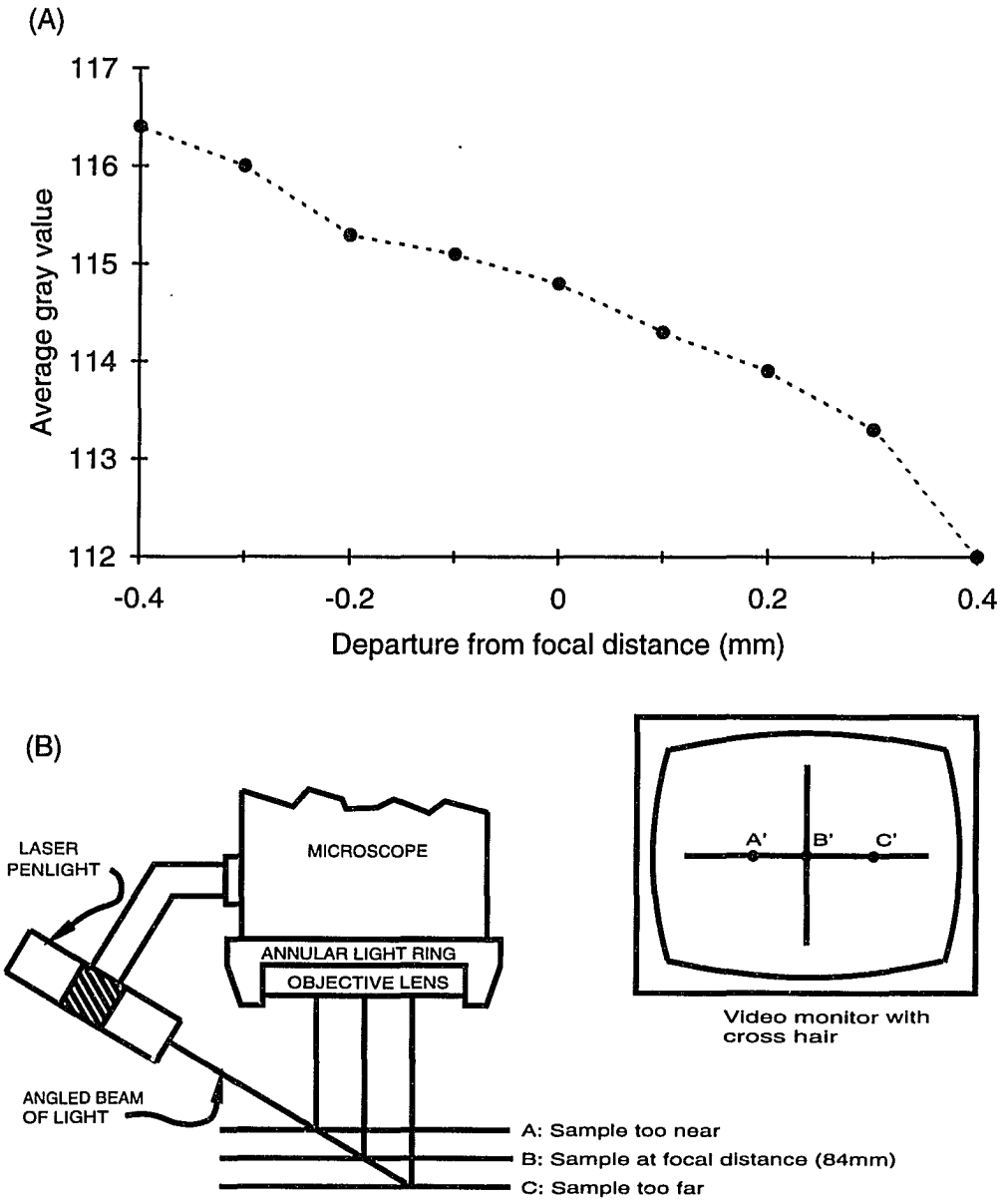

Fig. 5.2. Microscope Focus: (A) Average brightness of a stationary subject as a function of focus setting. A departure of 0.0 represents the known focal distance (84 mm) of the objective lens of the microscope. Relative to that focal distance, negative departures represent focus settings that are too short (<84 mm) and positive departures represent focus settings that are too long (>84 mm). (B) Detail of the focusing device.

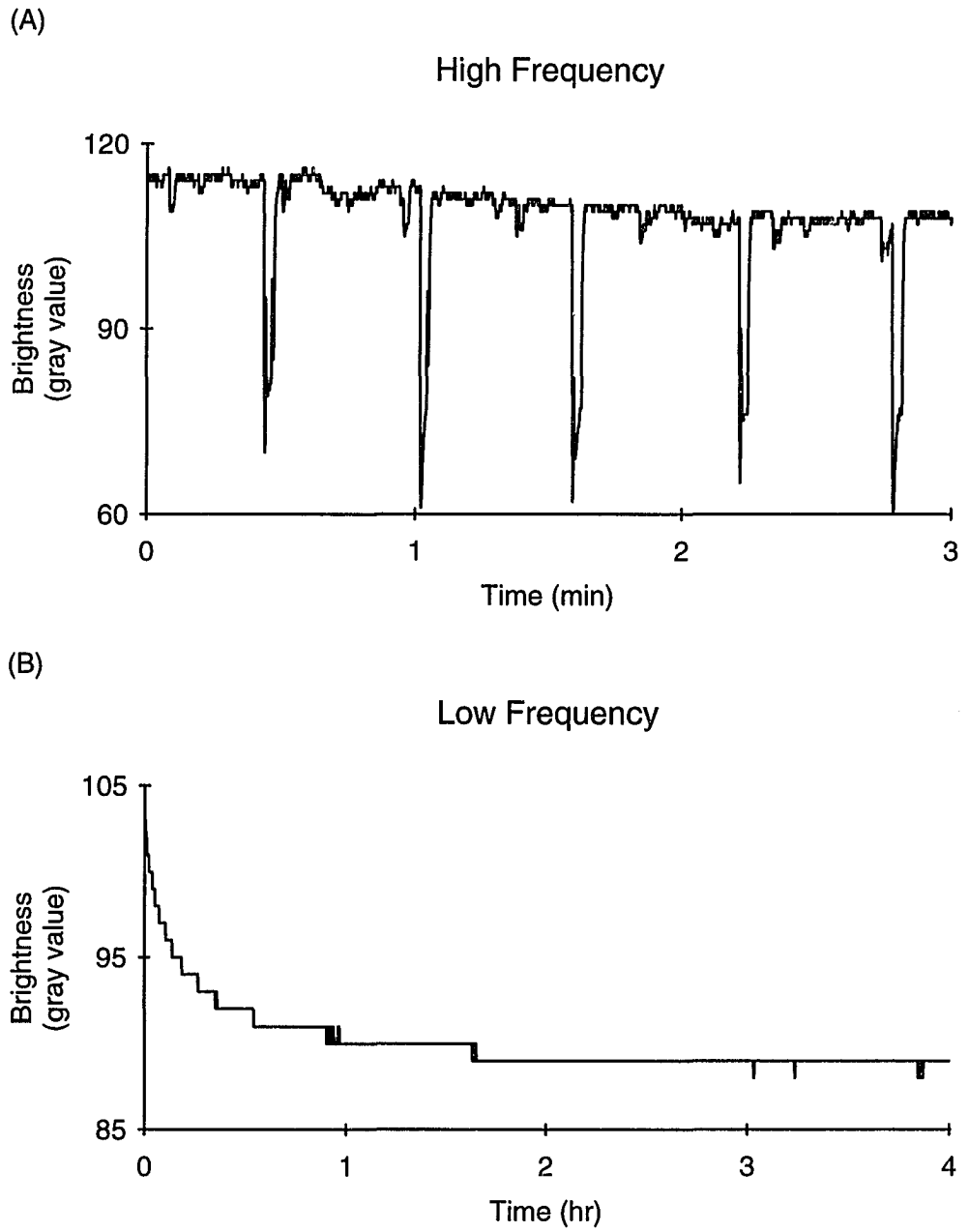

Fig. 5.3. Incident Light Variation: (A) High-amplitude variation, on the scale of minutes, and (B) low-frequency variation, on the scale of hours, as measured from a constant subject.

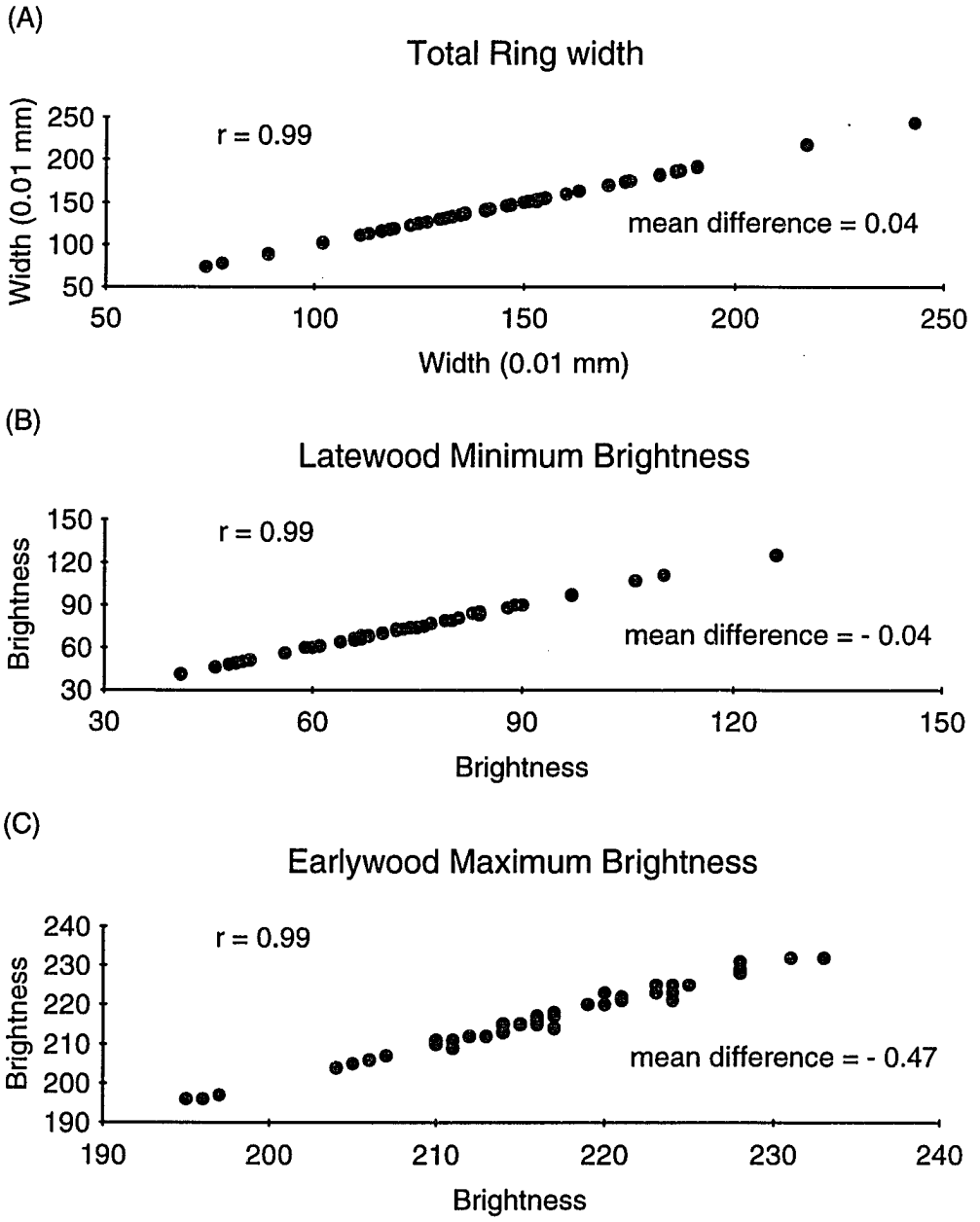

Fig. 5.4. Repeatability Tests: Repeatability results for (A) total ring width, (B) latewood minimum brightness, and (C) earlywood maximum brightness. For each variable, the x-axis represents data collected during one measurement session and the y-axis represents data collected during a different session.

6. PAST CLIMATE OF WESTERN MAINE USING REFLECTED-LIGHT IMAGE ANALYSIS OF RED SPRUCE OF ELEPHANT MOUNTAIN

INTRODUCTION

To demonstrate that conifer ring brightness can be used to reconstruct climate just as if density were used, I image analyzed cores from red spruce (*Picea rubens* Sarg.) growing at Elephant Mountain, Maine, (44° 46' N, 70° 46' W, 930 m elevation; Fig. 6.1). Conkey (1986) originally measured these cores densitometrically and reconstructed April–May temperature of western Maine. I compared statistical characteristics of density and brightness and climate-tree growth models using density or brightness (Sheppard et al. 1996).

METHODS

Site Characteristics

Elephant Mountain, western Maine, is within the Central Highlands section of the New England geologic province of Paleozoic metasedimentary and metavolcanic rocks (Denny 1982; Hack 1989). The present physiography of western Maine reflects Quaternary continental-scale glaciation, which left the highlands covered with till (Caldwell et al. 1985). Soils are coarsely textured (coarse-loamy to loamy), cool (frigid soil temperature regime) Spodosols that have mixed mineralogy and are typically shallow with either a fragipan or bedrock contact within 1 m of the surface (Rourke et al. 1978).

As typified by the meteorological record of Farmington, Maine (44° 40' N, 70° 09' W, 128 m elevation, 50 km southeast of and 800 m lower than Elephant Mountain; Fig. 6.1), western Maine has a mean annual air temperature of 5°C, a maximum mean monthly temperature of 19°C in July, and a minimum mean monthly tempera-

ture of −9°C in January (Fig. 6.2A). It is slightly cooler at the Elephant Mountain tree-ring site due to adiabatic cooling. Annual precipitation totals 1120 mm, which is evenly distributed throughout the year (Fig. 6.2B).

Elephant Mountain supports a mixed spruce-fir forest that is dominated by red spruce and also has balsam fir (*Abies balsamea* (L.) Mill.) (Oosting and Billings 1951). Other overstory trees include paper birch (*Betula papyrifera* Marsh.). Understory vegetation includes honeysuckle (*Viburnum* L.), blueberry (*Vaccinium* L.), and bramble (*Rubus* L.). Ground cover includes ferns, mosses, and liverworts.

Field Sampling, Sample Preparation, and Dating

In 1977, Laura E. Conkey (1982) increment cored red spruce growing at Elephant Mountain, Maine. She provided cores from that collection for comparison of X-ray densitometry data with imaging data. Using standard procedures for preparing tree-ring samples (Swetnam et al. 1985; Holmes et al. 1986), I air dried, mounted, and sanded all cores to expose a clear transverse sectional view.

I matched patterns of relatively wide and narrow rings across samples to identify and compensate for missing or intra-annual rings (Stokes and Smiley 1968); such ring-growth anomalies were not prevalent in the Elephant Mountain collection. Knowing the date of the last-formed ring of each sample, I then assigned a calendar year to each annual tree ring. Samples or segments of samples that could not be confidently dated were excluded from further analysis. I then measured all dated rings using reflected-light image analysis.

I checked all ring width and brightness series for dating and/or measuring errors by cross-correlating prewhitened measurement series with their respective mean-value series (Holmes 1983; Holmes et al. 1986). All identified dating and measuring errors were corrected. I verified the dating of the Elephant Mountain

ring-width chronology by matching it with nearby Traveler Mountain (46° 04' N, 68° 51' W) and Sugarloaf Mountain (45° 02' N, 70° 19' W) red spruce ring-width chronologies (Conkey 1986).

Data Reduction and Analysis

To correct for the normal decrease in ring widths as trees grow larger in diameter, I removed series-length growth trends from latewood, earlywood, and total ring-width series by dividing raw values by fitted values from negative-exponential curves or straight lines as estimated using iterative least squares regression (Fritts et al. 1969). Similarly, I removed series-length trends from brightness and density series using only straight lines as estimated using ordinary least squares regression. For each sample, this step resulted in dimensionless index series, which I averaged together into a standard chronology for each variable (Fritts 1976).

From the Historical Climatology Network (Karl et al. 1990), I obtained climate data and Palmer Drought Severity Indices (Palmer 1965) of the Farmington, Maine (44° 40' N, 70° 09' W, 128 m elevation, 50 km southeast of and 800 m lower than Elephant Mountain; Fig. 6.1) meteorological station for the Elephant Mountain climate modeling. Using best-subset regression (Draper and Smith 1981) with ring width and brightness or density variables as candidate predictors, I checked climate-tree growth relationships for all monthly and various seasonal temperature averages and precipitation totals. Tree-growth variables that were not highly cross-correlated and their 1-year forward and backward lagged series were included in this best-subset regression check.

I identified climate-tree growth models with optimum tradeoff between explained variance and number of included variables using Mallow's C_p statistic (Draper and Smith 1981). Models with low $C_p - p$ values, where p is the number of

predictors in the model, were tested for consistency across different time periods. I compared regression results for each model using the first half of the meteorological record to those using the second half. For each site, I chose the climate-tree growth model with the smallest difference across the two time periods for predictor coefficients; adjusted R^2 values, indicating percent variance shared by the tree-ring data and climate (Draper and Smith 1981); prediction R^2 values, indicating the true reconstruction skill of a model (Michaelsen 1987; Montgomery and Peck 1992; Haston and Michaelsen 1994); and with positive reduction of error statistics, indicating adequate skill for reconstructing climate (Fritts et al. 1990) as the strongest robust model for this site. I evaluated final climate-tree growth models for the full period of overlap with the meteorological data. Residuals of these models were checked for normality, correlation with predicted values, auto-correlation, and influence (Weisberg 1980). To equalize variances, I normalized reconstructed and actual climate series into series of departures relative to their respective means.

I inspected the variation of each normalized climate reconstruction across the frequency domain using spectral analysis (Chatfield 1975). I padded climate reconstructions to obtain a finer mesh of frequencies, tapered their ends (10%) to reduce the influence of estimates across frequency bands, and estimated each spectral density function by smoothing raw periodograms with a rectangular filter of an appropriate bandwidth.

RESULTS

Using reflected-light imaging analysis, I measured 15 Elephant Mountain red spruce cores (2045 rings total) in 25 hours, or about 45 seconds per ring. This measurement time included time spent setting up each measuring session, but it did not include time spent preparing the core samples. Sample preparation consisted of

fine sanding the transverse surfaces, which was no additional work beyond what is done for most dendrochronology studies. By contrast, several weeks were spent preparing and measuring the cores using X-ray densitometry (Conkey 1982).

Comparison of Density and Imaging Data

Density and brightness chronologies for earlywood (Fig. 6.3A) exhibit little variation compared to latewood (Fig 6.3B). Both brightness chronologies have low indices at their ends, a pattern of variation that differs from both density chronologies (Fig. 6.3A and B). Assuming this variation to be an anomalous end effect of the imaging system, I corrected latewood brightness indices of each sample by dividing them by their respective earlywood brightness indices. With this correction, anomalously low latewood brightness indices were raised by anomalously low earlywood brightness indices. The chronology of corrected latewood brightness more closely matches the chronology of latewood density than does the original latewood brightness.

Earlywood brightness index series have significantly higher first-order auto-correlation than density (Table 6.1); the earlywood brightness chronology also has higher first-order auto-correlation than density. There is no significant difference between density and brightness in cross-correlation of earlywood index series with their respective chronologies, but index series of both earlywood variables correlate only moderately strongly with their respective chronologies. Cross-correlation of brightness with density index series is negative and moderately strong for earlywood.

Latewood brightness index series also have significantly higher first-order auto-correlation than density, but the difference is less between density and corrected latewood brightness (Table 6.1). First-order auto-correlation of latewood is significantly less than that of earlywood, and no latewood chronology has significant

first-order auto-correlation. Cross-correlation of density index series with the density chronology is significantly higher than that for brightness, but not for corrected brightness. Index series of all latewood variables cross-correlate more strongly with their respective chronologies compared to earlywood. Cross-correlation of brightness with density index series is negative and significantly stronger for latewood than for earlywood.

April–May Temperature Reconstructed Using Density or Brightness

As with density and width chronologies, which do not significantly covary, most brightness chronologies do not significantly covary with width chronologies (Table 6.2). Neither the density chronologies nor the brightness chronologies covary significantly.

The strongest robust climate-tree growth models reconstruct April–May temperatures equally well using latewood density or corrected latewood brightness. Based on adjusted R^2 values and prediction R^2 values, climate models are stronger for the first-half time period than for the second half for both density and brightness (Table 6.3). Nonetheless, signs of estimated regression coefficients do not change between half periods, predicted values of each half period correlate significantly with actual climate values, and reduction of error statistics are all positive. For the full time period, density explains 30.8% of variation in April–May temperatures while brightness explains 29.0%. The prediction R^2 values match well between density and brightness and are only slightly lower than adjusted R^2 values.

Both reconstructions of April–May temperatures match actual values well for the 1910s, 1920s, and 1950s, but the match is relatively poor for the period since 1960 (Fig. 6.4A and B). Both reconstructions have no significant first-order auto-correlation for the full period, just as with the actual climate series. The two recon-

structions match each other well throughout most of their extents (Fig. 6.4C) and they cross-correlate significantly ($r = +0.86$). In spite of being corrected for end effects, latewood brightness results in higher positive temperature departures at the ends of the reconstruction than does density. Nonetheless, the spectral density functions of the reconstructions do not significantly differ from each other across the entire frequency domain (Fig. 6.5A), and they cohere strongly except for the lowest frequencies, i.e., periods > 20 years (Fig. 6.5B).

DISCUSSION

Density versus Image Analysis

In a small fraction of the time and expense needed to prepare and measure ring density of spruce cores, I used reflected-light image analysis to measure ring brightness. Latewood brightness correlates with April–May temperature such that both brightness and density reconstruct that climate variable equally well (Table 6.3, Fig. 6.4). This study indicates that reflected-light image analysis can aid in dendrochronological research to increase our understanding of climate of the latest Holocene.

As compared to ring density, the strong first-order auto-correlation of brightness (Table 6.1) is probably due to slight trends of color variation on the surface of the cores. While red spruce of Elephant Mountain does not exhibit severe heartwood-sapwood color variation, some core samples show 5- to 10-year periods of rings that are slightly lighter or darker than average. This variation may be due to twisting of the core, fungal staining, deposition by the tree of extractives, or some combination of these or still other factors. My method of correcting anomalous variation in latewood brightness–dividing by earlywood brightness–is simplistic and was only partially successful.

Variation in Past April–May Temperature

Both density and brightness reconstruct periods of below-average April–May temperatures during the 1830s, 1870s, and late 1880s, which combine to have an average departure of −0.30 (standard error = 0.19) (Fig. 6.4C). Notable single-year negative departures occurred in 1835, 1845, 1885, and 1888. Other red spruce density chronologies from western Maine reconstruct similar temperature patterns for the 19th century, indicating that these patterns are regional climate phenomena (Conkey 1986).

Both density and brightness reconstruct high annual variability for most of the 19th century (standard deviation = 1.16 for the period 1815–1890), though not for the 1890s (standard deviation = 0.56 for the decade). This pattern of climate variability corresponds well with historical documentation indicating great variability in lengths of growing seasons of southern New Hampshire until the end of the 19th century (Baron 1992a).

Both density and brightness fail to reconstruct a markedly below-average April–May temperature for 1816, a year that had a very short growing season in southern New Hampshire and that is known as one of the coldest years in the history of the northeastern United States (Baron 1992a, 1992b). This seemingly poor reconstruction for 1816 might be explained by the fact that various diarists of Maine, New Hampshire, and Vermont observed no remnant snow pack in mid April and that farmers were planting crops by early May (Baron 1992b). Not until mid May of 1816 was temperature of the northeastern United States below average. Furthermore, March–May temperature during 1816 was average relative to the entire meteorological record (1807–1837) for Brunswick, Maine (Baron 1992b). Therefore, the Elephant Mountain tree-ring chronologies should not be expected to

reconstruct a below-average April–May temperature for 1816, the so-called year without a summer.

The poor association between red spruce growth and climate at Elephant Mountain since 1960 corresponds with strikingly poor climate-tree growth modeling for that period for many transitional or boreal red spruce chronologies of New York and northern New England (Johnson et al. 1988). This regional breakdown of how red spruce are responding to climate variation since 1960 has been ascribed to the influence of extreme temperature and/or precipitation events, outbreaks of pathogens, pollution, or a combination of causes (Johnson et al. 1988).

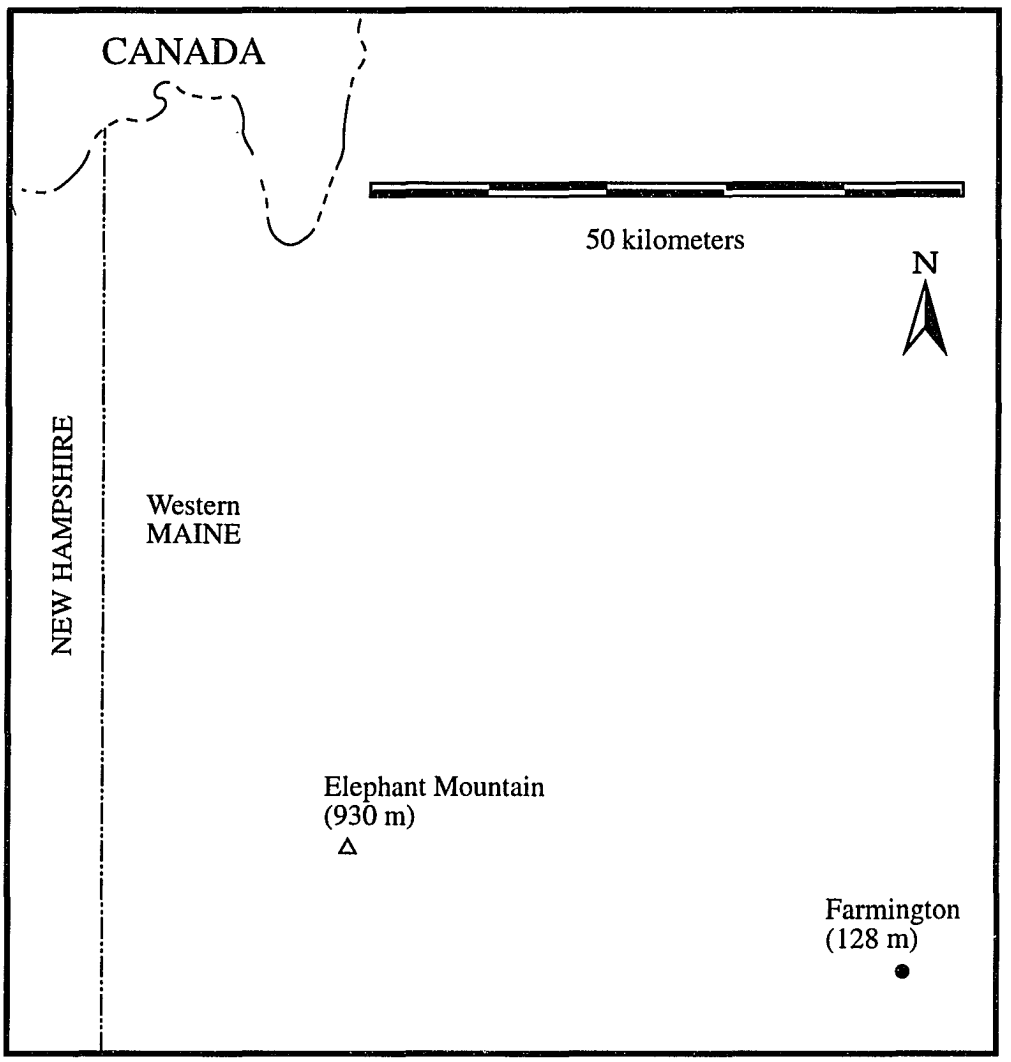

Fig. 6.1. Map of Western Maine: The Elephant Mountain tree-ring site is marked with an open triangle and the Farmington meterological station is marked with a closed circle; elevations are given in parentheses.

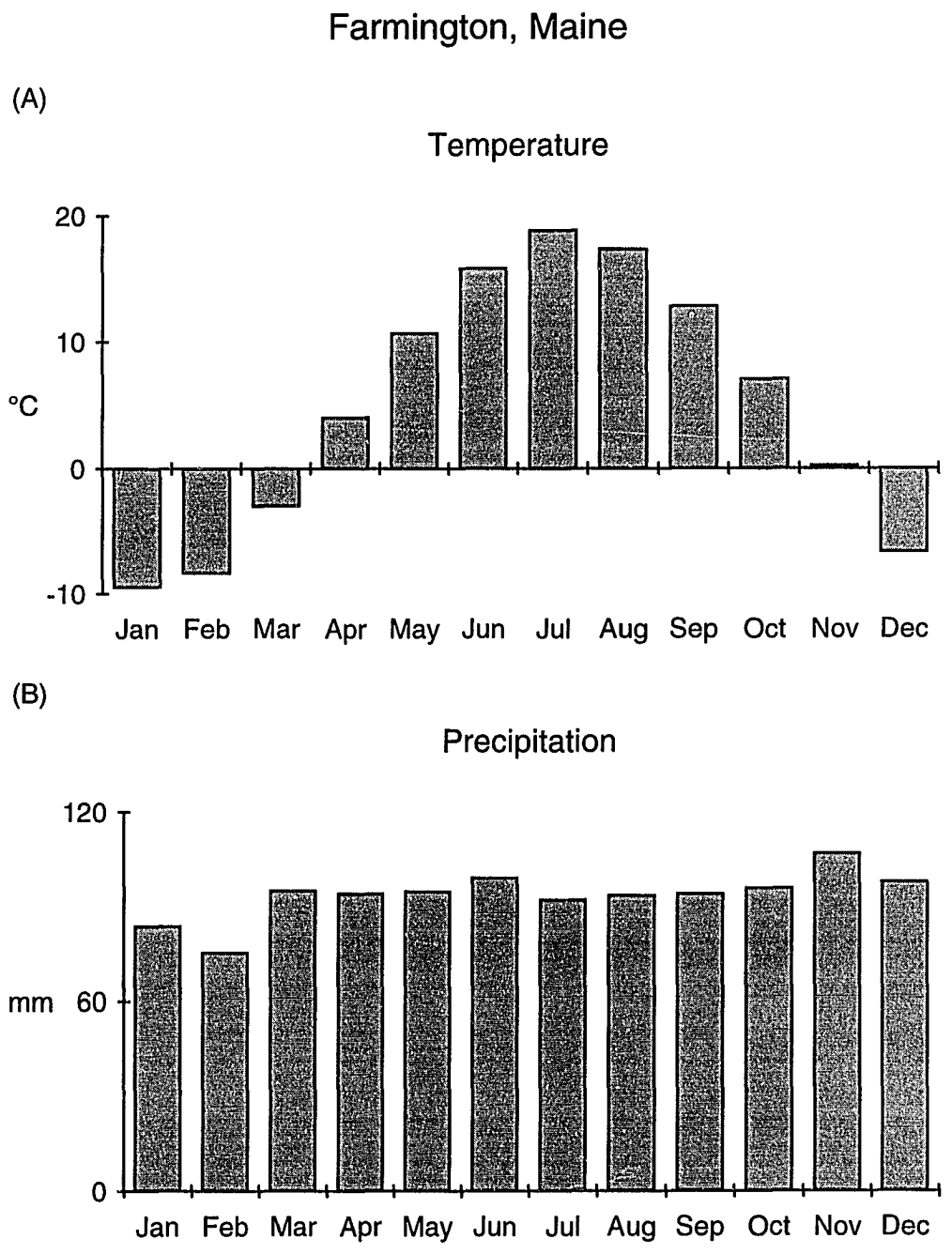

Fig. 6.2. Western Maine Climatographs: (A) Monthly average temperature and (B) monthly total precipitation for Farmington, Maine.

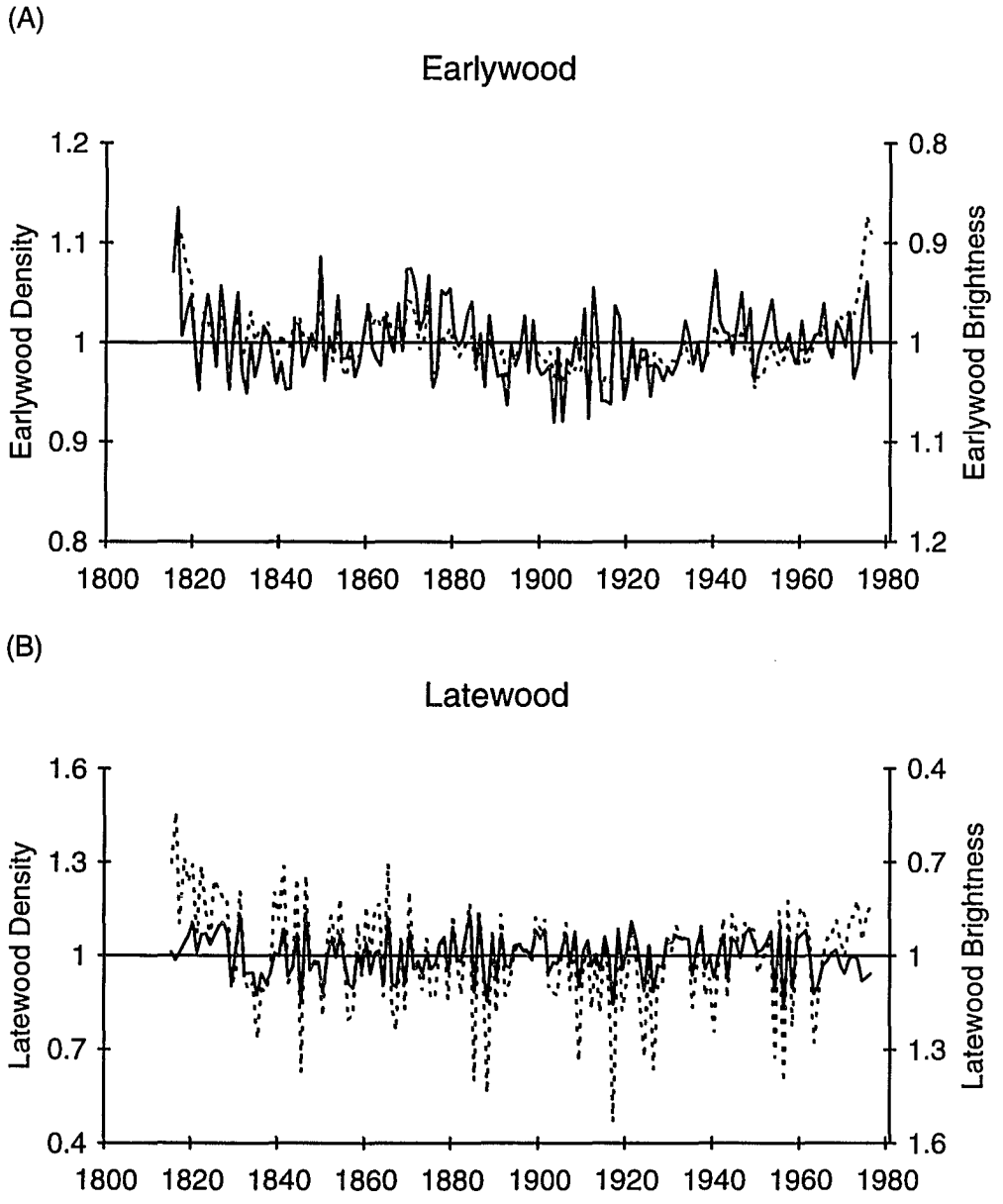

Fig. 6.3. Elephant Mountain Chronologies: Density (solid line) and brightness (dashed line) chronologies for (A) earlywood and (B) latewood. Brightness ordinate scales are reversed relative to density, and ordinate scales of earlywood are reduced relative to latewood.

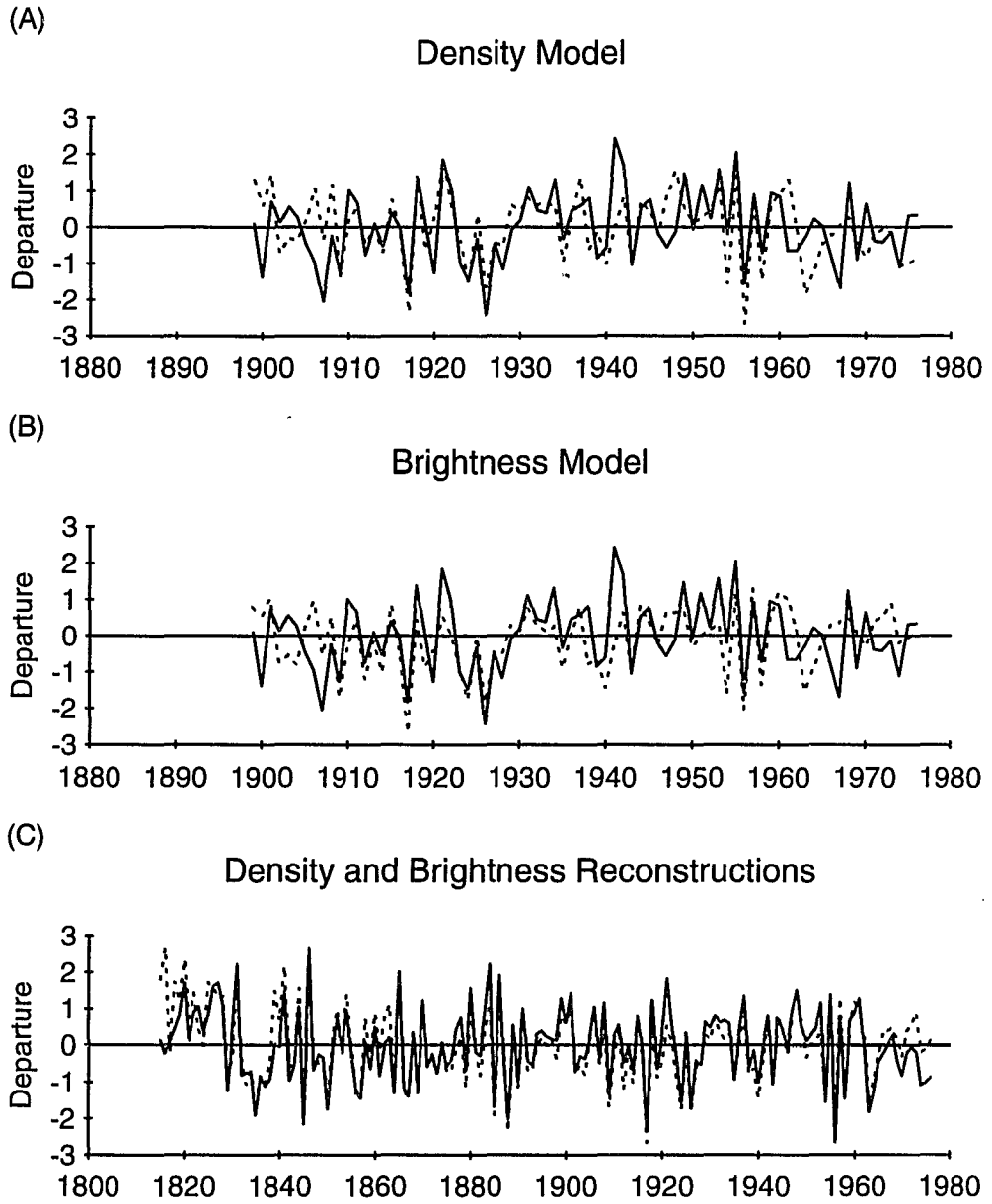

Fig. 6.4. Elephant Mountain Climate Models and Reconstructions: Actual (solid line) and predicted (dashed line) April-May temperature departures, relative to mean of entire time period, for (A) density and (B) brightness. (C) Density (solid line) and brightness (dashed line) reconstructions of temperature departures.

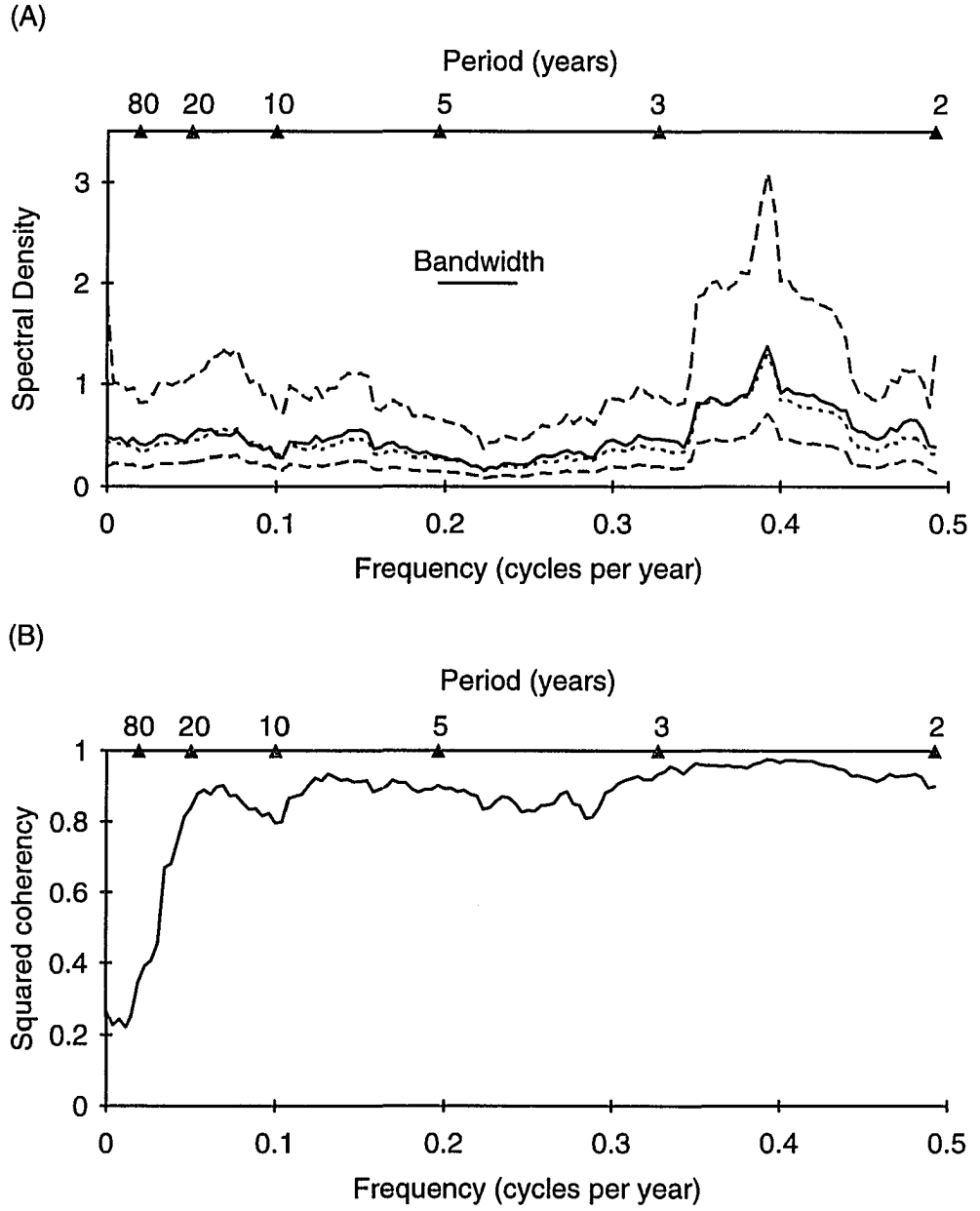

Fig. 6.5. Elephant Mountain Spectral Analysis: (A) Spectral density functions for April-May temperatures as reconstructed using density (solid line) or brightness (dotted line), with 95% confidence bands (dashed lines) for the brightness spectrum, and (B) squared coherency of the two spectral density functions. Bandwidth is 0.0508.

Table 6.1. Elephant Mountain Density and Brightness Chronologies: Mean and standard error (std. err.) of time-series and correlation statistics of brightness and density variables for earlywood and latewood.

	Earlywood				
	First-order Auto-correlation*		Cross-correlation with Chronology#		Between-system Cross-correlation*
	Density	Brightness	Density	Brightness	Density by Brightness
Mean	0.40	0.68	0.56	0.53	−0.55
Std. err.	0.04	0.03	0.03	0.05	0.04
Chronology#	0.21	0.64			

	Latewood							
	First-order Auto-correlation			Cross-correlation with Chronology			Between-system Cross-correlation	
	Density	Brightness	Corrected Brightness	Density	Brightness	Corrected Brightness	Density by Brightness	Density by Corrected Brightness
Mean	0.02	0.21	0.14	0.79	0.72	0.73	−0.75	−0.79
Std. err.	0.04	0.05	0.04	0.02	0.03	0.03	0.02	0.01
Chronology	−0.09	0.04	−0.06					

* Sample size is 15 for auto-correlation and between-system cross-correlation means.

Chronology refers to the single time series constructed for each variable by averaging individual index series. Sample size is 13 for mean cross-correlations with chronology for the common period (1850–1973) of the cores.

Table 6.2. Elephant Mountain Tree-Ring Correlation Matrices*.

	Densitometry			
	Earlywood Width	Latewood Width	Total Ring Width	Earlywood Density
Earlywood Density	−0.10	0.05	−0.10	
Latewood Density	0.05	0.02	0.04	0.02

	Image Analysis			
	Earlywood Width	Latewood Width	Total Ring Width	Earlywood Brightness
Earlywood Brightness	−0.02	−0.27	−0.02	
Latewood Brightness	−0.08	−0.12	−0.06	0.14

* Critical value is 0.16 for two series, 150 degrees of freedom, and an α level of 0.05.

Table 6.3. Elephant Mountain Climate Models Using Density or Brightness: Climate variable is Farmington April–May temperature.

Density						
Calibration				Verification		
Period	lxd^	R^2_{adj}* (%)	R^2_{pred}# (%)	Period	r§	RE¶
1899–1937	+0.001	45.3	41.5	1938–1976	0.50	+0.15
1938–1976	+0.001	22.6	17.5	1899–1937	0.68	+0.36
1899–1976	+0.001	30.8	28.3			

Brightness						
Calibration				Verification		
Period	lnb^	R^2_{adj}* (%)	R^2_{pred}# (%)	Period	r§	RE¶
1899–1937	−0.001	41.8	38.0	1938–1976	0.40	+0.10
1938–1976	−0.011	13.8	8.9	1899–1937	0.66	+0.36
1899–1976	−0.001	29.0	26.8			

^ The sign and probability level are given for each coefficient. Lxd is the slope of latewood maximum density, and lnb is the slope of corrected latewood minimum brightness.

* Coefficient of determination, adjusted for loss of degrees of freedom (Draper and Smith 1981).

\# Prediction coefficient of determination (Montgomery and Peck 1992).

§ Pearson coefficient of correlation between predicted and actual climate. Critical value is 0.32 for 35 degrees of freedom at the 0.05 level (Rohlf and Sokal 1980).

¶ Reduction of error statistic (Fritts et al. 1990).

7. PAST CLIMATE OF SOUTHEASTERN ARIZONA USING REFLECTED-LIGHT IMAGE ANALYSIS OF PONDEROSA PINE OF MICA MOUNTAIN

INTRODUCTION

Some conifer species exhibit extraneous color, i.e., color variation of wood that occurs after rings are formed and therefore has no relationship to environmental conditions at the time of ring formation. The most notable type of extraneous color is the heartwood-sapwood color change commonly seen in many conifer species. Extraneous color variation can also arise from fungal staining (Kreber and Byrne 1994) and/or compartmentalization of wounds (Shigo 1985). A reflected-light imaging system that can detect environmentally relevant brightness variation between rings can certainly detect extraneous color (Fig. 4.2), which would be statistical noise in later analyses. In species with extraneous color, the relationship between density and brightness is not constant throughout a sample and thus a primary requirement for applying reflected-light image analysis to approximate density is not met (Telewski and Jacoby 1987; Yanosky et al. 1987).

Tree species that exhibit highly pronounced heartwood-sapwood and other extraneous color include pines (*Pinus* L.) and Douglas-firs (*Pseudotsuga* Carr.), which comprise the majority of collections of the International Tree-Ring Data Bank (Grissino-Mayer 1995). To be widely applicable to dendrochronology, reflected-light image analysis must overcome the problem of extraneous color, either by chemically removing it from wood using organic extraction or bleaching, or by mathematically removing its effects from measured data (Yanosky et al. 1987).

Furthermore, given that ring density of pines and Douglas-firs has been used for reconstructing climate of the latest Holocene in semiarid Southwestern North

America (Cleaveland 1986), it is logical to attempt image analysis of these species. Park (1990) image analyzed ponderosa pines (*Pinus Ponderosa* Dougl. ex Laws.) growing at Mica Mountain, Arizona (32° 12' N, 110° 33', 2400 m elevation; Fig 7.1), and he modeled the lumen area:total cell area ratio to July–October precipitation. However, Park's image analysis method used very high magnification, light transmitted through thin sections of core samples, and binary object analysis of black cell walls versus white lumina. Consequently, while extraneous color was not a concern for Park, his image analysis method was time consuming such that he limited his climate-tree growth modeling to the period 1910–1930.

To investigate various strategies for overcoming extraneous color and to attempt low-magnification reflected-light image analysis on a semiarid Southwest tree-ring site, I image analyzed cores from ponderosa pine growing at Mica Mountain. I compared precipitation-tree growth models using brightness from various combinations of sample preparation, chronology type, and data strategies to overcome extraneous color.

METHODS

Site Characteristics

Mica Mountain, southeastern Arizona, is within the southern Basin and Range geologic province of numerous discrete mountain ranges of Precambrian metasedimentary and metavolcanic rocks and Oligocene metamorphic core complexes (Lingrey 1982). The present physiography of southeastern Arizona reflects late Miocene and younger extensional block faulting (Shafiqullah et al. 1978; Scarborough and Pierce 1978). Soils are coarsely textured (loamy-skeletal), moderately warm (mesic soil temperature regime) Mollisols that have mixed mineralogy and are moderately shallow with bedrock contact about 1 m below the surface (Soil Survey

Staff 1995).

As typified by the meteorological record at Tucson, Arizona (32° 16' N, 111° 00' W, 788 m elevation, 40 km west of and 1600 m lower than Mica Mountain; Fig 7.1), southeastern Arizona has a mean annual air temperature of 20°C, a maximum mean monthly temperature of 31°C in July, and a minimum mean monthly temperature of 11°C in January (Fig. 7.2A). It is several degrees cooler at the Mica Mountain tree-ring site due to adiabatic cooling. Annual precipitation totals 288 mm, most of which comes during summer (Fig. 7.2B) as a result of large-scale tropical storms from the Pacific Ocean and/or local convective storms (Sellers 1960).

Above 1800 m in elevation, Mica Mountain supports a montane mixed conifer forest that is dominated by ponderosa pine and has Douglas-fir (*Pseudotsuga menziesii* (Mirb.) Franco) on north-facing slopes (Lowe and Brown 1973). Other overstory trees include white fir (*Abies concolor* (Gord. and Glend.) Lindl. ex Hildebr.) and southwestern white pine (*Pinus strobiformis* Englm.). Understory vegetation includes buckbrush (*Ceanothus* L.), snowberry (*Symphoricarpos* Duhamel.), and bracken fern (*Pteridium* Scop.). Ground cover includes several grasses.

Field Sampling, Sample Preparation, and Dating

In October 1992, I increment cored 18 ponderosa pines growing on the southwest slope of Mica Mountain of the Rincon Range of Arizona. Following standard field techniques for dendrochronological research of past climate (Schweingruber et al. 1990), I identified apparently healthy trees, i.e., that were free of obvious scars, and then collected from each tree 5-mm-diameter increment core samples from opposing radii of the diameter that was perpendicular to the local slope. Whereas typically two cores are collected from each tree, I collected a total of four cores, i.e., two cores each from opposing radii. I used the extra samples for the investigation of

sample preparation treatments to remove extraneous color from the wood.

I investigated three chemical sample preparation treatments for removing extraneous color from wood. First, for each sampled ponderosa pine of Mica Mountain, I did no chemical treatment on one pair of cores (opposing radii), which were designated as NONE. Second, after measuring NONE cores with reflected-light image analysis, I removed them from their mounts and bleached them for two hours in a 70°C solution of 0.11 *M* $NaClO_2$ with glacial acetic acid (Leavitt and Danzer 1993). I then redried, remounted, and resanded bleached cores, which were redesignated as BLEACH. Third, I extracted the other pair of cores for four hours in toluene, then for four hours in a 50:50 mixture of ethanol-toluene, and then for one hour in distilled water (Park et al. 1992). Each solvent was alternately vaporized and distilled in a Soxhlet extraction apparatus. I then dried, mounted, and sanded extracted cores, which were designated as EXTRACT.

I matched patterns of relatively wide and narrow rings across samples to identify and compensate for missing or intra-annual rings (Stokes and Smiley 1968); such ring-growth anomalies were prevalent in the Mica Mountain collection. Knowing the date of the last-formed ring of each sample, I then assigned a calendar year to each annual tree ring. Samples or segments of samples that could not be confidently dated were excluded from further analysis. I then measured all dated rings using reflected-light image analysis.

I checked all ring width and brightness series for dating and/or measuring errors by cross-correlating prewhitened measurement series with their respective mean-value series (Holmes 1983; Holmes et al. 1986). All identified dating and measuring errors were corrected. I verified the dating of the Mica Mountain ring-width chronology by matching it with other ponderosa pine ring-width chronologies

made from earlier collections at the same study site (Drew 1972).

Data Reduction

To correct for the normal decrease in ring widths as trees grow larger in diameter, I removed series-length growth trends from latewood, earlywood, and total ring-width series by dividing raw values by fitted values from negative-exponential curves or straight lines as estimated using iterative least squares regression (Fritts et al. 1969). Similarly, I removed series-length trends from brightness and density series using only straight lines as estimated using ordinary least squares regression. For each sample, this step resulted in dimensionless index series, which I averaged together into a standard chronology for each variable (Fritts 1976).

STANDARD versus RESIDUAL Brightness Chronologies

In addition to containing year-to-year brightness variation of successive rings, brightness standard index series from Mica Mountain ponderosa pine contain low-frequency variation that is due to extraneous color, most notably from the heartwood-sapwood color change. In an analytical attempt to remove the effects of extraneous color from measured data, I autoregressively modeled each STANDARD brightness index series to its specific order as determined using the minimum Akaike Information Criterion (Akaike 1974). I then averaged residual index series across cores for each year into RESIDUAL brightness chronologies (Cook 1985).

SPLIT Versus FULL Brightness Data

Even after autoregressive modeling, it is possible for the residual chronology to have artifacts of extraneous color. To illustrate this potential problem, I measured 30 rings prior to and after the heartwood-sapwood boundary of a Mica Mountain ponderosa pine core for which ring brightness increases abruptly at the boundary (Fig. 5.7A). If the series is kept at its full length, the series-length trend is posi-

tive through time and the standard and, to a lesser degree, residual index series retain extraneous trends and/or spikes at the boundary (Fig. 7.3B).

If the brightness series is split into two at the heartwood-sapwood boundary, then the series-length trends are flat through time (Fig. 7.3A) and the standard and residual index series show no extraneous trends and/or spikes at the boundary (Fig. 7.3C); however, both index series show high variance for heartwood rings versus low variance for sapwood rings. This artifact can be corrected by normalizing each series (Fig. 7.3D).

Accordingly, I split each brightness series into two shorter series at the observed heartwood-sapwood boundary, removed series-length trends as previously described, normalized the standard index series, and re-attached the two split-length index series back into one series for every core. As before, I averaged these index series into chronologies that were designated as SPLIT to distinguish them from FULL chronologies.

Thus, for removing the effects of extraneous color from brightness data, this research design has three sample preparation treatments (NONE, EXTRACT, or BLEACH) crossed with two chronology treatments (STANDARD or RESIDUAL) crossed with two data treatments (FULL or SPLIT). Consequently, this design has 12 treatment combinations (Table 7.1). However, because of the potential drawback of the FULL treatment (Fig. 7.3), I initially restricted my analysis to the six SPLIT treatment combinations. I compared the strongest robust climate model from the SPLIT treatment combinations to its conjugate model from the FULL treatment combination.

Data Analysis

From the Historical Climatology Network (Karl et al. 1990), I merged climate

data and Palmer Drought Severity Indices (Palmer 1965) from the Tucson, Arizona (32° 16'N, 111° 00' W, 788 m elevation, 40 km west of and 1600 m lower than Mica Mountain; Fig 7.1) and Willcox, Arizona (32° 18' N, 109° 51' W, 1273 m, 68 km east of and 1125 m lower than Mica Mountain; Fig 7.1) meteorological stations for the Mica Mountain climate modeling. Using best-subset regression (Draper and Smith 1981) with ring width and brightness or density variables as candidate predictors, I checked climate-tree growth relationships for all monthly and various seasonal temperature averages and precipitation totals. Tree-growth variables that were not highly cross-correlated and their 1-year forward and backward lagged series were included in this best-subset regression check.

I identified climate-tree growth models with optimum tradeoff between explained variance and number of included variables using Mallow's Cp statistic (Draper and Smith 1981). Models with low $Cp - p$ values, where p is the number of predictors in the model, were tested for consistency across different time periods. I compared regression results for each model using the first half of the meteorological record to those using the second half. For each site, I chose the climate-tree growth model with the smallest difference across the two time periods for predictor coefficients; adjusted R^2 values, indicating percent variance shared by the tree-ring data and climate (Draper and Smith 1981); prediction R^2 values, indicating the true reconstruction skill of a model (Michaelsen 1987; Montgomery and Peck 1992; Haston and Michaelsen 1994); and with positive reduction of error statistics, indicating adequate skill for reconstructing climate (Fritts et al. 1990) as the strongest robust model for this site. I evaluated final climate-tree growth models for the full period of overlap with the meteorological data. Residuals of these models were checked for normality, correlation with predicted values, auto-correlation, and influ-

ence (Weisberg 1980). To equalize variances, I normalized reconstructed and actual climate series into series of departures relative to their respective means.

I inspected the variation of each normalized climate reconstruction across the frequency domain using spectral analysis (Chatfield 1975). I padded climate reconstructions to obtain a finer mesh of frequencies, tapered their ends (10%) to reduce the influence of estimates across frequency bands, and estimated each spectral density function by smoothing raw periodograms with a rectangular filter of an appropriate bandwidth.

RESULTS

July–October Precipitation Reconstructed Using Image Analysis

Regarding the common width and brightness variables, only earlywood brightness and total ring width covary significantly, though even these two variables share less than 10% variation in common (Table 7.2). Earlywood maximum brightness and latewood minimum brightness do no covary significantly.

With initially considering only SPLIT brightness data, the strongest robust climate-tree growth model predicts July–October precipitation with earlywood maximum and latewood minimum brightness and total ring width. This is true for NONE, EXTRACT, and BLEACH preparations and both STANDARD (Table 7.3) and RESIDUAL chronologies (Table 7.4).

For all six SPLIT preparation-chronology treatment combinations, earlywood maximum brightness has a negative coefficient while latewood minimum brightness and total ring width have positive coefficients, and no coefficient changes signs between full, first-half, and second-half periods of modeling. Based on adjusted R^2 values and prediction R^2 values, climate models are stronger for the first-half period than for the second-half (Tables 7.3 and 7.4).

Preparation and Chronology Treatments

BLEACH climate models are drastically weaker than NONE or EXTRACT (Tables 7.3 and 7.4). With very low—and even negative—prediction R^2 values, BLEACH climate models are too weak to warrant further analysis. Additionally, RESIDUAL climate models (Table 7.4) are stronger then STANDARD (Table 7.3).

For RESIDUAL chronologies, the EXTRACT climate model is slightly stronger than NONE (Table 7.4), i.e., the reduction of error for the second-half period of the NONE climate model is negative, indicating poor prediction skill. Thus, the EXTRACT-RESIDUAL treatment combination has the strongest robust climate model of the six SPLIT data sets in this research design.

Difference Brightness Variable

Because the coefficient for earlywood maximum brightness is negative while the coefficient for latewood minimum brightness is positive, I derived a new variable by subtracting latewood brightness from earlywood brightness. This difference variable should relate inversely to July—October precipitation. For the EXTRACT-RESIDUAL-SPLIT treatment combination, I redid best subset regression climate model checks using difference while excluding earlywood maximum and latewood minimum brightness, which significantly cross-correlate with difference (Table 7.2).

The strongest robust climate-tree growth model predicts July—October precipitation with difference, total ring brightness, and total ring width (Table 7.5), and this model is slightly stronger than that using earlywood maximum and latewood minimum brightness and total ring width (Table 7.4). As expected, the coefficient for difference is negative, as is the coefficient for total ring brightness, which is highly correlated with earlywood maximum brightness (Table 7.2).

SPLIT versus FULL Data

Using difference, total ring brightness, and total ring width from the EXTRACT-RESIDUAL data set, the FULL climate model is slightly stronger than SPLIT model (Table 7.5), i.e., both reduction of error statistics are stronger for the FULL model than for SPLIT. RESIDUAL-FULL brightness chronologies have no low-frequency variation and little variance relative to the total ring width chronology (Fig. 7.4).

For the full time period, the EXTRACT-RESIDUAL-FULL model explains 31.2% of variation in July–October precipitation. The prediction R^2 is only slightly lower than the adjusted R^2. For the full period, Tucson and Willcox share only ~25% variance in July–October precipitation (Fig. 7.5A). The FULL climate model matches actual values well for 1910–1930 and 1950–1970, but the match is relatively poor for 1930–1950 and the 1980s (Fig. 7.6A). Tucson and Willcox also match each other poorly with July–October precipitation for the period 1930–1950 (Fig. 7.5B). The FULL model matches well the below-average mean and variance of actual July–October precipitation for 1930–1950 period (Fig. 7.6A). The full reconstruction shows both high- and low-frequency variation (Fig. 7.6B).

DISCUSSION

Relationship of Tree Growth With Climate

This study supports Park's (1990) results relating latewood density, as approximated by the ratio of lumen area to total cell area, and total ring width of Mica Mountain ponderosa pine to July–October precipitation. Park (1990), however, did not image analyze earlywood and therefore could not have included earlywood variables in a climate model. By image analyzing full rings and measuring earlywood variables, I included earlywood maximum brightness in the July–October precipita-

tion model. This supports Cleaveland's (1983, 1986) results relating earlywood density to moisture availability for semiarid Southwest tree-ring sites.

Given that the usual growing season for ponderosa pine of southern Arizona begins by May and extends to late September (Budelsky 1969; Baisan and Swetnam 1994), the inverse relationship of earlywood brightness to July–October precipitation (Tables 7.3 and 7.4) of this study is phenologically logical. Earlywood tracheids are probably fully elongated but not finished with cell-wall thickening by July. Above-average July–October soil moisture should lead to above-average cell-wall thickening of earlywood cells, which would make earlywood denser and less bright. Conversely, below-average July–October soil moisture should lead to below-average cell-wall thickening of earlywood cells, which would make earlywood less dense and bright.

Similarly, the direct relationship of latewood brightness to July–October precipitation (Tables 7.3 and 7.4) is phenologically logical. Latewood tracheids are probably not fully elongated even as late as September. Above-average July–October soil moisture should lead to above-average elongation of latewood cells, which would make latewood less dense and bright. Conversely, below-average July–October soil moisture should lead to below-average elongation of latewood cells, which would make latewood denser and less bright.

By extension of that phenological logic, above-average July–October precipitation should reduce the difference between earlywood and latewood brightness, as is true in this study (Table 7.5). I know of no other dendrochronological research–either with densitometry or image analysis–in which climate has been modeled to such a difference variable. Consequently, it is difficult at this time to confidently infer wide applicability of this difference variable to dendrochronology.

Furthermore, difference is only one of several unusual and/or derivative variables of reflected-light image analysis (Fig. 4.1), and additional research is necessary to determine their usefulness.

Although tree growth responds strongly to summer precipitation for most of the period of the meteorological record, the relationship is weaker from 1930–1950, a time when summer precipitation for Tucson matches poorly that for Willcox (Fig. 7.5). Given that July–October precipitation for southeastern Arizona is the result of a combination of local convective storms during July–August and/or larger-scale tropical storms from the Pacific Ocean during September–October (Sellers 1960; Smith 1986), it is possible that 1930–1950 was a period of below-average tropical storm activity such that summer precipitation was unusually heterogeneous spatially during that time (Webb and Betancourt 1992).

Overcoming Extraneous Color

Sample Preparation Treatment

When sapwood tissue, which has living parenchyma cells, converts to heartwood, which has no living cells (Dadswell and Hillis 1962), soluble liquid tannins convert to an insoluble state and impart a dark color to the tissue (Chattaway 1952). Because solid tannins are not extractable, any chemical treatment to overcome extraneous color must oxidize them to a different state. However, at the same time, such a chemical treatment must not affect earlywood-latewood brightness variation, which is due primarily to differences in the light scattering power of the wood itself (Wilcox 1975).

Bleaching removed extraneous color, including heartwood-sapwood color changes, but bleaching did not effectively overcome the problem of extraneous color. In spite of bleaching with a weak solution and for only two hours, this treat-

ment was still too strong in that it also removed the ring brightness signal that relates to July–October precipitation (Table 7.3 and 7.4). For bleaching to be effective, a different bleaching agent and/or treatment will be necessary.

Bleaching had additional adverse side effects. The effectiveness of bleaching varied between cores, and it is difficult to know *a priori* what the correct bleaching treatment should be for any particular core. The effectiveness of bleaching varied within cores, both between heartwood and sapwood rings and between the surface area and interior of the core. Bleached cores were brittle, making them more difficult than normal to prepare for measuring. Bleached cores also contained numerous hairline fractures, which greatly slowed the rate of measurement using reflected-light image analysis because of discontinuous ring boundaries.

Many wood extractable materials, e.g., polyphenolic compounds, impart dark color on wood (Hillis 1968, 1971). However, organic extraction of cores did not greatly enhance the brightness signal that relates to July–October precipitation (Tables 7.3 and 7.4). Therefore, this treatment also did not effectively overcome the problem of extraneous color in this study. Organic extraction of wood is useful primarily for removing resins (Mutton 1962), which can obscure rings but is not the cause of severe extraneous color, e.g., heartwood-sapwood color variation.

Because the Mica Mountain ponderosa pine cores were not particularly resinous, organic extraction was not likely to overcome the problem of extraneous color in this study. However, in dendrochronological research of species known to be particularly resinous, e.g., bristlecone pine (*Pinus longeava* D.K. Bailey) and foxtail pine (*Pinus balfouriana* Grev. and Balf.), organic extraction to remove resins would likely be effective at enhancing the ring brightness signal from reflected-light image analysis.

Chronology Treatment

Autoregressively modeling brightness variables effectively overcame the problem of extraneous color. Climate models using residual brightness chronologies (Table 7.4) are all stronger than using standard chronologies (Table 7.3), and none of the residual brightness chronologies exhibit any unusual artifact attributable to heartwood-sapwood boundaries (Fig. 7.4A–D).

It is mathematically difficult for autoregressive modeling to differentiate between persistence due to extraneous color from that due to other environmental factors. Consequently, an adverse side effect of autoregressive modeling is the possibility of losing environmentally relevant information. Most tree-ring research using ring density has not shown it to exhibit low-frequency variation that was relevant to climate or any other environmental factor (Conkey 1986; Jacoby et al. 1988). Exceptions to this generalization include Briffa et al. (1992a), who observed low-frequency density variation in Scotch pine (*Pinus sylvestris* L.) of northern Fennoscandia, and Stahle et al. (1992), who observed a step change in baldcypress ring density–similar to the step change in brightness at a heartwood-sapwood boundary–due to the 1811-1812 New Madrid earthquake.

Data Treatment

Splitting brightness series at the heartwood-sapwood boundary prior to analysis theoretically overcomes the problem of extraneous color (Fig. 7.3). This data treatment uses the same rationale used for splitting ring-width series into segments of widely different mean values for trees exhibiting sharp growth releases (Blasing et al. 1983). A drawback of splitting series is the addition of yet more steps in a data-reduction process that is already complex.

While it is potentially risky not to split brightness series when image analyzing

samples with strong heartwood-sapwood color variation, keeping brightness series at full length worked well in this study (Table 7.5). There is no reason to expect heartwood-sapwood boundaries to be synchronous across trees of a noncommercial forest. If extraneous color is not synchronous across trees of a well replicated tree-ring collection, then averaging index series should eliminate the effects of that variation from final chronologies. This is especially true when using a robust averaging process (Cook 1985), which excludes far-outlying values from the calculation.

Variation in Past July–October Precipitation

As reconstructed using difference (earlywood brightness minus latewood brightness), total ring average brightness, and total ring width, July–October precipitation exhibits two prominent time-series characteristics (Fig 7.6B). One is strong low-frequency variation, as is highlighted by an appropriate cubic smoothing spline. Overlaid on that is strong high-frequency variation: Subtracting the spline from the reconstruction results in a series with a first-order autocorrelation of −0.19. Thus, July–October precipitation is highly variable year-to-year and has long-term departures, which is a typical precipitation pattern for semi-arid regions (Durrenberger and Wood 1979; Brazel 1985).

An independent verification of one feature of the reconstruction from this study is the regional die-off of cattle during an unusually persistent drought, including summer drought, of 1890–1892 (Bahre 1991). The July–October precipitation reconstruction has low values for those years, an extended period of drought that is unusual relative to the strong pattern of high-frequency variation for the rest of the series (Fig. 7.6B).

Few other opportunities exist for independently verifying the 19th Century events of this reconstruction. Tucson's meteorological record extends back to 1868,

but summer precipitation in southeastern Arizona is highly heterogeneous spatially (Brazel 1985), so much so that comparing one tree-ring reconstruction to one meteorological station is not meaningful. There are virtually no other historical documents that relate specifically to Mica Mountain prior to 1900. Thus, there currently is no verification of the period of below-average July–October precipitation for 1850–1890 (Fig. 7.6B).

A larger question remains as to whether this reconstruction truly reflects July–October precipitation, or if it also reflects annual or winter-spring precipitation, which is more commonly reconstructed from semiarid Southwest tree-ring sites (e.g., Brazel et al. 1978; Meko and Graybill 1995). Most past dendrochronological research in this region has reconstructed precipitation using only total ring width, which, in this study, is the source of the below-average reconstructed values for 1850–1890 (Fig. 7.4E). However, by itself, Mica Mountain ponderosa pine total ring width does not relate to any typically used climate variable, including winter precipitation, strongly enough to warrant a reconstruction (Fig. 7.7; Graybill and Rose 1989).

It is important to develop separate and defensible reconstructions of summer or winter precipitations because of ramifications to archeological research of past human cultures of the Southwest. A long-held hypothesis holds that summer precipitation was as important as that of winter to Pueblo people (Gladwin 1947). As yet, little dendrochronological research has spoken to this issue because most tree-ring reconstructions are of annual or winter-spring precipitation. If new tree-ring variables, such as those measured or derived using reflected-light image analysis, are useful for reconstructing summer precipitation, then this critical human-climate interaction theory can be tested more fully.

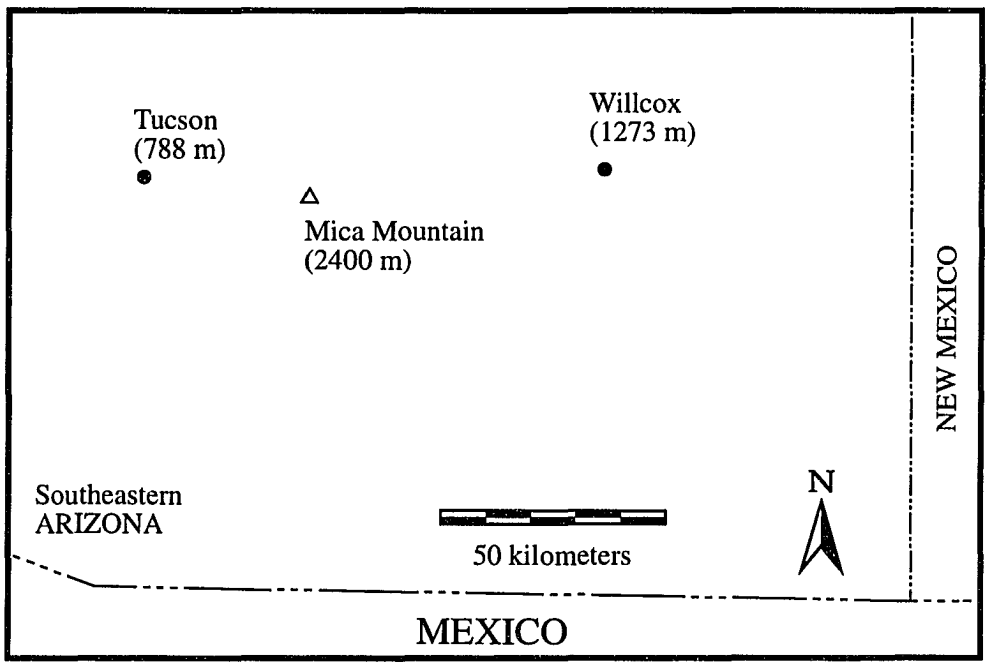

Fig. 7.1. Map of Southeastern Arizona: The Mica Mountain tree-ring site is marked with an open triangle and the Tucson and Willcox meteorological stations are marked with closed circles; elevations are given in parentheses.

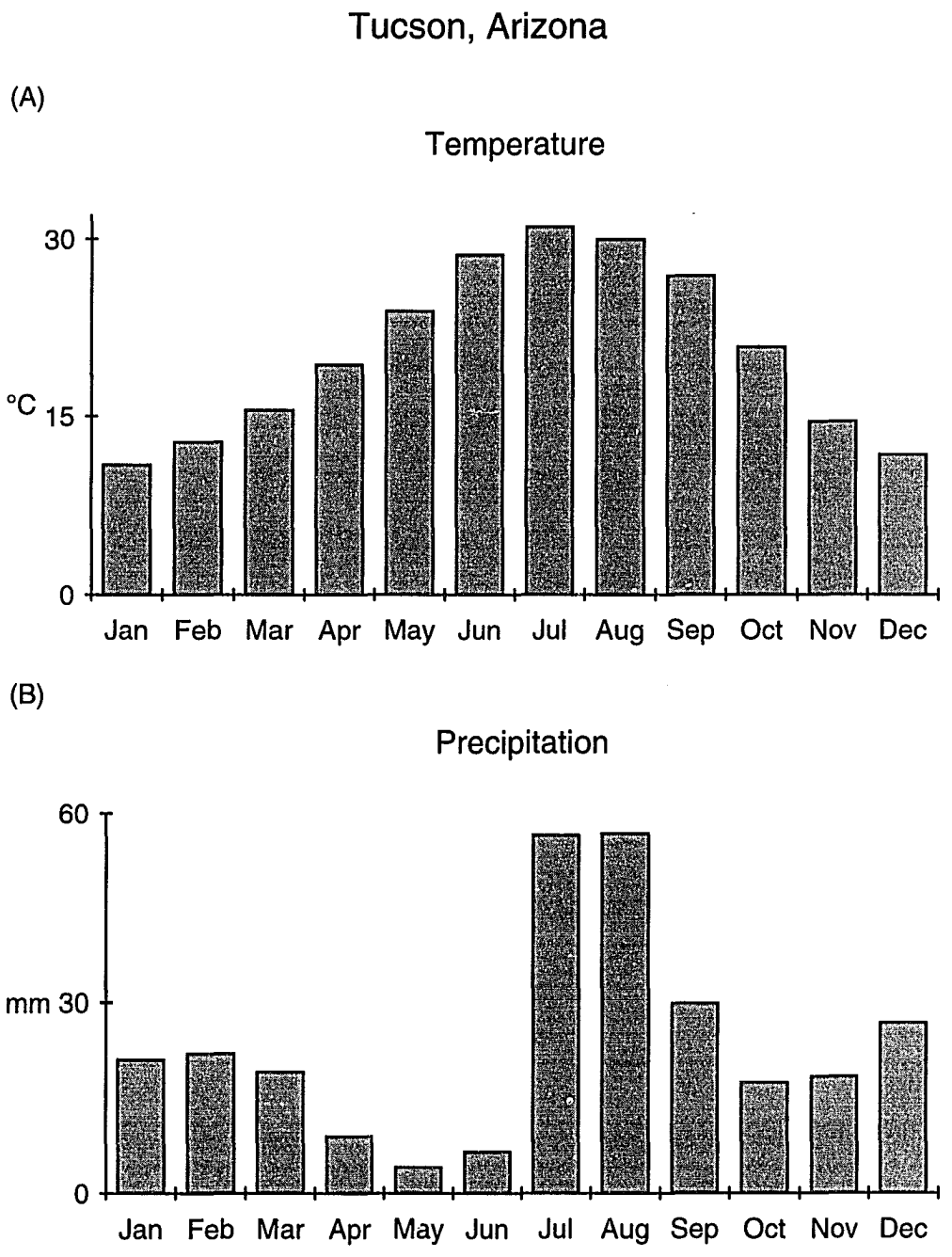

Fig. 7.2. Southeastern Arizona Climatographs: (A) Monthly average temperature and (B) monthly total precipitation for Tucson, Arizona.

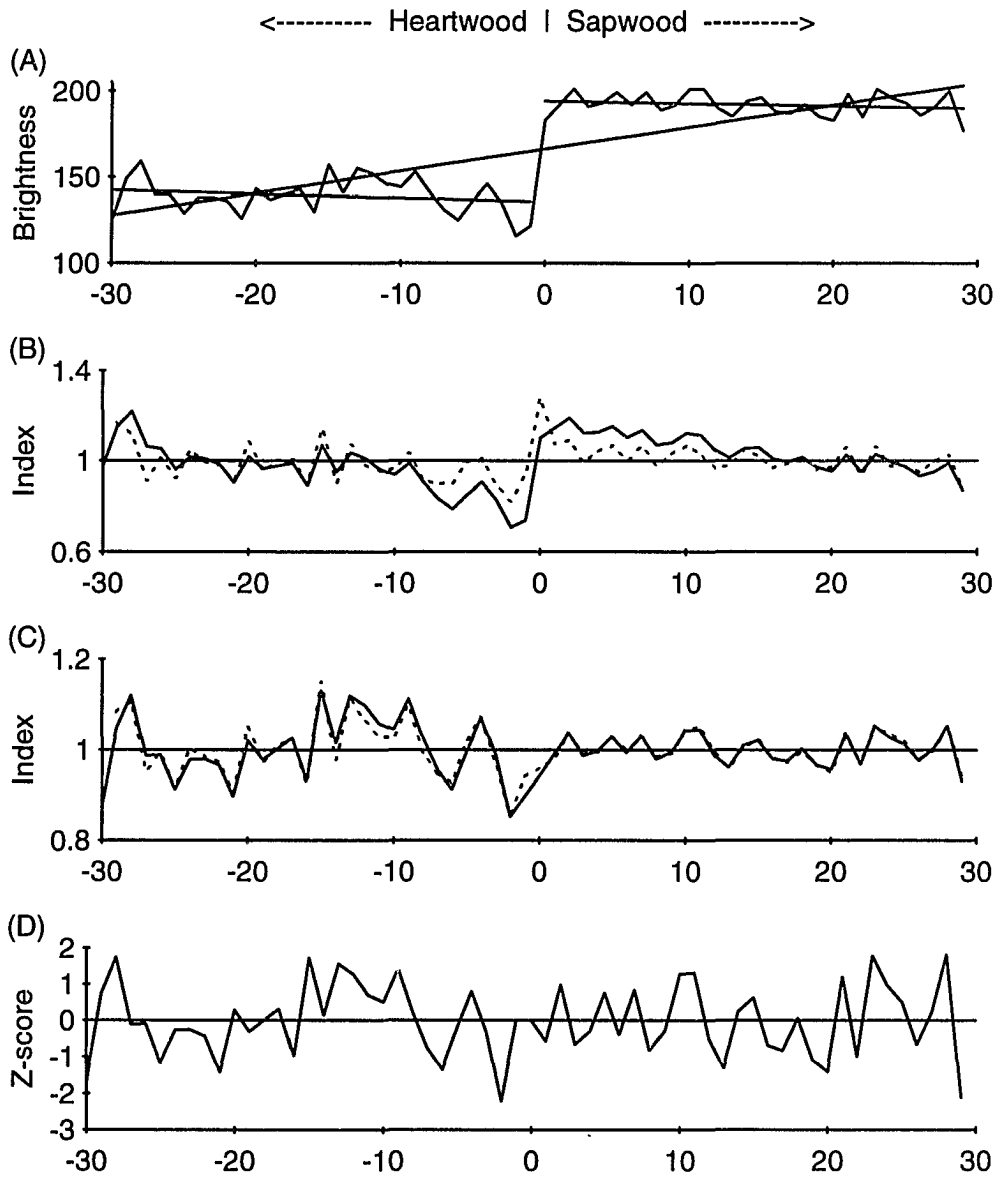

Fig. 7.3. Demonstration of Problem of Extraneous Color Variation: (A) Raw earlywood maximum brightness with trends lines, (B) standard (solid line) and residual (dashed line) indices after removing the full-length trend, (C) standard (solid line) and residual (dashed line) indices after removing split-length trends, and (D) normalized z-scores after removing split-length trends. For all time series, x-axis units are years relative to the heartwood-sapwood boundary, with 30 years measured before and after the boundary.

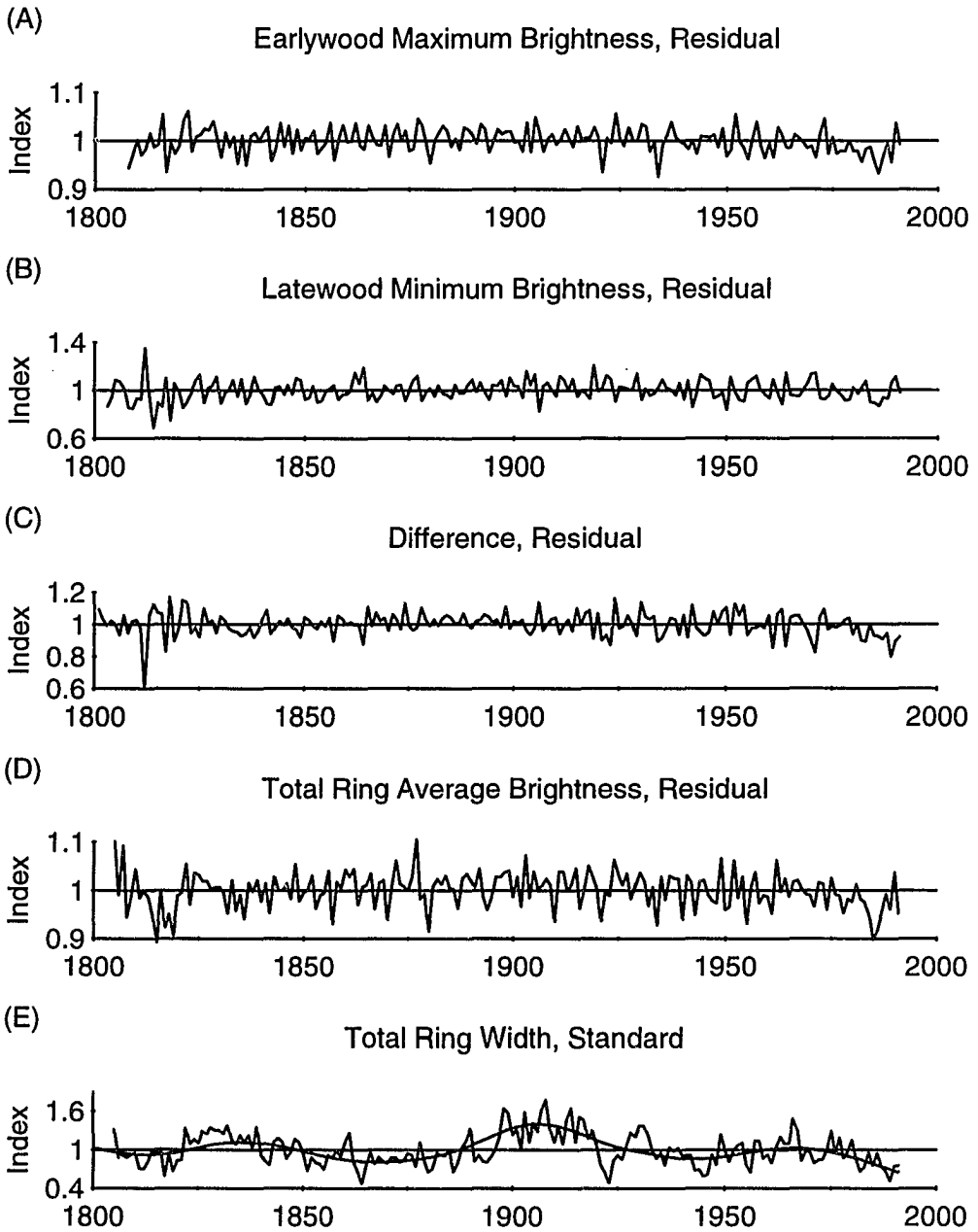

Fig. 7.4. Mica Mountain Full-Length Chronologies: (A) Earlywood maximum brightness, (B) latewood minimum brightness, (C) difference between earlywood and latewood, (D) total ring average brightness, and (E) total ring width with an appropriate cubic smoothing spline.

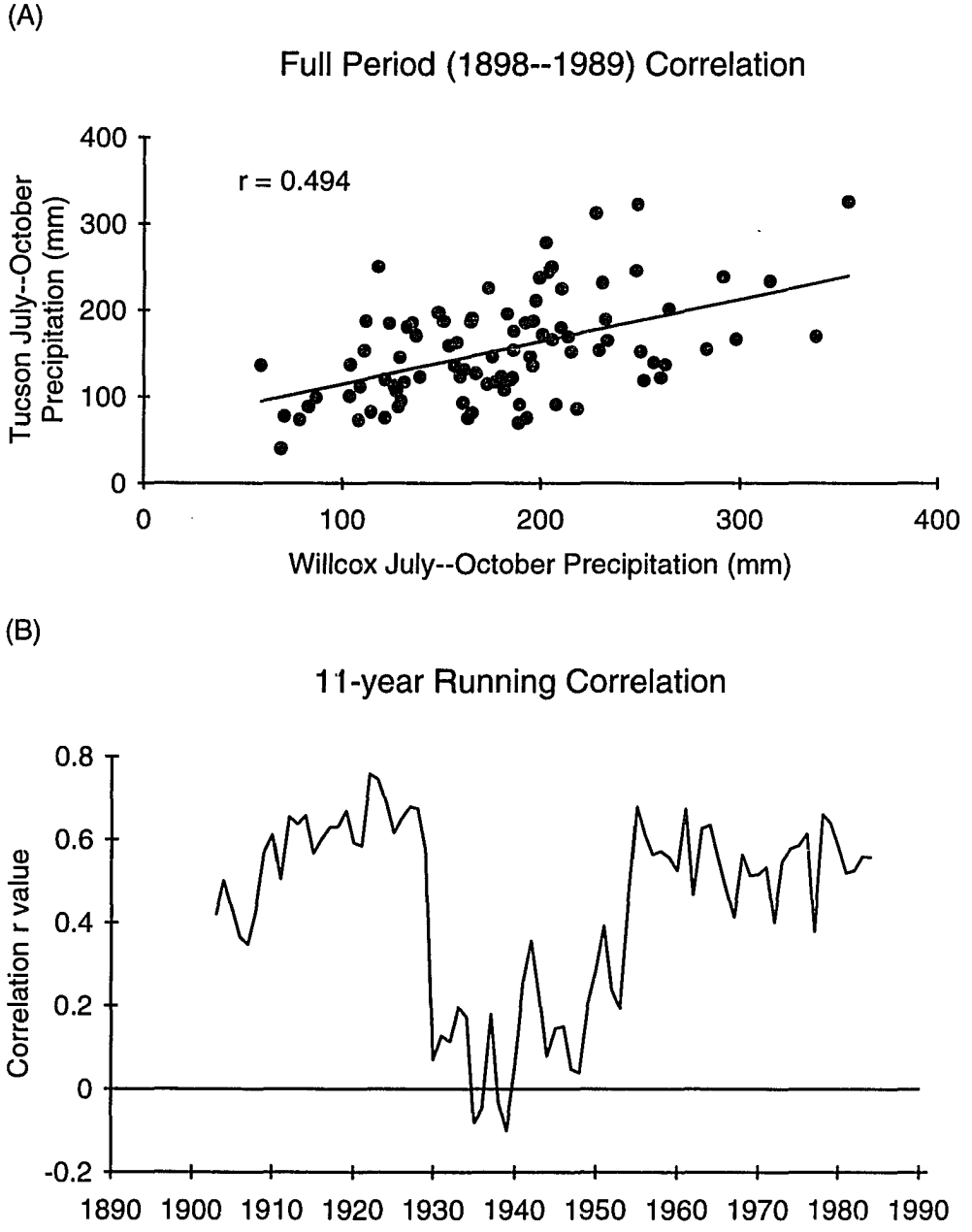

Fig. 7.5. Tucson versus Willcox July--October Precipitation: (A) Full-period (1898--1989) scatter plot and correlation and (B) 11-year running correlation values for July--October total precipitation between Tucson and Willcox.

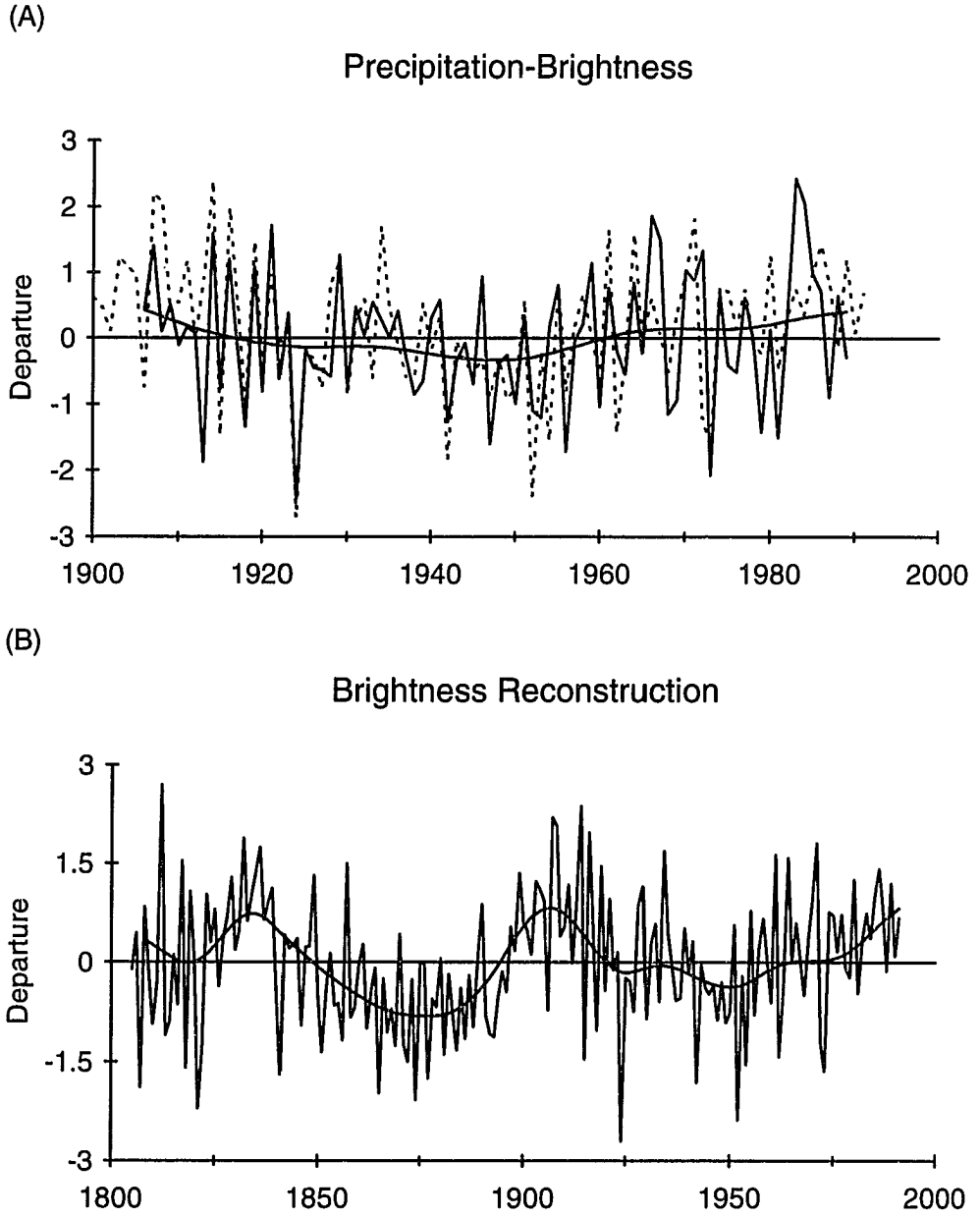

Fig. 7.6. Mica Mountain Climate Model and Reconstruction: (A) Actual with cubic smoothing spline (both solid lines) and predicted (dashed line) July--October precipitation departures, relative to the mean of the entire time period, using EXTRACT-RESIDUAL-FULL chronologies. (B) Reconstruction of precipitation departures with an appropriate cubic smoothing spline.

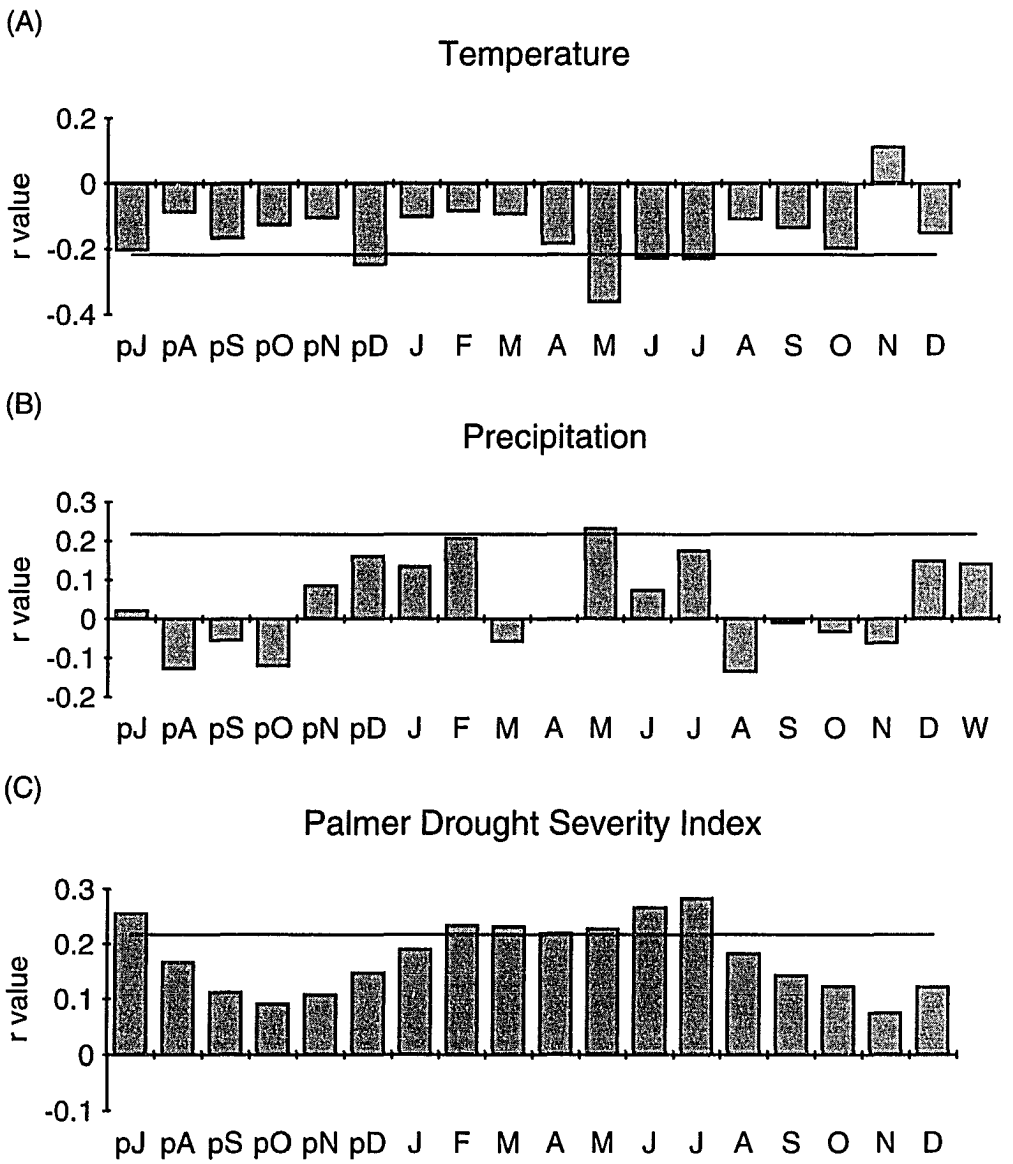

Fig. 7.7. Mica Mountain Total Ring Width Climate Correlations: Product moment *r* values for total ring width of Mica Mountain ponderosa pine and (A) temperature, (B) precipitation, and (C) Palmer Drought Severity Index recorded at Tucson, Arizona. X-axes are months from prior-year July to current-year December; the W for precipitation indicates winter (October--April). For all correlations, the time period is 1906-1989 without 1983, and values exceeding ±0.217 are significant at the 0.05 level.

Table 7.1. Mica Mountain Research Design to Overcome Extraneous Color Variation.

	NONE Preparation	EXTRACT Preparation	BLEACH Preparation
STANDARD Chronology	FULL data / SPLIT data	FULL data / SPLIT data	FULL data / SPLIT data
RESIDUAL Chronology	FULL data / SPLIT data	FULL data / SPLIT data	FULL data / SPLIT data

Table 7.2. Mica Mountain Tree-Ring Correlation Matrix*: Brightness chronologies are from the EXTRACT-RESIDUAL-SPLIT data set.

	Earlywood Brightness	Latewood Brightness	Difference	Total Ring Brightness
Latewood Brightness	0.07			
Difference	0.53	−0.73		
Total Ring Brightness	0.70	0.24	0.23	
Total Ring Width	0.31	−0.03	0.26	0.35

* Critical value is 0.15 for two series, 180 degrees of freedom, and an α level of 0.05.

Table 7.3. Mica Mountain Climate Models Using STANDARD-SPLIT Brightness Chronologies: The total ring width chronology was produced using standard analytical techniques (Fritts 1976). Climate variable is Tucson-Willcox July–October precipitation, with 1983 deleted as an extreme outlier.

NONE

Calibration							Verification		
	Coefficients^				R^2_{adj}*	R^2_{pred}#			
Period	bo	exb	lnb	trw	(%)	(%)	Period	r§	RE¶
1906–1947	23.7	−9.8	10.8	17.3	28.2	16.9	1948–1989	0.41	+0.16
1948–1989	10.1	−10.6	8.1	35.7	19.2	8.1	1906–1947	0.46	+0.06
1906–1989	20.7	−8.7	9.5	20.6	22.6	17.3			

EXTRACT

Calibration							Verification		
	Coefficients^				R^2_{adj}*	R^2_{pred}#			
Period	bo	exb	lnb	trw	(%)	(%)	Period	r§	RE¶
1906–1947	28.2	−12.0	11.2	14.6	30.5	19.0	1948–1989	0.40	+0.09
1948–1989	11.2	−9.7	7.5	34.5	21.5	10.4	1906–1947	0.44	+0.01
1906–1989	24.6	−9.0	8.6	18.0	22.9	16.5			

BLEACH

Calibration							Verification		
	Coefficients^				R^2_{adj}*	R^2_{pred}#			
Period	bo	exb	lnb	trw	(%)	(%)	Period	r§	RE¶
1906–1947	22.6	−10.8	9.7	18.7	16.5	3.1	1948–1989	0.26	+0.03
1948–1989	10.1	−6.1	9.1	30.5	7.9	−7.5	1906–1947	0.39	+0.06
1906–1989	19.4	−5.3	9.2	18.7	11.7	4.2			

^ bo is the intercept, exb and lnb are the slopes of earlywood maximum and latewood minimum brightness, and trw is the slope of total ring width.

* Coefficient of determination, adjusted for loss of degrees of freedom (Draper and Smith 1981).

Prediction coefficient of determination (Montgomery and Peck 1992).

§ Pearson coefficient of correlation between predicted and actual climate. Critical value is 0.30 for 40 degrees of freedom at the 0.05 level (Rohlf and Sokal 1980).

¶ Reduction of error statistic (Fritts et al. 1990).

Table 7.4. Mica Mountain Climate Models Using RESIDUAL-SPLIT Brightness Chronologies: The total ring width chronology was produced using standard analytical techniques (Fritts 1976). Climate variable is Tucson-Willcox July–October precipitation, with 1983 deleted as an extreme outlier.

NONE

Calibration							Verification		
	Coefficients^				R^2_{adj}*	R^2_{pred}#			
Period	bo	exb	lnb	trw	(%)	(%)	Period	r§	RE¶
1906–1947	29.3	−10.7	9.4	13.5	31.2	21.1	1948–1989	0.43	+0.18
1948–1989	16.8	−16.9	5.8	37.4	27.5	19.7	1906–1947	0.48	−0.05
1906–1989	29.0	−12.9	7.0	18.5	26.1	21.9			

EXTRACT

Calibration							Verification		
	Coefficients^				R^2_{adj}*	R^2_{pred}#			
Period	bo	exb	lnb	trw	(%)	(%)	Period	r§	RE¶
1906–1947	31.8	−13.8	10.8	12.6	39.2	28.7	1948–1989	0.38	+0.09
1948–1989	21.7	−13.6	4.0	30.4	21.0	10.8	1906–1947	0.49	+0.11
1906–1989	31.0	−12.7	6.7	16.7	26.6	21.8			

BLEACH

Calibration							Verification		
	Coefficients^				R^2_{adj}*	R^2_{pred}#			
Period	bo	exb	lnb	trw	(%)	(%)	Period	r§	RE¶
1906–1947	31.3	−13.8	9.0	14.0	24.0	9.8	1948–1989	0.20	−0.05
1948–1989	19.9	−7.8	5.2	25.9	4.2	−9.2	1906–1947	0.40	+0.09
1906–1989	26.8	−8.0	7.2	15.6	12.0	5.5			

^bo is the intercept, exb and lnb are the slopes of earlywood maximum and latewood minimum brightness, and trw is the slope of total ring width.

* Coefficient of determination, adjusted for loss of degrees of freedom (Draper and Smith 1981).

Prediction coefficient of determination (Montgomery and Peck 1992).

§ Pearson coefficient of correlation between predicted and actual climate. Critical value is 0.30 for 40 degrees of freedom at the 0.05 level (Rohlf and Sokal 1980).

¶ Reduction of error statistic (Fritts et al. 1990).

Table 7.5. Mica Mountain Climate Models Using Difference and Total Ring Average Brightness Chronologies: Brightness chronologies are from the EXTRACT-RESIDUAL data set. The total ring width chronology was produced using standard analytical techniques (Fritts 1976). Climate variable is Tucson-Willcox July–October precipitation, with 1983 deleted as an extreme outlier.

SPLIT

Calibration							Verification		
	Coefficients^				R^2_{adj}*	R^2_{pred}#			
Period	b_0	dif	trb	trw	(%)	(%)	Period	r§	RE¶
1906–1947	47.1	−13.1	−7.5	14.6	46.0	38.9	1948–1989	0.41	+0.06
1948–1989	23.8	−9.2	−6.2	35.0	24.1	14.8	1906–1947	0.53	+0.11
1906–1989	38.4	−10.1	−5.1	18.5	29.9	25.4			

FULL

Calibration							Verification		
	Coefficients^				R^2_{adj}*	R^2_{pred}#			
Period	b_0	dif	trb	trw	(%)	(%)	Period	r§	RE¶
1906–1947	211	−97	−88	16	45.0	37.5	1948–1989	0.43	+0.13
1948–1989	165	−71	−86	34	23.3	14.8	1906–1947	0.56	+0.19
1906–1989	173	−79	−73	20	31.2	27.4			

^ b_0 is the intercept, dif is the slope of the difference (earlywood maximum minus latewood minimum brightness), and trb and trw are the slopes of total ring average brightness and total ring width.

* Coefficient of determination, adjusted for loss of degrees of freedom (Draper and Smith 1981).

\# Prediction coefficient of determination (Montgomery and Peck 1992).

§ Pearson coefficient of correlation between predicted and actual climate. Critical value is 0.30 for 40 degrees of freedom at the 0.05 level (Rohlf and Sokal 1980).

¶ Reduction of error statistic (Fritts et al. 1990).

8. PAST GEOMORPHOLOGICAL EVENTS OF NORTHEASTERN CALIFORNIA USING REFLECTED-LIGHT IMAGE ANALYSIS OF CONIFERS OF STEPHENS PASS

INTRODUCTION

Among published studies using tree-ring techniques to the study of past earthquakes (e.g., see references in Sheppard and White 1995), only one study has noted a change in ring density due to an earthquake. Following the 1811–1812 earthquake at New Madrid, Missouri, baldcypresses (*Taxodium distichum* (L.) Rich.) growing in Tennessee responded with decreased latewood density in addition to increased ring-width (Stahle et al. 1992).

An opportunity arose to investigate an additional latewood brightness response to a past earthquake when, during the first half of August, 1978, a swarm of 200+ earthquakes occurred at Stephens Pass, California (41° 27' N, 121° 52' W, 1510 m elevation; Fig. 8.1). Although none of the earthquakes was large–the maximum magnitude was 4.6–they dropped a series of grabens that average 4.5 m in width, extend up to 3 m in depth, and occur intermittently along a 2-km-long rupture zone (Bennett et al. 1979). The formation of this graben series killed or otherwise affected many trees growing in or immediately adjacent to the rupture zone (e.g., see photos 2, 3, and 4 of Bennett et al. 1979). In addition to ring-width responses to this earthquake, one sampled red fir (*Abies magnifica* A. Murr.) responded with an apparent change in latewood brightness. To quantify this brightness response, I image analyzed the core samples from this tree (Sheppard and White 1995).

METHODS

Site Characteristics

Stephens Pass, northeastern California, is within the Modoc Plateau geologic province of Mesozoic metasedimentary and metavolcanic rocks (Gardner 1964) overlain by late Cenozoic basaltic flows and interbedded fluvial-lacustrine deposits. The Modoc Plateau province is transitional between the Cascade Range and the Basin and Range provinces (Saucedo et al. 1990; Grose et al. 1990). The present physiography of northeastern California reflects Quaternary normal faulting (Gardner 1964; Page et al. 1987). Soils are complexly textured (medial over loamy-skeletal), cool (frigid soil temperature regime) Andisols that are moderately deep with a paralithic contact deeper than 1 m below the surface (United States Forest Service, no date).

As typified by the meteorological record at Mt. Shasta, California (41° 19' N, 122° 19' W, 1094 m elevation, 24 km southwest of and 420 m lower than Stephens Pass; Fig. 8.1), northeastern California has a mean annual air temperature of 10°C, a maximum mean monthly temperature of 20°C in July, and a minimum mean monthly temperature of 1°C in January (Fig. 8.2A). Annual precipitation totals 919 mm, most of which comes during winter as snowfall (Fig. 8.2B).

The Modoc Plateau supports a montane mixed conifer forest that has white fir and incense-cedar (*Calocedrus decurrens* (Torr.) Florin) on mesic sites, ponderosa pine on north-facing slopes, and Jeffrey pine (*Pinus jeffreyi* Grev. and Balf.) on all aspects (Rundel et al. 1977). Other overstory trees include red fir, lodgepole pine (*Pinus contorta* Dougl. ex Laws), and western juniper (*Juniperus occidentalis* Hook.). Understory vegetation includes mountain-mahogany (*Cercocarpus* HBK), buck-brush, and sagebrush (*Artemisia* L.). Ground cover includes several grasses.

Field Sampling, Sample Preparation, and Dating

Between 1987 and 1992, tree-ring samples were collected from dominant or codominant white or red firs or Jeffrey, lodgepole, or ponderosa pines located in and around the Stephens Pass rupture zone. Two increment cores were collected per living tree as well as cross-sections from stumps of trees that were harvested in late 1990. Sampled trees located in, or immediately adjacent to, the rupture zone could have been affected by the 1978 event, so these trees were designated as event-response trees (Shroder and Butler 1987). Sampled trees located well away from the rupture zone probably could not have been affected by the 1978 event, so these trees were designated as control trees.

Using standard procedures for preparing tree-ring samples (Swetnam et al. 1985, Holmes et al. 1986), I air dried, mounted, and sanded all cores and cross-sections to expose a clear transverse sectional view. I matched patterns of relatively wide and narrow rings across samples to identify and compensate for missing or intra-annual rings (Stokes and Smiley 1968); such ring-growth anomalies were not prevalent in the Stephens Pass collection. Knowing the date of the last-formed ring of each sample, I then assigned a calendar year to each annual tree ring. Samples or segments of samples that could not be confidently dated were excluded from further analysis.

Using a computer-based incremental measuring system (Robinson and Evans 1980), I measured ring widths of all samples to the nearest 0.01 mm. Additionally, using reflected-light imaging analysis, I measured ring brightness in one particular event-response tree that exhibited density variation. From the intra-ring brightness scan, I extracted annual series of brightness and width for earlywood and latewood, which were analytically treated identically to the event-response ring-width series.

I checked all ring width and brightness series for dating and/or measuring errors by cross-correlating prewhitened measurement series with their respective mean-value series (Holmes 1983; Holmes et al. 1986). All identified dating and measuring errors were corrected. I verified the dating of the Stephens Pass ring-width control chronology by matching it with the nearby Grizzly Peak (41° 10' N, 122° 02' W), Black Cone (41° 11' N, 120° 07' W), and Greenville Saddle (40° 13' N, 122° 55' W) ponderosa pine ring-width chronologies (Graumlich 1987).

Data Reduction and Analysis

To correct for the normal decrease in ring widths as trees grow larger in diameter, I removed series-length growth trends from ring-width series of control trees by dividing raw values by fitted values from negative-exponential curves or straight lines as estimated using iterative least squares regression (Fritts et al. 1969). For each sample, this step resulted in dimensionless index series, which I averaged together into a standard chronology (Fritts 1976).

I also removed series-length growth trends from ring-width series of event-response trees similarly to the control trees, but the growth trend for each event-response series was estimated using data from the time period up to and including 1978. The growth trend was then extended through the remaining period of the sample (Mutch 1994). I visually compared event-response ring-width index series to the control chronology to identify anomalous ring-width departures that could be ascribed to the 1978 earthquake at Stephens Pass.

I removed series-length trends from brightness series using only straight lines as estimated using ordinary least squares regression, but the growth trend for each event-response series was estimated using data from the time period up to and including 1978. The growth trend was then extended through the remaining period

of the sample (Mutch 1994). I visually compared brightness for rings up to and including 1978 with that for rings since 1979 to identify anomalous brightness departures that could be ascribed to the 1978 earthquake at Stephens Pass.

RESULTS

Ring-Width Evidence

Although several of the sampled trees germinated during the 1800s, the adequately replicated part of the Stephens Pass control chronology extends from 1910 to 1990 with a maximum replication of 20 cores from 10 trees (Fig. 8.3, upper left). Trees in this area are sensitive to winter drought and therefore this chronology expresses variation in past precipitation (Graumlich 1987).

Although the Stephens Pass control chronology has a below-average value for 1979, it does not show an obviously anomalous growth pattern since 1978 (Fig. 8.3, upper left). Thus, this chronology represents coniferous tree-growth patterns across a wide region and serves as a control for expected tree growth (Sheppard and Jacoby 1989), i.e., how event-response trees at Stephens Pass should have grown in the absence of a disturbance such as the 1978 earthquake. Compared to the Stephens Pass control chronology, nine event-response trees show anomalously narrow ring widths beginning in 1979 and continuing for most of the remaining periods of the samples (Fig. 8.3, Trees 1-9).

Latewood Brightness Evidence

The event-response tree that was analyzed for ring brightness does not show an anomalous change in latewood brightness, i.e., latewood density (Fig. 8.4A). By contrast, this tree shows anomalously wide latewood, as a percentage of total ring width, beginning in 1979 and continuing for the remaining periods of the samples (Fig. 8.4B). This response is stronger in radius #2 than in radius #1.

DISCUSSION

The 1978 earthquake at Stephens Pass was unique in that it caused tree-ring responses despite its moderate magnitude and small rupture zone. All other documented examples of tree-growth responses to earthquakes involved large or great earthquakes with large rupture zones. In general, dendrochronological techniques can be applied to studies of any earthquake, regardless of magnitude or rupture zone, that results in ground-surface deformation or movement.

The 1978 earthquake at Stephens Pass was uncommon in that it caused a ring-density response (Fig. 8.4) in addition to a ring-width response (Fig. 8.3). As approximated using brightness, the density response at Stephens Pass was not a change in latewood density *per se*, but rather it was a substantial increase in the amount of latewood relative to the entire ring; this response gave the appearance of a change in density. It is puzzling that only one sampled tree responded to the earthquake with a change in relative amounts of latewood; this is probably an indirect response to a microsite change in available soil water. By quantifying this density response using reflected-light image analysis, I have demonstrated the general utility and potential for applying imaging techniques to tree-ring applications other than climatology.

These ring-width and ring-density changes constitute an example of tree-ring responses to a normal-fault earthquake within the intraplate Basin and Range. This example complements other cases of tree-growth responses to earthquakes of strike-slip (Page 1970; LaMarche and Wallace 1972; Wallace and LaMarche 1979; Meisling and Sieh 1980; Jacoby et al. 1988) and thrust tectonic settings (Jacoby and Ulan 1983; Sheppard and Jacoby 1989; Atwater and Yamaguchi 1991; Stahle et al. 1992). This addition to the list of dendrochronological studies of past earthquakes

further indicates that tree-ring dating should be considered as a complement to other geological dating techniques wherever possible (Ruzhich et al. 1982).

This example of tree-ring responses to intraplate, normal faulting at Stephens Pass has implications for dendrochronologically studying geomorphological events at Medicine Lake Highlands (41° 35' N, 121° 36' W; Fig. 8.1), a nearby collapsed shield volcano located northeast of Stephens Pass. Medicine Lake is located at the intersection of many northwest- and north-trending normal faults with east-west extension (Donnelly-Nolan 1990; Dzurisin et al. 1991), and it has an elliptical ring of several vents and domes around its caldera rim. Various types of geological evidence, including obsidian hydration dates of lava flows, radiocarbon dates of pumice tephras, and historical documents, indicate that this site has been volcanically active during the past 1000 years (Kilbourne and Anderson 1981). However, estimated dates of some Medicine Lake volcanic eruptions over the past 1000 years are not determined well enough to be confidently resolved from one another because of the level of uncertainty associated with radiocarbon dating of volcanic deposits (Donnelly-Nolan et al. 1990).

It is likely that Medicine Lake has also been seismically active over the past 1000 years. Extensional tectonism appears to be spatially linked to volcanism at Medicine Lake, as vents are aligned parallel to subparallel to the many normal faults of the area (Donnelly-Nolan et al. 1990; Dzurisin et al. 1990). High-precision dating of volcanic and seismic events is needed to discern the extent and nature of a temporal relation between these two geomorphological processes at Medicine Lake. Just as dendrochronological techniques are useful for studying past earthquakes, these same techniques are useful for studying past volcanic eruptions (Brantley et al. 1986). Complementing other dating techniques with annually resolved tree-ring

dating of past geologic events at Medicine Lake would help in evaluating the hypothesis that tectonism and volcanism are linked to such an extent that some earthquakes with ground deformation are accompanied by eruption of lava (Dzurisin et al. 1991).

Fortuitously, Medicine Lake supports a forest of several coniferous tree species, including white and red firs, western juniper, incense-cedar, and lodgepole, Jeffrey, ponderosa, and sugar (*Pinus lambertiana* Dougl.) pines. These species have been widely used in dendrochronology because they all date strongly, i.e., trees within a region exhibit synchronous patterns of wide and narrow annual rings (Grissino-Mayer 1995). In addition, each of these species is potentially long-lived, having trees that can live for hundreds of years or, in some cases, up to 1000 years.

Given that this resource of trees exists in an area of active tectonism and volcanism, questions about the temporal and spatial relation between these processes justify applying dendrochronological techniques, along with other geological techniques, for studying past volcanic and seismic events at Medicine Lake. This study, in which I have documented and described tree-growth responses—including a latewood brightness response, as quantified using reflected-light image analysis—to the 1978 normal-fault earthquake at Stephens Pass, serves as a specific calibration example for dendrochronologically studying prehistoric eruptions and earthquakes at Medicine Lake Highlands.

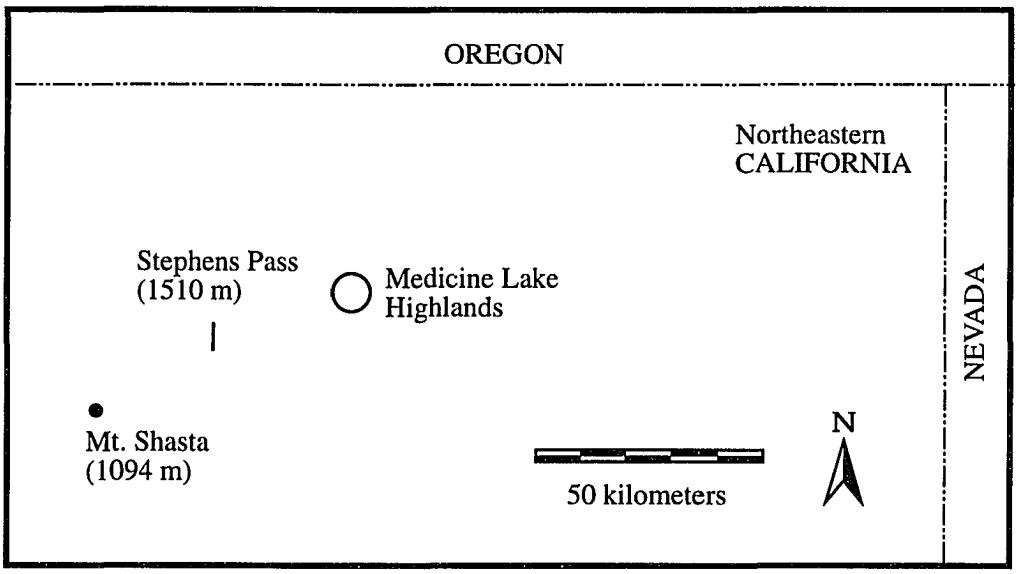

Fig. 8.1. Map of Northeastern California: The Stephens Pass rupture zone is marked with a north-south line, the Mt. Shasta meteorological station is marked with a closed circle, and the Medicine Lake Highlands is marked with an open circle; elevations are given in parentheses.

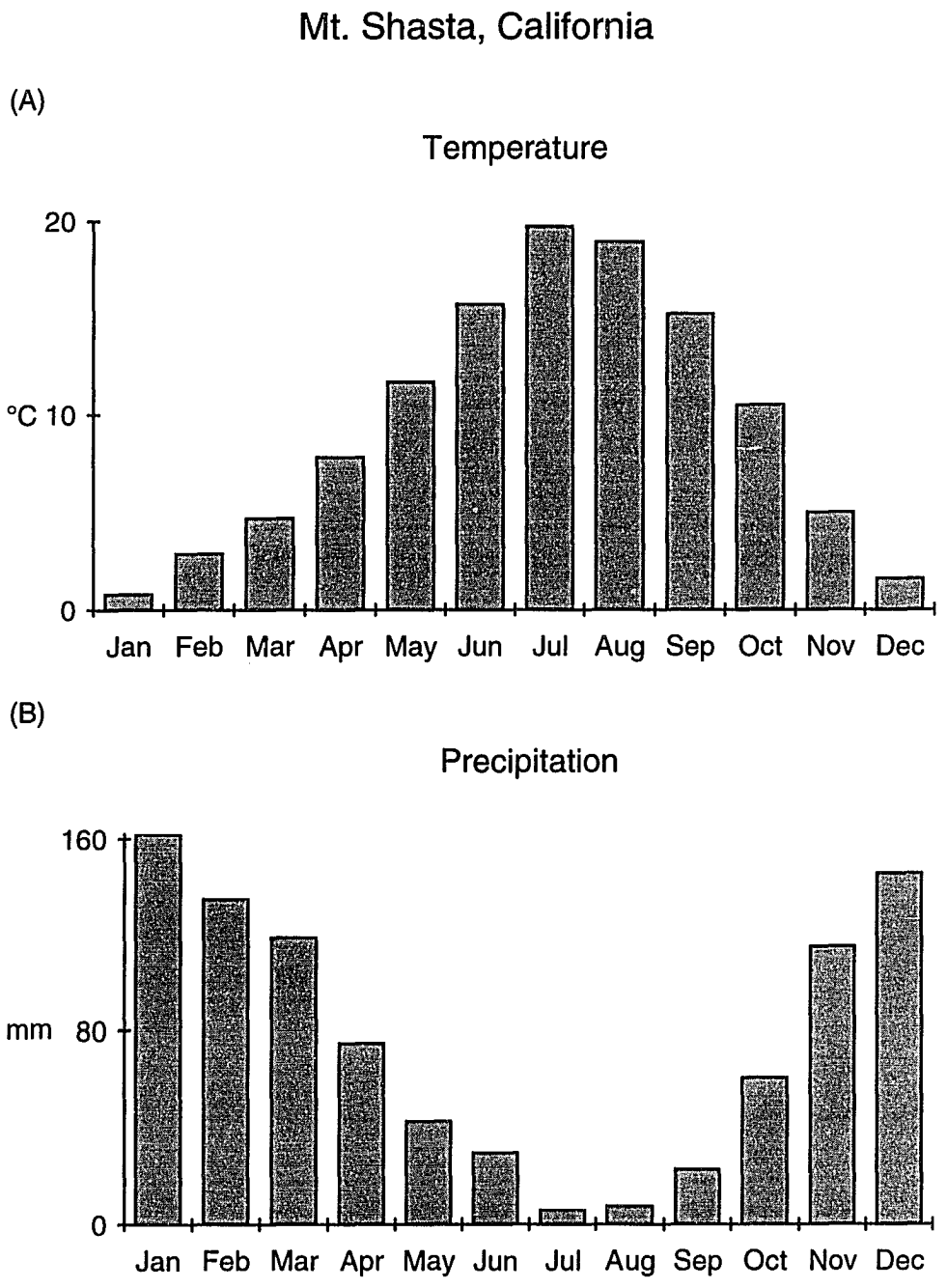

Fig. 8.2. Northeastern California Climatographs: (A) Monthly average temperature and (B) monthly total precipitation for Mt. Shasta, California.

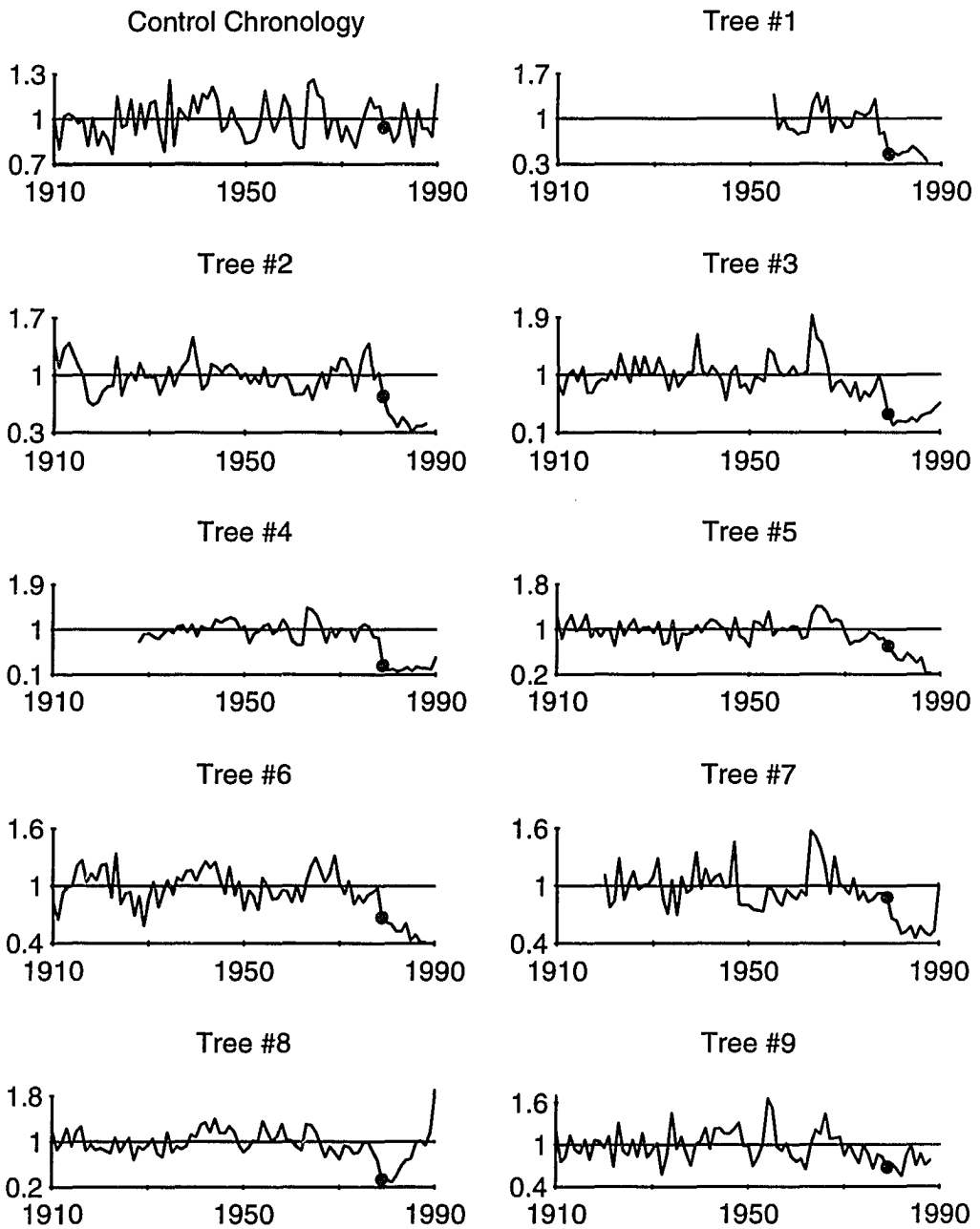

Fig. 8.3. Ring Width Response to 1978 Stephens Pass Earthquake: Stephens Pass control chronology (upper left) and index series of nine event-response trees. Solid circles indicate 1979 values, and all y-axis units are dimensionless indices.

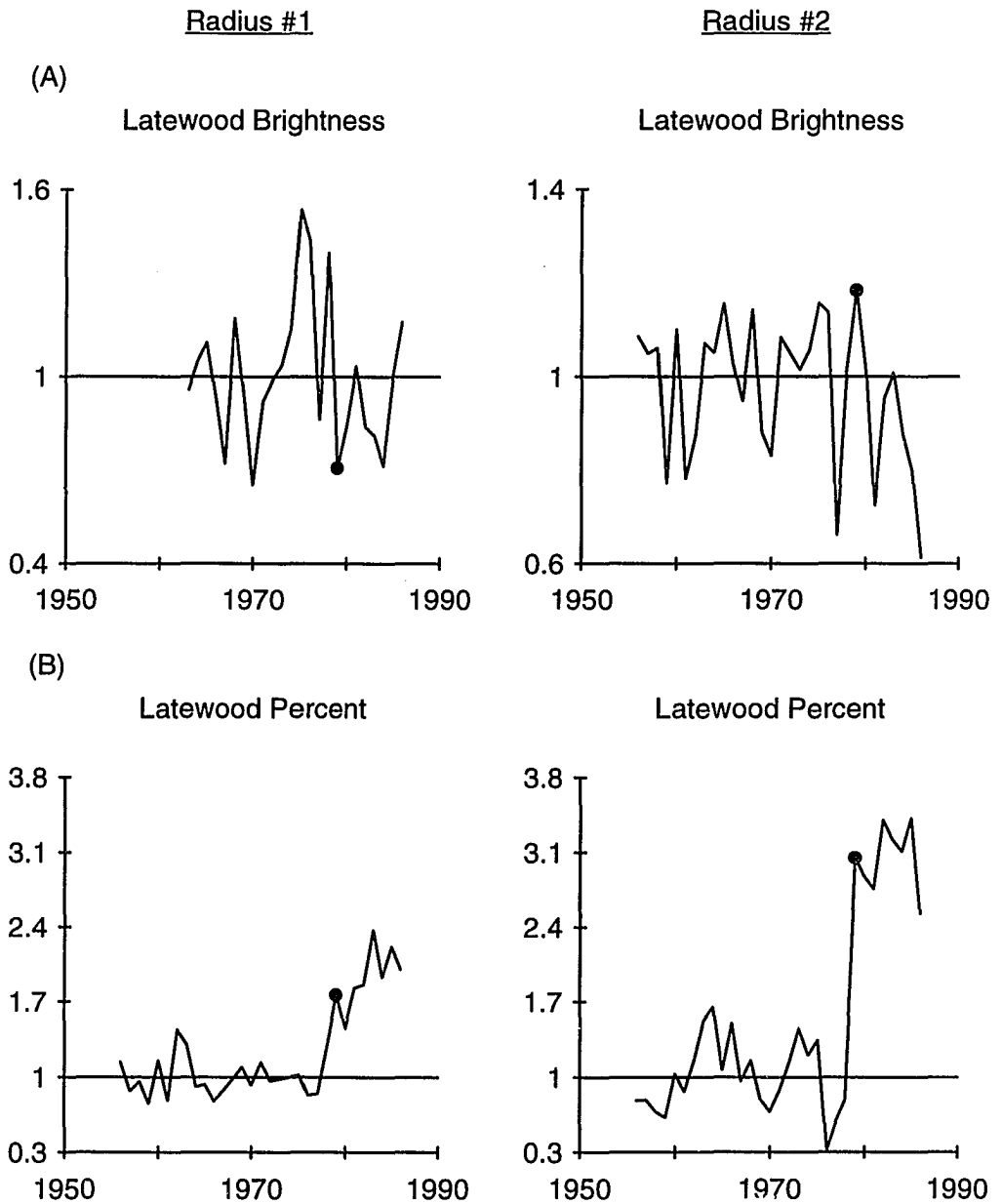

Fig. 8.4. Brightness Response to 1978 Stephens Pass Earthquake: (A) Latewood brightness and (B) latewood width as a percentage of total ring width for both radii of one tree at Stephens Pass. Solid circles indicate 1979 values, and all y-axis units are dimensionless indices.

9. IDENTIFICATION OF LOW-FREQUENCY VARIATION IN TREE-RING DATA

INTRODUCTION

Dendrochronological research is replete with studies that, in part, identify and interpret low-frequency variation (period length > 10 years) in tree-ring chronologies (LaMarche 1974; Jacoby et al. 1985; Norton et al. 1989; Briffa et al. 1990). A common approach to identifying low-frequency tree-ring variation is (1) to construct a standard chronology using several samples from a homogeneous stand of trees (Fritts 1976), (2) to generate a smoothed index series from that standard chronology, e.g., with a cubic smoothing spline (Cook and Peters 1981), and (3) to overlay the standard chronology with its smoothed index series. Trends in low-frequency variation, i.e., departures from a reference line, are commonly interpreted as responses to biological or physical events.

As stated, this common approach has two inadequacies that arise from the fact that the smoothed index series is generated from only a single time series. First, the smoothed index series does not have accompanying confidence intervals with which trends might be evaluated as being significant or important. Second, the smoothed index series does not reflect changing sample depth through time, even though sample depths of tree-ring chronologies range from as low as a single sample at the beginning year to a maximum value, commonly >20 trees, sometime before the ending year. While it is tempting to interpret low-frequency trends for the full length of a chronology, there should be some distinction between well-replicated portions of a chronology, where low-frequency variation is robustly estimated, and poorly replicated portions of a chronology, where low-frequency variation is weakly estimated (Shiyatov et al. 1990).

To overcome these two inadequacies, I propose a method of re-ordering the individual steps commonly used in constructing tree-ring chronologies. This method provides approximate 95% confidence intervals for a chronology of low-frequency variation so that a level of significance or importance for trends may be inferred, and it visually reveals the portions of a chronology where sample depth is so poor that low-frequency variation is not robustly estimated, i.e., when the mean value is significantly affected by the addition or deletion of a single sample. Because this method is merely a re-ordering of the individual steps commonly used in constructing tree-ring chronologies. Consequently, this method is computationally simple for researchers who already routinely construct standard tree-ring chronologies, especially for those who have access to the library of data-reduction programs compiled under the auspices of the International Tree-Ring Data Bank, of the National Geophysical Data Center. The secondary objective for this dissertation research is to demonstrate this method for identifying low-frequency variation of tree-ring chronologies and/or past climate as reconstructed using tree-rings.

METHODS

Chronologies: Coddington Lake, Northern Minnesota

To illustrate this method of identifying low-frequency tree-ring variation, I applied it to a tree-ring collection of ring-width series from white oak (*Quercus alba* L.) growing at Coddington Lake, Minnesota (47° 44' N, 94° 03' W, 128 m). The standard chronology from this site exhibits strong low-frequency variation (Sheppard 1991), which makes it useful for illustrating this method.

As illustrated using ring-width data of white oak growing at Coddington Lake, identifying low-frequency tree-ring variation begins with constructing a standard index chronology using conventional steps (Table 9.1, left column; Fritts 1976). I

removed series-length growth trends from ring-width series as previously described. This step purposely removed variation at frequencies longer than the fundamental frequency of 1/n, where n is the series length (Cook et al. 1995); frequencies longer than the series length are difficult to interpret with respect to causal mechanisms because they can not be differentiated from pure trend (Cook et al. 1990). I then averaged the standard index series into a chronology.

Determining the frequency of interest can be accomplished using various strategies. Researchers may hypothesize *a priori* the existence of a specific causal mechanism, with a known frequency of variation, that might affect tree growth; examples of such mechanisms include regimes of periodic wildfire, cyclic budworm infestations, or any of the solar cycles that might affect climate. In these cases, researchers have predetermined the frequency of variation that is pertinent to their study.

Lacking an *a priori* hypothesis, researchers can use the standard chronology itself to determine the frequency of variation to analyze. If a chronology expresses a sine wave pattern, then the peak frequency can be determined using spectral analysis (Mazepa 1990), which I used for the Coddington Lake oak site. I then generated a smoothed index series to represent that frequency by fitting the appropriate cubic smoothing spline to the standard chronology. Specifically, I fit the spline with a frequency response retention of 90% of the frequency of interest. Lastly, I overlaid the spline series with the standard chronology.

As its name implies, the re-ordered approach uses the same steps used to construct the standard chronology, but those steps are executed in a slightly different order (Table 9.1, right column). As a result of having constructed the standard chronology, the index series were already created and the pertinent frequency of

variation was already determined. I generated smoothed index series to represent that frequency by fitting to all standard index series the same cubic smoothing spline that was used on the standard chronology. By fitting the spline to all index series, each year of the chronology had a distribution of smoothed index values. I then averaged the smoothed index values for each distribution, i.e., for each year of the chronology, and thereby created a chronology of low-frequency variation.

An important benefit of the fact that each year of the chronology had a distribution of smoothed index values is the ability to estimate confidence intervals around the chronology of low-frequency variation. One method for estimating confidence intervals around tree-ring data is bootstrap sampling of the distributions of values for up to hundreds—or even thousands—of times, as demonstrated by Cook (1990) for smoothed ring-width chronologies. Cook opted for bootstrap estimation of confidence intervals primarily because distributions of smoothed ring-width values may not be normal.

However, a benefit of converting ring-width series into index series is that distributions of smoothed index values are not likely to violate the assumption of normality. Consequently, I opted to estimate confidence intervals by using the common parametric equation (Sokal and Rohlf 1981), which is computationally less arduous than bootstrap estimation. Thus, I calculated 95%-confidence intervals as follows:

$$95\%\text{-confidence interval}_t = \bar{x}_t \pm se_{\bar{x}(t)} \cdot t_{0.05[d.f.(t)]}$$

where $\bar{x}_t$ is the mean smoothed index value of the t^{th} year, $se_{\bar{x}(t)}$ is the standard error of the mean of the t^{th} year, and $t_{0.05[d.f.(t)]}$ is the critical value of the Student's t distribution for $\alpha = 0.05$ and degrees of freedom (sample depth − 1) of the t^{th} year (Rohlf and Sokal 1981). Lastly, I overlaid the low-frequency chronology and its

associated 95% confidence intervals with the standard chronology.

Reconstructions: Mica Mountain, Southeastern Arizona

Analyzing variation in tree-ring chronologies is not usually the ultimate goal of dendrochronological research. Rather, researchers seek to analyze and understand variation in environmental factors that cause tree growth to vary. Accordingly, I applied this method of identifying low-frequency variation to past July–October precipitation as reconstructed using tree-ring chronologies of brightness and width variables from ponderosa pines growing on Mica Mountain.

The logic of identifying low-frequency variation in tree-ring chronologies can be extended one level to identify low-frequency variation of paleoenvironmental reconstructions, such as the climate reconstruction from using reflected-light image analysis to study the Mica Mountain tree-ring site. I began by reconstructing climate using conventional steps (Table 9.2, left column; Cook and Kairiukstis 1990), as described in Chapter 7 of this dissertation. I calibrated and verified the climate-precipitation model and used it to reconstruct past climate. Using spectral analysis, I determined the prominent frequency of the full reconstruction.

I Identified low-frequency variation of the precipitation reconstruction using four additional steps (Table 9.2, right column). I evaluated the climate-tree growth model for each individual sample of the tree-ring collection. I then fit the appropriate cubic smoothing spline to highlight the frequency of interest for all individual-sample reconstructions and averaged those splines into a low-frequency reconstruction. As previously described, for each year of the reconstruction I calculated the 95% confidence interval and then overlaid that interval with the low-frequency reconstruction.

RESULTS

The Coddington Lake oak standard chronology clearly expresses low-frequency variation (Fig. 9.1A). The prominent frequency of variation in this standard chronology is at 74 years (Fig. 9.2), which I highlighted with the appropriate cubic smoothing spline (Figure 9.1A). The low-frequency chronology (Figure 9.1B) is similar to the spline generated from the standard chronology (Figure 9.1A); differences between these two smoothed series are restricted to early decades of the chronology.

However, the low-frequency chronology and its 95% confidence intervals permit visual identification of important low-frequency tree-ring variation (Figure 9.1B). Negative departures of 1825–1855 and 1890–1935 are significant and worthy of interpretation, as are positive departures of 1855–1890 and of 1935–1980. Because of the erratic nature of the low-frequency chronology and its wide 95% confidence intervals prior to 1820 (Figure 9.1B), low-frequency variation is not robustly estimated during the chronology's first 50 years, primarily due to poor sample depth (Figure 9.1C). It would not be prudent to interpreting low-frequency variation prior to 1820 of this chronology.

The Mica Mountain July–October precipitation reconstruction clearly expresses low-frequency variation (Fig. 9.3A). The prominent frequency of variation in this standard chronology is at 54 years (Fig. 9.4), which I highlighted with the appropriate cubic smoothing spline (Figure 9.3A). The low-frequency chronology (Figure 9.3B) is similar to the spline generated from the reconstruction (Figure 9.3A); differences between these two smoothed series are restricted to early decades of the reconstruction.

However, the low-frequency reconstruction and its 95% confidence intervals

permit visual identification of important low-frequency July–October precipitation variation (Figure 9.3B). The negative departure of 1850–1890 is significant and worthy of interpretation. Because of the erratic nature of the low-frequency reconstruction and its wide 95% confidence intervals prior to 1850 (Figure 9.3B), low-frequency variation is not robustly estimated during the reconstruction's first 50 years, primarily due to poor sample depth (Figure 9.3C). It would not be prudent to interpret low-frequency variation prior to 1850 of this reconstruction.

DISCUSSION

The slight flaring of the 95%-confidence intervals in the late part (after 1970) of the Coddington Lake chronology (Fig. 9.1B) and Mica Mountain reconstruction (Fig. 9.3B) occur because smoothing spline values are successively less influenced at that point by future index values, which do not exist; this illustrates the end-effect phenomenon, whereby values at the end of a time series exert more influence on an estimated fit line than do values in the middle of a time series. The much wider flaring of the 95%-confidence intervals in the early part of the chronology and reconstruction (Figs. 9.1B and 9.3B) occur because of poor sample depth (Figs. 9.1C and 9.3C), which leads to poor estimation of the standard error of the mean and to large critical values of the Student's t distribution that are associated with few degrees of freedom (Rohlf and Sokal 1981). Flaring of 95%-confidence intervals should occur in most cases when using this method.

This method of identifying low-frequency tree-ring variation appears to provide a basis for testing of significance of low-frequency departures from the reference line for either chronologies or reconstructions. It could be argued, however, that this approach also constitutes multiple significance testing of means, which causes the α level for the confidence interval to be unknown (Sokal and Rohlf 1981);

consequently, it is difficult to know the level of significance for low-frequency tree-ring trends. Given that a chronology constitutes a single experiment of multiple tests (Miller 1981), a new error level (α') is necessary for each test in order to yield a known error level (α) for the single experiment. The new error level could be determined as follows:

$$\alpha' = 1 - (1 - \alpha)^{1/k}$$

where α' is the error level for each of the k tests and α is the error level of the single experiment (Sokal and Rohlf 1981). As an example, for chronologies or reconstructions 200 years in length and for an experiment with $\alpha = 0.05$ and $k = 215$ tests, α' must be ~0.0002. Regardless of sample depth for any year of the chronology, the critical values of the Student's t distribution that correspond to an α' of ~0.0002 are very large. Such a conservative adjustment would make it highly unlikely that any departure could be deemed significant at the experiment α level of 0.05.

However, adjusting the α level to account for multiple significance testing assumes that the k tests are independent, which is usually not true. Consequently, the number of actual tests (k) should be adjusted downward to a number of effective, independent tests (k') as follows:

$$\frac{k'}{k' - 1} = \left[1 - \frac{1 - r^2}{k(1 - r)^2} + \frac{2r(1 - r^k)}{k^2(1 - r)^2}\right]^{-1}$$

where k' is the number of effective, independent tests, r is the estimated first-order autocorrelation of the low-frequency chronology, and k is the number of actual tests, i.e., the length of the chronology (Dawdy and Matalas 1969, modified from equations 8-III-41 and 8-III-42). Because low-frequency chronologies and reconstructions have extreme autocorrelation, they comprise a k' of ~1 effective, independent test, which nullifies the adjustment of α levels to account for multiple significance

testing. Thus, the desired experiment α level of 0.05 is approximately obtained even when the α' level of 0.05 is used for the calculation of the confidence interval around each mean.

However, even if the experiment error level is considered to be known only approximately, then this approach remains useful in that it still provides the means to evaluate the probable importance of low-frequency departures expressed in tree-ring chronologies. In the Coddington Lake oak chronology (Fig. 9.1B), the approximate 95% confidence intervals associated with trends since 1790 clearly do not enclose the 1.0 reference line. Similarly, in the Mica Mountain July–October precipitation reconstruction (Fig. 9.3B), the approximate 95% confidence intervals associated with the trend of 1850–1900 clearly do not enclose the 1.0 reference line. It can not be argued reasonably that these trends do not exist, and this method demonstrates that low-frequency trends expressed by the Coddington Lake oak chronology and the Mica Mountain reconstruction are real and warrant further investigation.

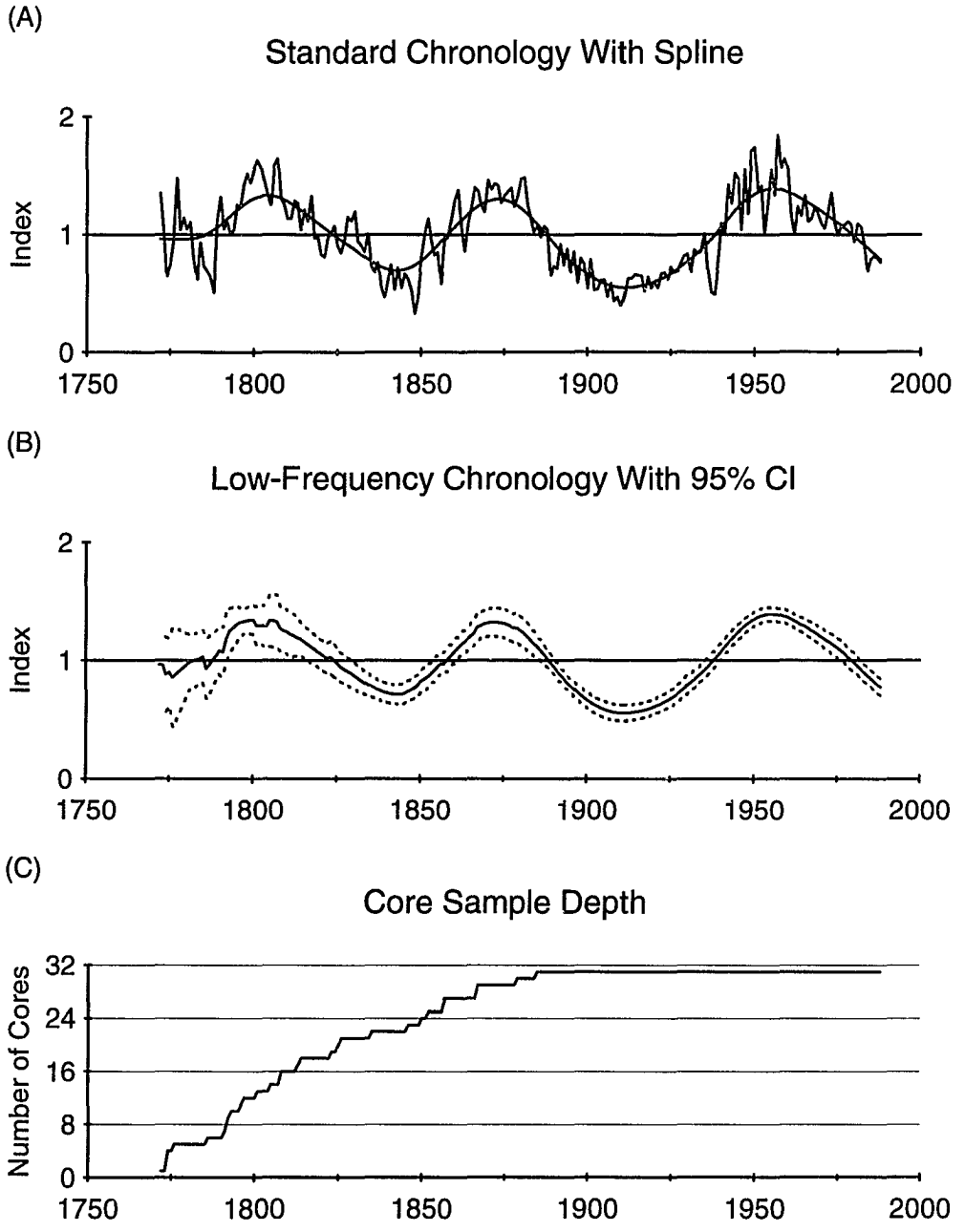

Fig. 9.1. Coddington Lake Low-Frequency Variation: (A) Standard index chronology with appropriate cubic smoothing spline, (B) low-frequency chronology (solid line) with ±95% confidence interval (dashed lines), and (C) core sample depth through time.

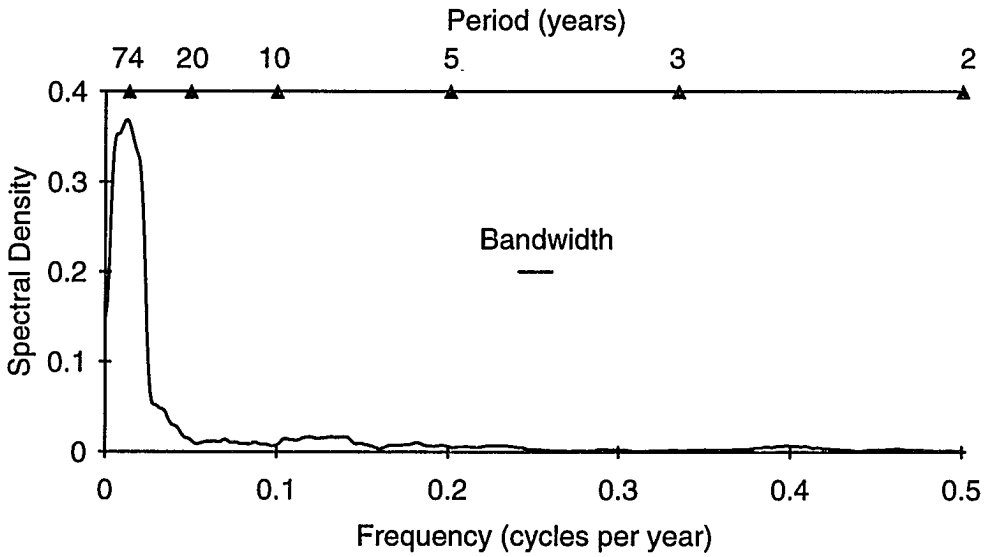

Fig. 9.2. Coddington Lake Spectral Analysis: Spectral density function for standard index chronology derived from ring widths. Bandwidth is 0.0205.

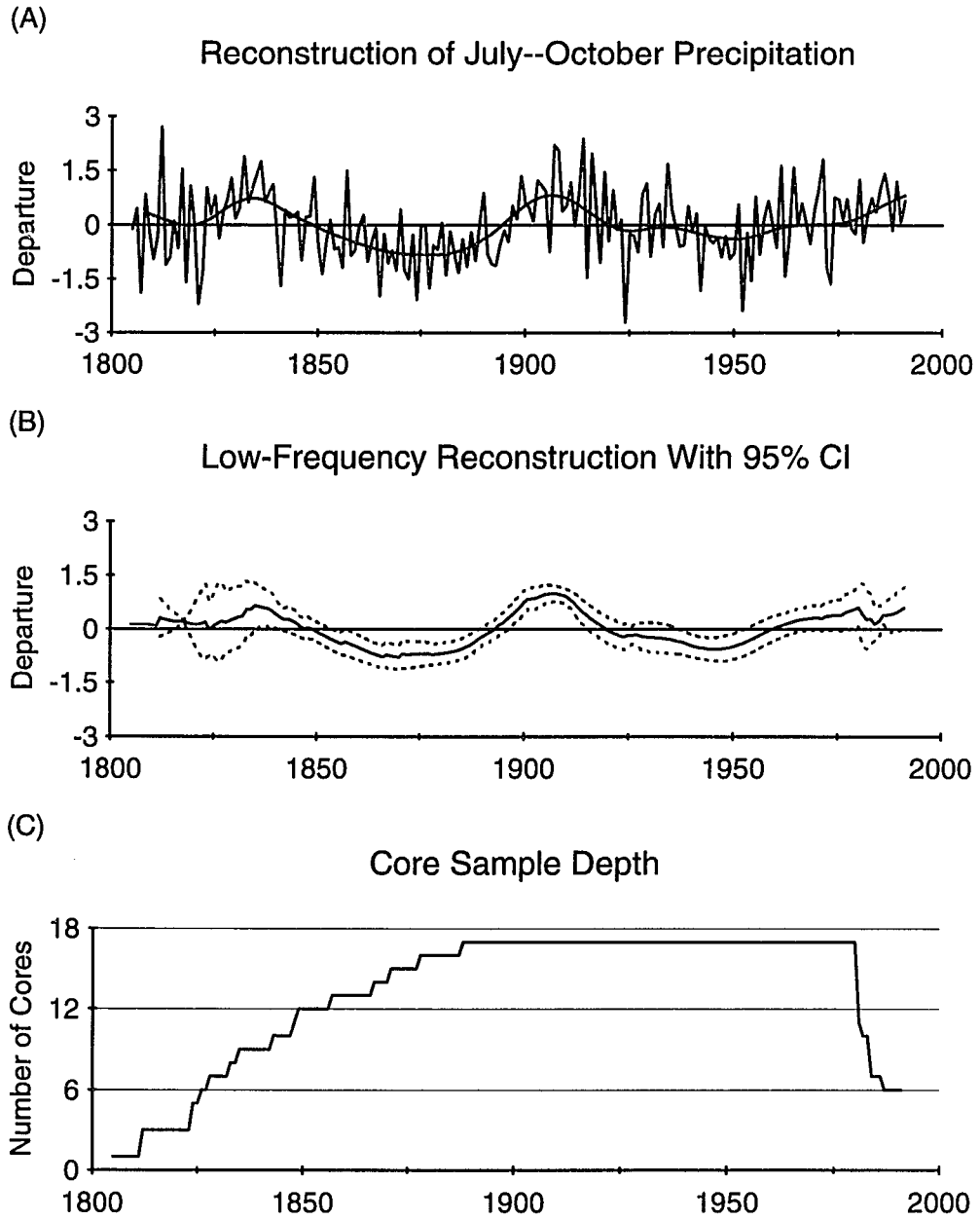

Fig. 9.3. Mica Mountain Low-Frequency Variation: (A) Reconstruction of July--October precipitation with an appropriate cubic smoothing spline (identical to Fig. 7.6B), (B) low-frequency reconstruction of July--October precipitation (solid line) with ±95% confidence interval (dashed lines), and (C) core sample depth through time.

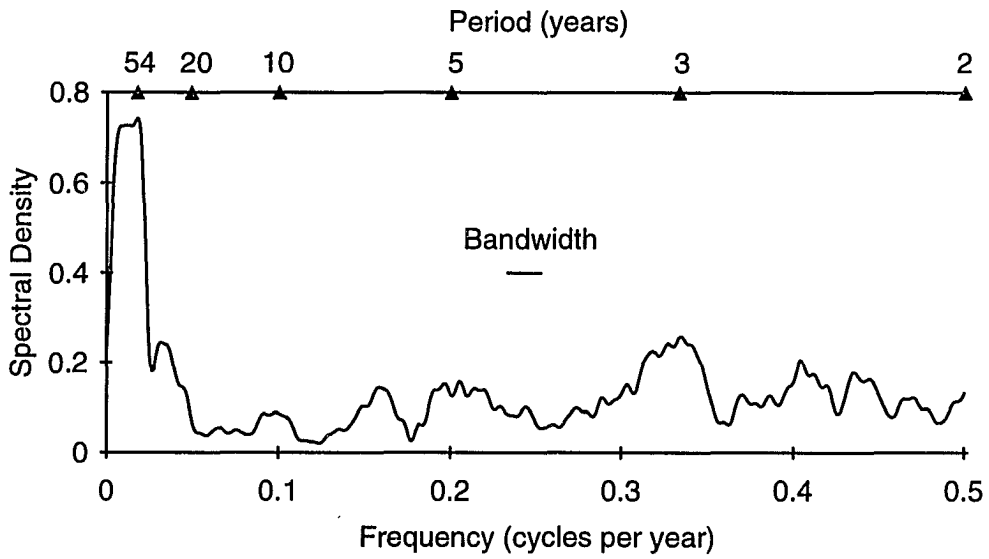

Fig. 9.4. Mica Mountain Spectral Analysis: Spectral density function for July-October precipitation departures as reconstructed using full-length difference (earlywood minus latewood brightness), total ring average brightness, and total ring width measured from extracted cores. Bandwidth is 0.0205.

Table 9.1. Identifying Low Frequency Variation in Chronologies: Steps for constructing a standard tree-ring chronology and for constructing a chronology of low-frequency variation with associated confidence intervals.

Constructing a Standard Tree-Ring Chronology	Re-ordered Approach for Constructing a Chronology of Low-Frequency Variation With Associated Confidence Intervals
1. Create index series by removing series-length trend from each ring-width series	1. Create index series by removing series-length trend from each ring-width series (1)*
2. Average the index series into a standard chronology	2. Determine the frequency of interest (3)
3. Determine the frequency of interest	3. Generate a smoothed low-frequency series for each index series (4)
4. Generate a smoothed low-frequency series for the single, standard chronology	4. Average the smoothed index series into a chronology of low-frequency variation (2)
5. Overlay the standard chronology and the smoothed low-frequency series	5. Overlay the standard chronology and the chronology of low-frequency variation (5)
	6. Calculate the 95% confidence interval for each mean value of the low-frequency chronology
	7. Overlay the 95% confidence intervals with the low-frequency chronology

*Number in parentheses refers to corresponding step in constructing a standard tree-ring chronology (left column).

Table 9.2. Identifying Low Frequency Variation in Reconstructions: Steps for reconstructing climate using tree-rings and for reconstructing low-frequency climate variation with associated confidence intervals.

Constructing a Tree-Ring Climate Reconstruction	Additional Steps for Constructing a Reconstruction of Low-Frequency Variation With Associated Confidence Intervals
1. Calibrate and verify a climate-tree-ring model for period of meteorological record	1. Reconstruct climate for individual samples of the tree-ring collection
2. Reconstruct climate for full extent of chronologies	2. Generate a smoothed low-frequency series for each individual-sample reconstruction
3. Determine the frequency of interest in reconstruction	3. Average the smoothed series into a low-frequency reconstruction
	4. Calculate the 95% confidence interval for each year of the low-frequency reconstruction
	5. Overlay the 95% confidence intervals with the low-frequency reconstruction

10. GENERAL CONCLUSIONS

REFLECTED-LIGHT IMAGE ANALYSIS OF CONIFERS

Current Status

Using reflected-light image analysis, ring brightness can be measured at a fraction of the cost and time required to measure ring density. Given that research funds will always be scarce—especially in science budgets of developing countries—reflected-light image analysis is an attractive alternative to X-ray densitometry. This study indicates that reflected-light image analysis is an excellent tool in dendrochronological research for increasing our understanding paleoenvironmental processes of the latest Holocene.

Latewood brightness was useful for reconstructing past temperature at a cold, moist tree-ring site. Ring density has been useful in several studies to reconstruct temperature of cold, forest ecotones (Conkey 1986; Briffa et al. 1988, 1990, and 1992; Jacoby et al. 1988), and ring brightness should be just as useful in future research at similar sites. Such treeline and/or alpine tree-ring sites are critical for evaluating the significance of the current trend of rising temperature (Hansen and Lebedeff 1988) and for detecting an anthropogenic signal from increasing concentrations of greenhouse gases (Briffa et al. 1990). It would be especially interesting to use reflected-light image analysis on very long-lived species, such as upper treeline bristlecone pine, where ring widths have been interpreted for past temperature (LaMarche 1974; Hughes and Graumlich, in press). Additionally, reflected-light image analysis should be useful for quantifying the phenomenon of light rings, which are commonly associated with short-term extreme climate events of potentially great impact to humans (Filion et al. 1986; Delwaide et al. 1991; Yamaguchi et al. 1993).

Multiple ring brightness variables were useful for reconstructing past precipi-

tation at a warm tree-ring site where tree growth is limited by moisture. Ring density has been useful for reconstructing precipitation of the semiarid Southwest (Cleaveland 1983, 1986; Park 1990; Park and Telewski 1992). Ring brightness should also be useful in future research of these sites, which are critical for understanding the link between climate and forcing factors such as El Niño-Southern Oscillation (Andrade and Sellers 1988; Swetnam and Betancourt 1990). Especially intriguing is the uncommon opportunity to reconstruct and understand past summer precipitation using reflected-light image analysis. If the relationship of ring brightness and summer precipitation is verified in additional dendrochronological studies, then archeological research will have a powerful line of evidence for testing theories associating agricultural production and cultural dynamics to summer rain (Van West 1990).

Ring brightness was useful in documenting tree-growth responses to a known earthquake, and ring brightness should be generally useful in geomorphological research. In particular, the coexistence of 1000-year-old trees and evidence of both earthquakes and volcanic eruptions over the last 1000 years at Medicine Lake (Kilbourne and Anderson 1981) makes it an obvious area for adding dendrochronological techniques—including reflected-light image analysis—to multidisciplinary geomorphological research. For assessing geologic hazards to humans, it is especially critical to demonstrate the existence, or lack, of a temporal-spatial link of individual eruptions and earthquakes.

Future Research

An irony of magnification must be solved. Although the microscope in this imaging system has zoom magnification, I was limited to taking advantage of that feature only between cores, not within cores. Altering magnification alters the

optical configuration of the imaging system, and doing that while measuring a sample would alter the relationship between density and brightness and thereby violate that requirement for using reflected-light image analysis to study conifers.

No single level of magnification suffices for imaging all rings of a sample that has up to two orders of magnitude variation in ring width. Consequently, for reflected-light image analysis to become widely applicable in dendrochronological studies of conifers, changes in the optical configuration that accompany changing the level of magnification must be compensated for so that the relationship between density and brightness remains constant while measuring a core. Whereas I hold constant the absolute video signal response to light, ideally the relative shape of the video signal response to light should remain constant while allowing the absolute signal to vary with changes in magnification. This problem requires more research in analog/digital image analysis.

Several unusual tree-ring variables are either directly measurable or indirectly derivable from the ring brightness scan of reflected-light image analysis. For example, the area beneath the brightness scan (Fig. 4.1) incorporates both ring width and brightness. More specifically, the area beneath the earlywood brightness scan can be used to quantify the presence and strength of false rings, which are related to particular intra-seasonal patterns of summer precipitation and which lower values of earlywood area. Future research using reflected-light image analysis of conifers should continue exploring these and other variables.

IDENTIFYING LOW-FREQUENCY TREE-RING VARIATION

A current challenge in paleoenvironmental research is associating low-frequency (decade- to century-scale) climate variation to its causal factor (Rind and Overpeck 1993). In meeting this challenge, researchers should explicitly know the

significance of low-frequency climate departures as reconstructed using paleoenvironmental data. Researchers should also know how robustly a departure is estimated. Interpreting an insignificant or poorly estimated climate departure runs the risk of incorrectly linking it to a causal factor.

As demonstrated in this study, identifying low-frequency tree-ring variation provides a way to judge the significance or importance of low-frequency departures, either in tree-ring chronologies or in environmental reconstructions derived from tree-ring data. Additionally, this method provides a visual basis for determining whether or not low-frequency variation is robustly estimated by tree-ring data. Given that this method uses computations already commonly used in dendrochronology and is therefore analytically simple, dendrochronologists should use this method, or something else to achieve the same objectives, before interpreting low-frequency tree-ring variation.

11. APPENDIX I: Pascal Code to Find Ring Boundaries

I use the following program of Pascal code interactively on a PC system with Image−1® to locate boundaries between rings and between earlywood and latewood portions within rings. This program reads in binary data from .IMG files of images generated with Image−1®. At the time of publication of this dissertation, this code was compilable on a PC system by Turbo Pascal, version 6. I include this code in this dissertation for documentation purposes only; I disclaim any responsibility for how others use this code.

```
program newboundary (input, output);
uses dos,crt;

CONST VERTEDGE = 25;
      HOOD = 3;
      MAXROW = 479;
      MAXCOL = 511;
      MAXRINGS = 11;

type real_row_array = array[0..MAXROW]  of real;
type real_row_array_ptr = ^real_row_array;
type int_row_array = array[-1..MAXROW] of integer;
type int_row_array_ptr = ^int_row_array;

type int_col_array = array[-1..MAXCOL] of integer;
type int_col_array_ptr = ^int_col_array;
type int_short_col_array = array[0..MAXRINGS] of integer;
type int_short_col_array_ptr = ^int_short_col_array;
type real_short_col_array = array[-1..MAXRINGS] of real;
type real_short_col_array_ptr = ^real_short_col_array;

type byte_col_array = array[0..MAXCOL] of byte;
type byte_col_array_ptr = ^byte_col_array;
type bool_col_array = array[0..MAXCOL] of boolean;
type bool_col_array_ptr = ^bool_col_array;

type byte_row_col_array = array[0..MAXROW] of
byte_col_array_ptr;
type byte_row_col_array_ptr = ^byte_row_col_array;
```

```
type int_row_short_col_array = array[0..MAXROW] of
  int_short_col_array_ptr;
type int_row_short_col_array_ptr =
  ^int_row_short_col_array;
type bool_row_col_array = array[0..MAXROW] of
  bool_col_array_ptr;
type bool_row_col_array_ptr = ^bool_row_col_array;

var file_path, core_name, str_year, boundary_ok    :string;

    num_rings, year, x,
    up, down, left, right,
    row, col, mean_row, retrace_col,
    pixel_num,
    first_dig, second_dig, third_dig, fourth_dig,
    height, width,
    marker, edge,
    right_most_b_on_b, left_most_b_on_b,
    fourth, second,
    max_fourth, max_second :integer;

    early_late_col,
    early_late_row                :int_short_col_array_ptr;

    mean_gray                          :int_col_array_ptr;

    byte_point,
    lo_width, hi_width, lo_height, hi_height          :char;

    ew_pct                        :real_short_col_array_ptr;

    gray                            :byte_row_col_array_ptr;
    boundary                   :int_row_short_col_array_ptr;

    black_on_boundary               :bool_row_col_array_ptr;

    bad_row, no_problem,
    doing_mean_scan, doing_first_mean, file_ok    :boolean;

    path_file, log_file, dat_file,
    out_file, img_file                                :text;

procedure row_scan;
{to find boundary addresses of 1-row scans than are checked
and good}
```

```
begin
max_fourth := 0; fourth := 0;
{look in 7-pixel neighborhood of boundaries of previous
row}
for col := (boundary^[row+up+down]^[marker]-HOOD) to
  (boundary^[row+up+down]^[marker]+HOOD) do begin
  if (gray^[row]^[col-2] <> 0) and (gray^[row]^[col-1] <>
    0) and (gray^[row]^[col] <> 0) and
    (gray^[row]^[col+1] <> 0) and (gray^[row]^[col+2] <> 0)
    then begin
    fourth := gray^[row]^[col+2] - gray^[row]^[col-2];
    if (fourth > max_fourth) then begin
      max_fourth := fourth;
      boundary^[row]^[marker] := col;
      end; {if fourth > max_fourth}
    end; {if all 5 pixels not black [fourth is calculated]}
  end; {for col loop}
if max_fourth = 0 then begin
  writeln('No positive 4th difference was found for
  row ',row:1,', marker # ',marker:1,'.');
  max_second := 0; second := 0;
  for col := (boundary^[row+up+down]^[marker]-HOOD) to
    (boundary^[row+up+down]^[marker]+HOOD) do begin
    if (gray^[row]^[col-1] <> 0) and (gray^[row]^[col] <>
      0) and (gray^[row]^[col+1] <> 0) then begin
      second := gray^[row]^[col+1] - gray^[row]^[col-1];
      if (second > max_second) then begin
        max_second := second;
        boundary^[row]^[marker] := col;
        end; {if second > max_second}
      end; {if all 3 pixels not black [second calculated]}
    end; {for col loop}
  if max_second = 0 then begin
    writeln('No positive 2nd difference was found for
    row ',row:1,', marker # ',marker:1,'.');
    writeln('The program is aborting and writing out
    boundaries found so far.');
    no_problem := false;
    end; {if no max_second}
  end; {if no max_fourth, look for a max_second}
if boundary^[row]^[marker] <> 0 then
  gray^[row]^[boundary^[row]^[marker]] := 255;
end; {procedure row_scan}

procedure mean_scan;
```

```
{To find 13-row mean scan for locating ring boundaries find
start_ and end_addresses}
begin
if (marker = 0) and (gray^[row]^[VERTEDGE] = 255) then
  begin
  writeln('Found white out on the left for marker
  # ',marker:1,'.');
  col := VERTEDGE;
  while gray^[row]^[col] = 255 do inc(col);
  boundary^[row]^[marker] := col; gray^[row]^[col] := 0;
  end {if first col is white}
else {marker <> 0 and/or first pixel <> 255}
  if (marker = num_rings) and (gray^[row]^[width-1-
    VERTEDGE] = 255) then begin
    writeln('Found white out on the right for marker
    # ',marker:1,'.');
    col := width - 1 - VERTEDGE;
    while gray^[row]^[col] = 255 do dec(col);
    boundary^[row]^[marker] := col; gray^[row]^[col] := 0;
    end {if last col is white}
  else {not first or last marker with white outs} begin
    doing_mean_scan := true;
    {initialize, sum, and divide by 13 for 13-row mean
    variables}
    for col := 0 to (width-1) do begin
      mean_gray^[col] := 0;
      for mean_row := (row+up) to (row+down) do
        mean_gray^[col] := mean_gray^[col] +
        gray^[mean_row]^[col];
      mean_gray^[col] := round(mean_gray^[col]/13);
      {if any of the 13 rows is 0 at this col, then assign
      col mean 0}
      for mean_row := (row+up) to (row+down) do
        if gray^[mean_row]^[col] = 0 then
          mean_gray^[col] := 0;
      end; {for col = 0 to (width-1) loop}

    {find boundary point of 13-row mean scan by maxing
    4th-diffs}
    fourth := 0; max_fourth := 0;
    if doing_first_mean then begin
      if marker = 0 then col := early_late_col^[1] - 2
      else col := early_late_col^[marker] + 2;
      while ((max_fourth = 0) or (fourth = max_fourth)) and
        ((col >= 2) and (col <= width-3)) do begin
```

```
      if marker = 0 then dec(col)
      else inc(col);
      if (mean_gray^[col-2] <> 0) and (mean_gray^[col-1]
        <> 0) and (mean_gray^[col] <> 0) and
        (mean_gray^[col+1] <> 0) and (mean_gray^[col+2]
        <> 0) then begin
        fourth := mean_gray^[col+2] - mean_gray^[col-2];
        if (fourth >= 40) and (fourth > max_fourth) then
          max_fourth := fourth;
        end; {if all 5 pixels are not black [fourth is
        calculated]}
      end; {while conditional}
    if max_fourth = 0 then begin
      writeln('No 4th-difference >= 40 was found in
      row ',row:1,' for marker # ',marker:1,';');
      writeln('The program is aborting and writing out
      boundaries found so far.');
      no_problem := false;
      end {if no large 4th difference}
    else {yes large 4th diff and not doing first or last
    with white outs}
      if marker = 0 then boundary^[row]^[marker] := col+1
      else boundary^[row]^[marker] := col - 1;
    end {if doing first mean}
  else {not doing_first_mean} begin
    if marker = 0 then col := right_most_b_on_b + 5
    else col := left_most_b_on_b - 5;
    while (col >= (left_most_b_on_b - 5)) and (col <=
    (right_most_b_on_b + 5)) do begin
      if marker = 0 then dec(col)
      else inc(col);
      if (mean_gray^[col-2] <> 0) and (mean_gray^[col-1]
        <> 0) and (mean_gray^[col] <> 0) and
        (mean_gray^[col+1] <> 0) and (mean_gray^[col+2]
        <> 0) then begin
        fourth := mean_gray^[col+2] - mean_gray^[col-2];
        if fourth > max_fourth then begin
          max_fourth := fourth; boundary^[row]^[marker]
          := col;
          end; {if 4th > max_4th}
        end; {if all 5 pixels are not black [fourth is
        calculated]}
      end; {while conditional}
    if boundary^[row]^[marker] = 0 then begin
      writeln('No 4th-difference >= 0 was found in
```

```
        row ',row:1,' for marker # ',marker:1,';');
        writeln('The program is aborting and writing out
        boundaries found so far.');
        no_problem := false;
        end {if no large 4th difference}
      else {a boundary col was identified}
        gray^[row]^[boundary^[row]^[marker]] := 255;
      end; {else not doing first mean}
    end; {else not first or last with white outs}
right_most_b_on_b := 0; left_most_b_on_b := width - 1;
doing_first_mean := false;
end; {procedure mean_scan}

procedure check_row;
{to check rows for black pixels on or near boundaries}
begin
if (marker = 0) and (gray^[row]^[VERTEDGE] = 255) then
  begin
  col := VERTEDGE;
  while gray^[row]^[col] = 255 do inc(col);
  boundary^[row]^[marker] := col; gray^[row]^[col] := 0;
  end {if first col is white}
else {marker <> 0 and/or first pixel <> 255}
  if (marker = num_rings) and (gray^[row]^[width-1-
  VERTEDGE] = 255) then begin
    col := width - 1 - VERTEDGE;
    while gray^[row]^[col] = 255 do dec(col);
    boundary^[row]^[marker] := col; gray^[row]^[col] := 0;
    end {if last col is white}
  else {not first or last marker with white outs} begin
    bad_row := false;
    {if black in this row is adjacent to black on
    boundaries in previous row, then reject this row}
    if boundary^[row+up+down]^[marker] <> 0 then
      if marker = 0 then col :=
      boundary^[row+up+down]^[marker] + 10
      else col := boundary^[row+up+down]^[marker] - 10
    else {previous row has no column for this boundary}
      if marker = 0 then col := right_most_b_on_b + 5
      else col := left_most_b_on_b - 5;
    while (col >= 3) and (col <= (width - 4)) do begin
      if marker = 0 then dec(col)
      else inc(col);
      if (gray^[row]^[col] = 0) and
      (((col >= boundary^[row+up+down]^[marker]-2) and
```

```
(col<= boundary^[row+up+down]^[marker]+2) and
      (boundary^[row+up+down]^[marker] <> 0)) or
(black_on_boundary^[row+up+down]^[col-2] or
      black_on_boundary^[row+up+down]^[col-1] or
      black_on_boundary^[row+up+down]^[col] or
      black_on_boundary^[row+up+down]^[col+1] or
black_on_boundary^[row+up+down]^[col+2] or
      black_on_boundary^[row]^[col-1] or
      black_on_boundary^[row]^[col+1])) then begin
        black_on_boundary^[row]^[col] := true;
        retrace_col := col;
        if marker = 0 then begin
        right := 1; left := 0; end
        else begin
        right := 0; left := -1; end;
        while black_on_boundary^[row]^[retrace_col] and
        ((gray^[row]^[retrace_col+left+right] = 0) and
        (not black_on_boundary^[row]^[retrace_col+left+
        right])) do begin
          if marker = 0 then inc(retrace_col)
          else dec(retrace_col);
          black_on_boundary^[row]^[retrace_col] := true;
          if retrace_col < left_most_b_on_b then
            left_most_b_on_b := retrace_col;
          if retrace_col > right_most_b_on_b then
            right_most_b_on_b := retrace_col;
          end; {while black_on_boundary[row,col]}
        bad_row := true;
        if col < left_most_b_on_b then
          left_most_b_on_b := col;
        if col > right_most_b_on_b then
          right_most_b_on_b := col;
        end; {if a black pixel is near a boundary or
        black_on_boundary of previous row}
      end; {while col conditional}
    if not bad_row then
      if (boundary^[row+up+down]^[marker] <> 0) then
        row_scan
      else {good row following a bad row} begin
        if up = -1 {looking down the image} then begin
          up := 0; down := 12;
          end {if looking down the image}
        else {looking up the image} begin
          up := -12; down := 0;
          end; {else looking up the image}
```

```
        mean_scan;
        end; {else good row following bad row}
    end; {else not first or last with white outs
    conditional}
end; {procedure check_row}

procedure quicksort (start,finish:integer; var
data:int_short_col_array_ptr);
var starting_value, left, right, temp: integer;
begin
left := start; right := finish;
starting_value := data^[(start+finish) div 2];
repeat
  while data^[left] < starting_value do
    inc(left);
  while starting_value < data^[right] do
    dec(right);
  if left <= right then begin
    temp := data^[left]; data^[left] := data^[right];
    data^[right] := temp;
    temp := early_late_row^[left];
    early_late_row^[left] := early_late_row^[right];
    early_late_row^[right] := temp;
    inc(left); dec(right);
    end; {if not too far}
  until right <= left;
if start < right then quicksort(start,right,data);
if left < finish then quicksort(left,finish,data);
end; {procedure quicksort}

begin{main}
assign(path_file,'c:\image1\data\filepath.dat');
reset(path_file);
readln(path_file,file_path);
close(path_file);

assign(log_file,file_path+'log.log');
{$I-} reset(log_file); {$I+}
file_OK := (IOResult = 0);
if file_OK then begin
  reset(log_file);
  while not eof(log_file) do
    readln(log_file,year);
  inc(year);
  end
```

```
else begin
  rewrite(log_file);
  close(log_file);
  assign(dat_file,file_path+'dat.dat'); reset(dat_file);
  readln(dat_file,year); close(dat_file);
  end;
str(year,str_year);writeln(str_year);readln;

{process .img files}
assign(img_file,file_path+str_year+'.img');
reset(img_file);
writeln; writeln('Processing ',file_path+str_year,'.img');
{val(copy(paramstr(1),length(paramstr(1))-3,4),year,x);}
read(img_file,byte_point,byte_point,lo_width,hi_width,
lo_height,hi_height);
width:=ord(lo_width)+256*ord(hi_width);     {page A59 of    }
height:=ord(lo_height)+256*ord(hi_height); {Image-1 manual}

new(mean_gray); new(gray); new(ew_pct);
new(early_late_row); new(early_late_col);
new(black_on_boundary); new(boundary);
for row := 0 to MAXROW do begin
  new(gray^[row]); new(black_on_boundary^[row]);
  new(boundary^[row]);
  end;

{read in all data from the .img file}
writeln('Reading in byte data.');
row := 0; marker := 0;
while row <= (height - 1) do begin
  col := 0;
  while col <= (width - 1) do begin
    read(img_file,byte_point);
    if (row = 0) and (col = 0) then begin
      edge := ord(byte_point);
      writeln('Horizontal edge is ',edge:1,'.');
      end; {if first pixel}
    if (row = (edge - 1)) or (row = (height - 1 - edge +
      1)) then
      gray^[row]^[col] := 255
    else
      gray^[row]^[col] := ord(byte_point);
    black_on_boundary^[row]^[col] := false;
    if gray^[row]^[col] = 254 then begin
      inc(marker);
```

```
      if marker > MAXRINGS then begin
        writeln('The maximum rings allowed is ',MAXRINGS:1,
        ';on row ',row:1,' and col ',col:1,', you exceeded
        the limit by one.');
        writeln('Hit control-break to stop.'); readln;
        end; {if too many markers}
      early_late_col^[marker] := col;
      early_late_row^[marker] := row;
      gray^[row]^[col] := 0;
      end; {if gray = 254}
    inc(col);
    end; {while col loop}
  inc(row);
  end; {while row loop}
num_rings := marker;
writeln('Number of rings = ',num_rings:1,'.');
close(img_file);

for row := 0 to (height - 1) do
  for marker := 0 to num_rings do
    boundary^[row]^[marker] := 0;

quicksort(1,marker,early_late_col);
early_late_row^[0] := early_late_row^[1];
writeln('The following ',num_rings:1, ' early-latewood
markers were found, in order from left to right:');
writeln('Marker  column   row    year');
writeln('------  ------  ------  ----');
for marker := 1 to num_rings do begin
  writeln(marker:4,early_late_col^[marker]:8,
  early_late_row^[marker]:8,year:8);
  inc(year);
  end; {for all markers}

writeln('Finding boundaries.');
{find boundary addresses of each 1-row scan by maxing
4th-diffs}
no_problem := true; marker := -1;
while no_problem and (marker < num_rings) do begin
  inc(marker); writeln('Finding boundary # ',marker:1,'.');
  row := early_late_row^[marker]; doing_first_mean := true;
  up := -6; down := 6; mean_scan;

  {looking down the image}
  while no_problem and (row < (height - 1 - edge)) do begin
```

```
      inc(row); up := -1; down := 0; check_row;
      end; {while no_problem for all rows looking down}

    {looking up the image}
    row := (early_late_row^[marker]);
    while no_problem and (row > (0 + edge)) do begin
      dec(row); up := 0; down := 1; check_row;
      end; {while no_problem for all rows looking up}

    {calculate ew_pct}
    if no_problem and (marker > 0) then begin
      ew_pct^[marker] := (early_late_col^[marker]-
      boundary^[early_late_row^[marker]]^[marker-1]+1)/
      (boundary^[early_late_row^[marker]]^[marker]-
      boundary^[early_late_row^[marker]]^[marker-1]+1);
      if (ew_pct^[marker] < 1) and (ew_pct^[marker] > 0) then
        for row := (0 + edge) to (height - 1 - edge) do
          if (boundary^[row]^[marker-1] <> 0) and
          (boundary^[row]^[marker] <> 0) and
          (boundary^[row]^[marker-1] <
          boundary^[row]^[marker]) then
            gray^[row]^[round(ew_pct^[marker]*
            (boundary^[row]^[marker]-
            boundary^[row]^[marker-1]+1))+
            boundary^[row]^[marker-1]] := 0;
      end; {if no_problem and marker > 0}
    end; {while no_problem and marker < num_rings}

writeln('Writing out c:\image1\images\boundary.img.');
assign(out_file,'c:\image1\images\boundary.img');
rewrite(out_file);
write(out_file,chr(0),chr(0),lo_width,hi_width,lo_height,
hi_height);
for row := 0 to (height-1) do
  for col := 0 to (width-1) do
    write(out_file,chr(gray^[row]^[col]));
close(out_file);
if no_problem then writeln('Done.')
else begin
  writeln('Take note of the location of the problem, then
  hit control-break.');
  readln;
  end; {else there was a problem}
end.
```

12. APPENDIX II: Pascal Code to Reduce Images to Tree-Ring Data

I use the following procedures of Pascal code in batch mode on the VAX mainframe of The University of Arizona to reduce binary data from .IMG files of images generated with Image−1© to files of tree-ring data that can be analyzed further using programs of the International Tree-Ring Data Bank (Grissino-Mayer et al. 1992). I use these procedures after finding and checking ring boundaries on each image (Appendix I), and for these procedures to work, they must be joined with the code to find ring boundaries. At the time of publication of this dissertation, this code was compilable on the VAX mainframe of The University of Arizona. I include this code in this dissertation for documentation purposes only; I disclaim any responsibility for how others use this code.

```
CONST HOOD = 2;
CONST VERTEDGE = 25;
CONST MAXROW = 479;
CONST MAXCOL = 511;
CONST MAXRINGS = 11;
CONST MISSING_VAL = -1;

type real_col_array = array[0..MAXCOL] of real;
type real_short_col_array  = array[-1..MAXRINGS] of real;
type int_col_array = array[0..MAXCOL] of integer;
type int_short_col_array  = array[0..MAXRINGS] of integer;

type real_row_array = array[0..MAXROW]  of real;
type int_row_array  = array[-1..MAXROW] of integer;
type bool_row_array = array[-1..MAXROW]  of boolean;

type real_row_col_array = array[0..MAXROW,0..MAXCOL] of
  real;
type int_row_col_array = array[0..MAXROW,0..MAXCOL] of
  integer;
type int_row_short_col_array = array[0..MAXROW,0..MAXRINGS]
  of integer;
type bool_row_col_array = array[0..MAXROW,0..MAXCOL] of
  boolean;
```

```
type real_year_array = array[1..2000] of real;
type int_year_array = array[1..2000] of integer;
type bool_year_array = array[1..2000] of boolean;

type char_array = packed array[1..6] of char;

var core_name                  :char_array; {input file name}

    year,                                      {counter for year}
    first_year,                              {to remember first year}
    last_year,                                {to remember last year}
    past_year,
    current_year,
    up, down, left, right, retrace_col,
    row, col, mean_row,
    scan_num, max_scan_num,
    pixel_num,          {counter for pixels w/i row w/i year}
    just_below,                {the pixel just below new one}
    just_above,                {the pixel just above new one}
    final_pixel_num,       {integer series for avg gray row}
    avg_max_pixel_num,     {avg max pixel for rows w/i year}
    rel_max,                              {max_dens / min_dens}
    dif_max,                              {max_dens - min_dens}
    max_ew_area,          {max area beneath earlywood curve}
    max_lw_area,           {max area beneath latewood curve}
    min_ew_area,          {min area beneath earlywood curve}
    min_lw_area,           {min area beneath latewood curve}
    ewa_divisor,           {to adjust earlywood area values}
    lwa_divisor,            {to adjust latewood area values}
    first_dig, second_dig,
    third_dig, fourth_dig,
    byte_num, edge,
    height, width,
    marker, num_rings,
    right_most_b_on_b,
    left_most_b_on_b,
    fourth, second, first,
    max_fourth, max_second, max_first,
    fourth_boundary, second_boundary,
    early_max_gray,        {maximum ew value, w/i earlywood}
    early_avg_gray,        {average ew value, w/i earlywood}
    early_min_gray,        {minimum ew value, w/i earlywood}
    late_max_gray,         {maximum lw value, w/i  latewood}
    late_avg_gray,         {average lw value, w/i  latewood}
```

```
late_min_gray,          {minimum lw value, w/i  latewood}
num_miss_ew_col,
num_miss_lw_col,
minitab, x                                        :integer;

early_late_col,
early_late_row                        :int_short_col_array;

mean_gray, avg_gray,
second_diff, max_row_num                   :int_col_array;

sum_gray                                  :real_col_array;

pixel_size                               :real_year_array;

ew_area,          {area beneath latewood curve w/i year}
lw_area           {area beneath latewood curve w/i year}
                                          :int_year_array;

byte_point,
lo_width, hi_width,
lo_height, hi_height,
one_char                                             :char;

ew_pct                                :real_short_col_array;

scan_conversion                           :real_row_array;
       {a ratio, mean of 1.0, to stretch/contract rows}

start_address, end_address,
max_pixel_num                              :int_row_array;
                {value of last latewood pixel, w/i row}

new_pixel_num,      {ranging from 0 to avg_max_ew_pixel}
adj_gray          {avg values for entire row, by pixel}
                                    :real_row_col_array;

gray                                   :int_row_col_array;

boundary                          :int_row_short_col_array;

black_on_boundary                     :bool_row_col_array;

all_black                                 :bool_row_array;
```

```
    missing_ring, ew_area_ok, lw_area_ok  :bool_year_array;

    bad_row, doing_first_mean                        :boolean;

    early_width,                          {earlywood ring width}
    late_width,                           { latewood ring width}
    total_width,                          {    total ring width}
    late_percent,
    early_max_value,     {earlywood maximum gray (min dens)}
    early_avg_value,     {earlywood average gray (avg dens)}
    early_min_value,     {earlywood minimum gray (max dens)}
    late_max_value,      { latewood minimum gray (max dens)}
    late_avg_value,      { latewood average gray (avg dens)}
    late_min_value,      { latewood maximum gray (min dens)}
    total_value,                    {total ring average gray}
    early_area,                {earlywood area beneath curve}
    late_area,                  {latewood area beneath curve}
    rel_max_gray,  {late_min_gray / early_max_gray * const}
    dif_max_gray,           {early_max_gray - late_min_gray}
    num_of_rows                       {a minitab naming file}
                                                    :text;

procedure writedata;
begin
if year = first_year then begin
  writeln; writeln; writeln('Now opening output files.');
  open(early_width,'xlarge:[grad12.temp]'+
  CORE_NAME+'.eww',new);
  rewrite(early_width);
  write(early_width,substr(CORE_NAME,1,5)+'eww',
  first_year:4);
  open(late_width,'xlarge:[grad12.temp]'+
  CORE_NAME+'.lww',new);
  rewrite(late_width);
  write(late_width,substr(CORE_NAME,1,5)+'lww',
  first_year:4);
  open(total_width,'xlarge:[grad12.temp]'+
  CORE_NAME+'.trw',new);
  rewrite(total_width);
  write(total_width,substr(CORE_NAME,1,5)+'trw',
  first_year:4);
  open(late_percent,'xlarge:[grad12.temp]'+
  CORE_NAME+'.lwp',new);
  rewrite(late_percent);
  write(late_percent,substr(CORE_NAME,1,5)+'lwp',
```

```
first_year:4);
open(early_max_value,'xlarge:[grad12.temp]'+
CORE_NAME+'.exg',new);
rewrite(early_max_value);
write(early_max_value,substr(CORE_NAME,1,5)+'exg',
first_year:4);
open(early_avg_value,'xlarge:[grad12.temp]'+
CORE_NAME+'.eag',new);
rewrite(early_avg_value);
write(early_avg_value,substr(CORE_NAME,1,5)+'eag',
first_year:4);
open(early_min_value,'xlarge:[grad12.temp]'+
CORE_NAME+'.eng',new);
rewrite(early_min_value);
write(early_min_value,substr(CORE_NAME,1,5)+'eng',
first_year:4);
open(late_max_value,'xlarge:[grad12.temp]'+
CORE_NAME+'.lxg',new);
rewrite(late_max_value);
write(late_max_value,substr(CORE_NAME,1,5)+'lxg',
first_year:4);
open(late_avg_value,'xlarge:[grad12.temp]'+
CORE_NAME+'.lag',new)
rewrite(late_avg_value);
write(late_avg_value,substr(CORE_NAME,1,5)+'lag',
first_year:4);
open(late_min_value,'xlarge:[grad12.temp]'+
CORE_NAME+'.lng',new);
rewrite(late_min_value);
write(late_min_value,substr(CORE_NAME,1,5)+'lng',
first_year:4);
open(total_value,'xlarge:[grad12.temp]'+
CORE_NAME+'.trg',new);
rewrite(total_value);
write(total_value,substr(CORE_NAME,1,5)+'trg',
first_year:4);
open(rel_max_gray,'xlarge:[grad12.temp]'+
CORE_NAME+'.rel',new);
rewrite(rel_max_gray);
write(rel_max_gray,substr(CORE_NAME,1,5)+'rel',
first_year:4);
open(dif_max_gray,'xlarge:[grad12.temp]'+
CORE_NAME+'.dif',new); rewrite(dif_max_gray);
write(dif_max_gray,substr(CORE_NAME,1,5)+'dif',
first_year:4);
```

```
  open(num_of_rows,'xlarge:[grad12.temp]'+
  CORE_NAME+'.nos',new);
  rewrite(num_of_rows);
  write(num_of_rows,substr(CORE_NAME,1,5)+'nos',
  first_year:4);
  end;  {if year = first_year}
if missing_ring[year] then begin
  write(early_width,MISSING_VAL:6);
  write(late_width,MISSING_VAL:6);
  write(total_width,MISSING_VAL:6);
  write(late_percent,MISSING_VAL:6);
  write(early_max_value,MISSING_VAL:6);
  write(early_avg_value,MISSING_VAL:6);
  write(early_min_value,MISSING_VAL:6);
  write(late_max_value,MISSING_VAL:6);
  write(late_avg_value,MISSING_VAL:6);
  write(late_min_value,MISSING_VAL:6);
  write(total_value,MISSING_VAL:6);
  write(rel_max_gray,MISSING_VAL:6);
  write(dif_max_gray,MISSING_VAL:6);
  write(num_of_rows,MISSING_VAL:6);
  if (year = first_year) or (year mod 20 = 0) then begin
    writeln;
    writeln('year eww lww trw lwp exg eag eng lxg lag lng
    trg       ewa       lwa rel dif nos');
    writeln('---- --- --- --- --- --- --- --- --- --- ---
    --- --------- --------- --- --- ---');
    end;  {if header is needed}
  writeln(year:4,'   *   *   *   *   *   *   *   *   *   *
  *         *   *   *   *');
  end {if missing_ring}
else {not missing_ring} begin
  write(early_width,round(ew_pct[marker]*
  (avg_max_pixel_num+1)*pixel_size[year]*100):6);
  write(late_width,round((1-ew_pct[marker])*
  (avg_max_pixel_num+1)*pixel_size[year]*100):6);
  write(total_width,round((avg_max_pixel_num+1)*
  pixel_size[year]*100):6);
  write(late_percent,round(100*(1-ew_pct[marker])):6);
  write(early_max_value,early_max_gray:6);
  write(early_avg_value,early_avg_gray:6);
  write(early_min_value,early_min_gray:6);
  write(late_max_value,late_max_gray:6);
  write(late_avg_value,late_avg_gray:6);
  write(late_min_value,late_min_gray:6);
```

```
  write(total_value,round(((early_avg_gray*ew_pct[marker]*
  (avg_max_pixel_num+1))+(late_avg_gray*(1-ew_pct[marker])*
  (avg_max_pixel_num+1)))/(avg_max_pixel_num+1)):6);
  write(rel_max_gray,rel_max:6);
  write(dif_max_gray,dif_max:6);
  write(num_of_rows,max_scan_num:6);
  if (year = first_year) or (year mod 20 = 0) then begin
    writeln;
    writeln('year eww lww trw lwp exg eag eng lxg lag lng
    trg       ewa       lwa rel dif nos');
    writeln('---- --- --- --- --- --- --- --- --- --- ---
    --- --------- --------- --- --- ---');
    end;  {if header is needed}
  writeln(year:4,
  round(ew_pct[marker]*(avg_max_pixel_num+1)*
  pixel_size[year]*100):4,
  round((1-ew_pct[marker])*(avg_max_pixel_num+1)*
  pixel_size[year]*100):4,
  round((avg_max_pixel_num+1)*pixel_size[year]*100):4,
  round(100*(1-ew_pct[marker])):4,
  early_max_gray:4,
  early_avg_gray:4,
  early_min_gray:4,
  late_max_gray:4,
  late_avg_gray:4,
  late_min_gray:4,
  round(((early_avg_gray*ew_pct[marker]*
  (avg_max_pixel_num+1))+(late_avg_gray*(1-ew_pct[marker])*
  (avg_max_pixel_num+1)))/(avg_max_pixel_num+1)):4,
  ew_area[year]:10,
  lw_area[year]:10,
  rel_max:4,
  dif_max:4,
  max_scan_num:4);
  end; {else not missing_ring}
if (year + 1) mod 10 = 0 then begin
{end of output line wrap around}
  writeln(early_width);
  write(early_width,substr(CORE_NAME,1,5)+'eww',
  (year+1):4);
  writeln(late_width);
  write(late_width,substr(CORE_NAME,1,5)+'lww',
  (year+1):4);
  writeln(total_width);
  write(total_width,substr(CORE_NAME,1,5)+'trw',
```

```
    (year+1):4);
    writeln(late_percent);
    write(late_percent,substr(CORE_NAME,1,5)+'lwp',
    (year+1):4);
    writeln(early_max_value);
    write(early_max_value,substr(CORE_NAME,1,5)+'exg',
    (year+1):4);
    writeln(early_avg_value);
    write(early_avg_value,substr(CORE_NAME,1,5)+'eag',
    (year+1):4);
    writeln(early_min_value);
    write(early_min_value,substr(CORE_NAME,1,5)+'eng',
    (year+1):4);
    writeln(late_max_value);
    write(late_max_value,substr(CORE_NAME,1,5)+'lxg',
    (year+1):4);
    writeln(late_avg_value);
    write(late_avg_value,substr(CORE_NAME,1,5)+'lag',
    (year+1):4);
    writeln(late_min_value);
    write(late_min_value,substr(CORE_NAME,1,5)+'lng',
    (year+1):4);
    writeln(total_value);
    write(total_value,substr(CORE_NAME,1,5)+'trg',
    (year+1):4);
    writeln(rel_max_gray);
    write(rel_max_gray,substr(CORE_NAME,1,5)+'rel',
    (year+1):4);
    writeln(dif_max_gray);
    write(dif_max_gray,substr(CORE_NAME,1,5)+'dif',
    (year+1):4);
    writeln(num_of_rows);
    write(num_of_rows,substr(CORE_NAME,1,5)+'nos',
    (year+1):4);
    end;  {if a decade year is coming up}
  if year = last_year then begin
    writeln; writeln('Now closing output files.');
    write(early_width,'   999'); close(early_width);
    write(late_width,'   999'); close(late_width);
    write(total_width,'   999'); close(total_width);
    write(late_percent,'   999'); close(late_percent);
    write(early_max_value,'   999'); close(early_max_value);
    write(early_avg_value,'   999'); close(early_avg_value);
    write(early_min_value,'   999'); close(early_min_value);
    write(late_max_value,'   999'); close(late_max_value);
```

```
write(late_avg_value,'   999'); close(late_avg_value);
write(late_min_value,'   999'); close(late_min_value);
write(total_value,'   999'); close(total_value);
write(rel_max_gray,'   999'); close(rel_max_gray);
write(dif_max_gray,'   999'); close(dif_max_gray);
write(num_of_rows,'   999'); close(num_of_rows);
x := 0;
while max_ew_area / exp(x*ln(10)) > 1 do
  x := x + 1;
if x > 3 then
  ewa_divisor := x - 3
else
  ewa_divisor := 0;
x := 0;
while max_lw_area / exp(x*ln(10)) > 1 do
  x := x + 1;
if x > 3 then
  lwa_divisor := x - 3
else
  lwa_divisor := 0;
writeln;
writeln;
writeln('Now writing out the last two output files.');
writeln;
open(early_area,'xlarge:[grad12.temp]'+
CORE_NAME+'.ewa',new);
rewrite(early_area);
write(early_area,substr(CORE_NAME,1,5)+'ewa',
first_year:4);
open(late_area,'xlarge:[grad12.temp]'+
CORE_NAME+'.lwa',new);
rewrite(late_area);
write(late_area,substr(CORE_NAME,1,5)+'lwa',
first_year:4);
for year := first_year to last_year do begin
  if not missing_ring[year] then begin
    if ew_area_ok[year] then
      write(early_area,round(ew_area[year]/
      exp(ewa_divisor*ln(10))):6)
    else {should be -1}
      write(early_area,ew_area[year]:6);
    if lw_area_ok[year] then
      write(late_area,round(lw_area[year]/
      exp(lwa_divisor*ln(10))):6)
    else {should be -1}
```

```
        write(late_area,lw_area[year]:6);
      end {if not missing ring}
    else {yes missing year} begin
      write(early_area,MISSING_VAL:6);
      write(late_area,MISSING_VAL:6);
      end; {else yes missing ring}
    if ((year+1) mod 10 = 0) then begin
      writeln(early_area);
      write(early_area,substr(CORE_NAME,1,5)+'ewa',
      (year+1):4);
      writeln(late_area);
      write(late_area,substr(CORE_NAME,1,5)+'lwa',
      (year+1):4);
      end;  {if ((year+1) mod 10 = 0) conditional}
    end;  {for year := start_year to end_year loop}
  write(early_area,'   999');
  close(early_area);
  write(late_area,'   999');
  close(late_area);
  end;  {else year = last_year}
end;  {procedure writedata}

procedure reducedata;
{takes final ew and lw smoothed series from RUBBERBAND,
evaluates brightness variables and calls WRITEDATA}
begin
if year = first_year then begin
  min_ew_area := MAXINT;
  min_lw_area := MAXINT;
  max_ew_area := -MAXINT;
  max_lw_area := -MAXINT;
  end;  {if year = first_year conditional}

num_miss_ew_col := 0;
early_min_gray := MAXINT;
early_max_gray := -MAXINT;
early_avg_gray := 0;
{search through earlywood}
for pixel_num := 0 to round(ew_pct[marker]*
(avg_max_pixel_num+1)-1) do
  if avg_gray[pixel_num] < 255 then begin
    if pixel_num > (0.5*ew_pct[marker]*
    (avg_max_pixel_num+1)) then       {look in 2nd half}
      if early_min_gray > avg_gray[pixel_num] then
        {find minimum value}
```

```
          early_min_gray := avg_gray[pixel_num];
      if early_max_gray < avg_gray[pixel_num] then
        {find maximum value}
        early_max_gray := avg_gray[pixel_num];
      early_avg_gray := early_avg_gray + avg_gray[pixel_num];
      end  {if a good column within earlywood}
    else {an earlywood column without any good pixels} begin
      ew_area_ok[year] := false;
      num_miss_ew_col := num_miss_ew_col + 1;
      end;  {else a bad column}
if ew_area_ok[year] then begin
  ew_area[year] := round(early_avg_gray*
  pixel_size[year]*10000); {area under earlywood curve}
  {Note: early_avg_gray is still a sum at this point}
  { This is based on the following math:
    sum(gray)*pixel-basis    x.xx mm    sum(gray)*mm-basis
    --------------------- * ------- = ------------------
            ring                pixel            ring        }
  if ew_area[year] < min_ew_area then
    {find minimum ew area for core}
    min_ew_area := ew_area[year];
  if ew_area[year] > max_ew_area then
    {find maximum ew area for core}
    max_ew_area := ew_area[year];
  end {if ew_area_ok}
else {ew_area not ok}
  ew_area[year] := -1;
early_avg_gray := round(early_avg_gray/((ew_pct[marker]*
(avg_max_pixel_num+1))-num_miss_ew_col)); {divide by n}

num_miss_lw_col := 0;
late_min_gray := MAXINT;
late_max_gray := -MAXINT;
late_avg_gray := 0;
{search through latewood}
for pixel_num := (round(ew_pct[marker]*
(avg_max_pixel_num+1))) to avg_max_pixel_num do
  if avg_gray[pixel_num] < 255 then begin
    if late_min_gray > avg_gray[pixel_num] then
      {find minimum value}
      late_min_gray := avg_gray[pixel_num];
    if pixel_num < (0.5*(ew_pct[marker]*
    (avg_max_pixel_num+1)+(avg_max_pixel_num+1))) then
      {look in 1st half}
      if late_max_gray < avg_gray[pixel_num] then
```

```
        {find maximum value}
        late_max_gray := avg_gray[pixel_num];
    late_avg_gray := late_avg_gray + avg_gray[pixel_num];
    end  {if a good column within latewood}
  else {a latewood column without any good pixels} begin
    lw_area_ok[year] := false;
    num_miss_lw_col := num_miss_lw_col + 1;
    end;  {else a bad column}
if lw_area_ok[year] then begin
  lw_area[year] := round(late_avg_gray*
  pixel_size[year]*10000);  {area under latewood curve}
  {Note: late_avg_gray is still a sum at this point}
  { This is based on the following math:
    sum(gray)*pixel-basis   x.xx mm   sum(gray)*mm-basis
    --------------------- * ------- = ------------------
            ring              pixel           ring        }
  if lw_area[year] < min_lw_area then
    {find minimum lw area for core}
    min_lw_area := lw_area[year];
  if lw_area[year] > max_lw_area then
    {find maximum lw area for core}
    max_lw_area := lw_area[year];
  end  {if lw_area_ok}
else {lw_area not ok}
  lw_area[year] := -1;
late_avg_gray := round(late_avg_gray/
(((avg_max_pixel_num+1)-(ew_pct[marker]*
(avg_max_pixel_num+1)))-num_miss_lw_col)); {divide by n}

rel_max := round(late_min_gray / early_max_gray * 1000);
dif_max := early_max_gray - late_min_gray;
writedata;
end;  {procedure reducedata}

procedure rubberband;
{to stretch or contract total ring scans, average them, and
call REDUCEDATA}
begin
for marker := 1 to num_rings do begin
  {convert all row,col to scan_num (starts at 1),pixel_num
  (starts at 0) notation}
  scan_num := 0;
  avg_max_pixel_num := 0;
  for row := (0 + edge) to (height - 1 - edge) do begin
    pixel_num := -1;
```

```
    if (boundary[row,marker-1] <> 0) and
    (boundary[row,marker] <> 0) then begin
      scan_num := scan_num + 1;
      for col := (boundary[row,marker-1]+1) to
      boundary[row,marker] do begin
        pixel_num := pixel_num + 1;
        gray[scan_num,pixel_num] := gray[row,col];
        end; {for col := boundary[row,marker-1] to
        boundary[row,marker]}
      max_pixel_num[scan_num] := pixel_num;
      avg_max_pixel_num := avg_max_pixel_num +
      max_pixel_num[scan_num];
      end; {if (boundary[row,marker-1] <> 0) and
      (boundary[row,marker] <> 0)}
    end; {for row := (0 + edge) to (height - 1 - edge)}
max_scan_num := scan_num;
avg_max_pixel_num:=round(avg_max_pixel_num/max_scan_num);
{divide by n and round to integer}

for scan_num := 1 to max_scan_num do begin
  scan_conversion[scan_num] := avg_max_pixel_num/
  max_pixel_num[scan_num];
  for pixel_num := 0 to max_pixel_num[scan_num] do
    new_pixel_num[scan_num,pixel_num] := pixel_num*
    scan_conversion[scan_num];  {new, real pixel numbers}
  end;  {for scan_num := 1 to max_scan_num loop}

for scan_num := 1 to max_scan_num do begin
  pixel_num := 0;  {counter to find pair of gray values}
                   {to be used in weighted mean        }
  for final_pixel_num := 0 to avg_max_pixel_num do begin
    while (new_pixel_num[scan_num,pixel_num] <=
    final_pixel_num) and (pixel_num <>
    max_pixel_num[scan_num]) do begin
      just_below := pixel_num;
      pixel_num := pixel_num + 1;
      end; {while pixels are ok}
    just_above := pixel_num;
    if (gray[scan_num,just_below] = 0) and
    (gray[scan_num,just_above] = 0) then
      adj_gray[scan_num,final_pixel_num] := 0
      else if (gray[scan_num,just_below] = 0) or
      (gray[scan_num,just_above] = 0) then
        adj_gray[scan_num,final_pixel_num] :=
        abs(gray[scan_num,just_below] -
```

```
        gray[scan_num,just_above])
        else
          adj_gray[scan_num,final_pixel_num] :=
          (final_pixel_num -
          new_pixel_num[scan_num,just_below])/
          (new_pixel_num[scan_num,just_above] -
          new_pixel_num[scan_num,just_below])*
          (gray[scan_num,just_above] -
          gray[scan_num,just_below])+
          gray[scan_num,just_below];
    end; {for final_pixel_num := 0 to avg_max_pixel_num}
  end; {for all scans}
```

13. REFERENCES

Abramovitz, M.J. 1989. A fiber optic illumination system. American Laboratory 21(4):48–50.

Adams, A. 1981. The Negative. The New Ansel Adams Photography Series, Vol. 2. Boston: Little, Brown and Company.

Akaike, H. 1974. A new look at the statistical model identification. IEEE Transactions on Automatic Control AC19: 716–723.

Amparado, R.F., H. Beeckman and R. Lemeur. 1990. Thin section preparation of poplar tree-rings for computer-aided image analysis in dendrochronological investigations. Silva Gandavensis 55:81–85.

Andrade, E.R. and W.D. Sellers. 1988. El Niño and its effect on precipitation in Arizona and western New Mexico. Journal of Climatology 8:403–410.

Arkin, A.P., E.R. Goldman, S.J. Robles, C.A. Goddard, W.J. Coleman, M.M. Yang and D.C. Youvan. 1990. Applications of imaging spectroscopy in molecular biology. II. Colony screening based on absorption spectra. Bio/technology 8:746–749.

Atwater, B.F. and D.K. Yamaguchi. 1991, Sudden, probably coseismic submergence of Holocene trees and grass in coastal Washington state. Geology 19:706–709.

Bahre, C.J. 1991. A Legacy of Change: Historic Human Impact on Vegetation of the Arizona Borderlands. Tucson, Arizona: The University of Arizona Press.

Baisan, C.H. and T.W. Swetnam. 1994. Assessment of Phenological Growth Patterns in Four Coniferous Species, Rhyolite Canyon, Chiricahua National Monument: Final Report to Southwest Parks and Monuments Association. Tucson, Arizona: Laboratory of Tree-Ring Research, The University of Arizona.

Baron, W.R. 1992a. Historical climate records from the northeastern United States,

1640 to 1900. Pp. 74–91 in Climate Since A.D. 1500, R.S. Bradley and P.D. Jones, editors. London: Routledge.

Baron, W.R. 1992b. 1816 in perspective: the View from the northeastern United States. Pp. 124–144 in The Year Without a Summer? World Climate in 1816, C.R. Harington, editor. Ottawa: Canadian Museum of Nature.

Bennett, J.H., R.W. Sherburne, C.H. Cramer, C.W. Chesterman, and R.H. Chapman. 1979. Stephens Pass earthquakes, Mount Shasta–August 1978, Siskiyou County, CA. California Geology 32(2):27–34.

Blasing, T.J., D.N. Duvick, and E.R. Cook. 1983. Filtering the effects of competition from ring-width series. Tree-Ring Bulletin 43:19–30.

Brantley, S., D. Yamaguchi, K. Cameron, and P. Pringle. 1986. Tree-ring dating of volcanic deposits. Earthquakes and Volcanoes 18(5):184–194.

Brazel, A.J. 1985. Statewide temperature and moisture trends, 1895–1983. Pp. 79–84 in Arizona Climate: One Hundred Years, W.D. Sellers, R.H. Hill, and M. Sanderson-Rae, editors. Tucson, Arizona: University of Arizona.

Brazel, A.J., H.C. Fritts, and S.B. Idso. 1978. The Climate of Arizona: Prospects for the Future. Tempe, Arizona: Climatological Publications, Scientific Papers No. 2.

Briffa, K.R., T.S. Bartolin, D. Eckstein, P.D. Jones, W. Karlén, F.H. Schweingruber, and P. Zetterberg. 1990. A 1,400-year tree-ring record of summer temperatures in Fennoscandia. Nature 346:434–439.

Briffa, K.R., P.D. Jones, T.S. Bartolin, D. Eckstein, F.H. Schweingruber, W. Karlén, P. Zetterberg, and M. Eronen. 1992a. Fennoscandia summers from AD 500: temperature changes on short and long timescales. Climate Dynamics 7:111–119.

Briffa, K.R., P.D. Jones, J. R. Pilcher, and M.K. Hughes. 1988a. Reconstructing summer temperatures in northern Fennoscandinavia back to A.D. 1700 using tree-ring data from Scots pine. Arctic and Alpine Research 20:385–394.

Briffa, K.R., P.D. Jones, and F.H. Schweingruber. 1988b. Summer temperature patterns over Europe: A reconstruction from 1750 A.D. based on maximum latewood density indices of conifers. Quaternary Research 30:36–52.

Briffa, K.R., P.D. Jones, and F.H. Schweingruber. 1992b. Tree-ring density reconstructions of summer temperature patterns across western North America since AD 1600. Journal of Climate 5:735–754.

Briffa, K.R., P.D. Jones, F.H. Schweingruber, S.G. Shiyatov, and E.R. Cook. 1995. Unusual twentieth-century summer warmth in a 1,000-year temperature record from Siberia. Nature 376:156–159.

Budelsky, C.A. 1969. Variation in Transpiration and Its Relationship With Growth for *Pinus ponderosa* Lawson in Southern Arizona. Ph.D. Dissertation, The University of Arizona, Tucson.

Caldwell, D.W., L.S. Hanson, and W.B. Thompson. 1985. Styles of deglaciation in central Maine. Pp. 45–58 in Late Pleistocene History of Northeastern New England and Adjacent Quebec, H.W. Borns, P. LaSalle, and W.B. Thompson, editors. Boulder, Colorado: The Geological Society of America.

Chatfield, C. 1975. The Analysis of Time Series: Theory and Practice. London: Chapman and Hall.

Chattaway, M.M. 1952. The sapwood-heartwood transition. Australian Forestry 16:25–34.

Clauson, M.L. and J.B. Wilson. 1991. Comparison of video and X-ray for scanning wood density. Forest Products Journal 41(3):58–62.

Cleaveland, M.K. 1983. X-Ray Densitometric Measurement of Climatic Influence on the Intra-Annual Characteristics of Southwestern Semiarid Conifer Tree Rings. Ph.D. Dissertation, The University of Arizona, Tucson.

Cleaveland, M.K. 1986. Climatic response of densitometric properties in semiarid site tree rings. Tree-Ring Bulletin 46:13–29.

Commare, D.L. 1988. Video microscopy: An integrated systems approach. American Laboratory 20(12):56–65.

Conkey, L.E. 1982. Eastern U.S. Tree-Ring Widths and Densities as Indicators of Past Climate. Ph.D. Dissertation, The University of Arizona, Tucson.

Conkey, L.E. 1986. Red spruce tree-ring widths and densities in eastern North America as indicators of past climate. Quaternary Research 26:232–243.

Cook, E.R. 1985. A Time Series Approach to Tree-Ring Standardization. Ph.D. Dissertation, The University of Arizona, Tucson.

Cook, E.R. 1990. Bootstrap confidence intervals for red spruce ring-width chronologies and an assessment of age-related bias in recent growth trends. Canadian Journal of Forest Research 20:1326-1331.

Cook, E.R., K.R. Briffa, D.M. Meko, D.A. Graybill, and G. Funkhouser. 1995. The 'segment length curse' in long tree-ring chronology development for paleoclimatic studies. The Holocene 5:229–237.

Cook, E.R., K. Briffa, S. Shiyatov, and V. Mazepa. 1990. Tree-ring standardization and growth-trend estimation. Pp. 104–123 in Methods of Dendrochronology: Applications in the Environmental Sciences, E.R. Cook and L.A. Kairiukstis, editors. Boston: Kluwer Academic Publishers.

Cook, E.R. and L.A. Kairiukstis. 1990. Methods of Dendrochronology: Applications in the Environmental Sciences, Boston: Kluwer Academic Publishers.

Cook, E.R. and K. Peters. 1981. The smoothing spline: A new approach to standardizing forest interior tree-ring width series for dendroclimatic studies. Tree-Ring Bulletin 41:45-53.

Dadswell, H.E. and W.E. Hillis. 1962. Wood. Pp. 3–55 in Wood Extractives and Their Significance to the Pulp and Paper Industries, W.E. Hillis, editor. New York: Academic press.

Dawdy, D.R. and N.C. Matalas. 1969. Statistical and probability analysis of hydrologic data. Part III: Analysis of variance, covariance, and time series. Pp. 8.68-8.90 in Handbook of Applied Hydrology: A Compendium of Water-Resources Technology, V.T. Chow, editor. New York: McGraw-Hill Book Company.

Delwaide, A., L. Filion, and S. Payette. 1991. Spatiotemporal distribution of light rings in subarctic black spruce, Quebec. Canadian Journal of Forest Research 21:1828–1832.

Denny, C.S. 1982. Geomorphology of New England. USGS Professional Paper 1208.

Donnelly-Nolan, J.M. 1990. Medicine Lake Volcano, northern California: Cascade or Basin and Range volcano? EOS, Transactions of the American Geophysical Union: 71(43):1614.

Donnelly-Nolan, J.M., D.E. Champion, C.D. Miller, T.L. Grove, and D.A. Trimble. 1990. Post-11,000-year volcanism at Medicine Lake volcano, Cascade Range, northern California. Journal of Geophysical Research 95(B12):19693–19704.

Draper, N. and H. Smith. 1981. Applied Regression Analysis, Second edition. New York: Wiley.

Drew, L.G. 1972. Tree-Ring Chronologies of Western America. II. Arizona, New Mexico, Texas: Chronology Series I. Tucson, Arizona: Laboratory of Tree-Ring Research, The University of Arizona.

Durrenburger, R.W. and R. Wood. 1979. Climate and Energy in the Tucson Region. Tempe, Arizona: The Laboratory of Climatology, Arizona State University.

Dustin, I., P. Vollenweider, R.M. Hofer, and P. Hainard. 1994. A study of the cambial zone and conductive phloem of common beech (*Fagus sylvatica* L.) using an image analysis method. II. Automated measurement procedure. Trees 9:113–117.

Dzurisin, D., J.M. Donnelly-Nolan, J.R. Evans, and S.R. Walter. 1990. Relation between magmatism and tectonism near Medicine Lake volcano, California, inferred from historical subsidence, seismicity and crustal structure. EOS, Transactions of the American Geophysical Union 71(43):1608.

Dzurisin, D., J.M. Donnelly-Nolan, J.R. Evans, and S.R. Walter. 1991. Crustal subsidence, seismicity, and structure near Medicine Lake volcano, California. Journal of Geophysical Research 96(B10):16319–16333.

Ebding, T., M.G. Schinker, and H. Spiecker. 1995. Methods of empirical studies of cell structures and of cell development in tree-rings including sample collection, sample preparation and image analysis: Optical and mechanical analysis of cross sections of wood. Pp. 69–70 in Proceedings of the Workshop, Modeling of Tree-Ring Development–Cell Structure and Environment, H. Spiecker and P. Kahle, editors. Freiburg, Germany: Institut für Walwachstum.

Filion, L., S. Payette, L. Gauthier, and Y. Boutin. 1986. Light rings in subarctic conifers as a dendrochronological tool. Quaternary Research 26:272–279.

Fritts, H.C. 1976. Tree Rings and Climate. New York: Academic Press.

Fritts, H.C., J. Guiot, and G.A. Gordon. 1990. Verification. Pp. 178–185 in Methods of Dendrochronology: Applications in the Environmental Sciences, E.R. Cook and L.A. Kairiukstis, editors. Boston: Kluwer Academic Publishers.

Fritts, H.C., J.E. Mosimann, and C.P. Bottorff. 1969. A revised computer program for standardizing tree-ring series. Tree-Ring Bulletin 29:15–20.

Gardner, M.C. 1964. Cenozoic Volcanism in the High Cascade and Modoc Plateau Provinces of Northeastern California. Ph.D. Dissertation, The University of Arizona, Tucson.

Gladwin, H.S. 1947. Tree-Ring Analysis: Tree-Rings and Drought. Medallion Papers No. 37. Globe, Arizona: Gila Pueblo.

Graumlich, L. J. 1987. Precipitation variation in the Pacific Northwest (1675–1975) as reconstructed from tree rings. Annals of the Association of American Geographers 77(1):19–29.

Graybill, D.A. and M.R. Rose. 1989. Analysis of Growth Trends and Variation in Conifers From Central Arizona. I. Network and Chronology Development and Analysis, Final and Revised Report. Corvallis, Oregon: Western Conifers Research Cooperative, Forest Response Program, Environmental Protection Agency.

Green, H.V. and J. Worrall. 1964. Wood quality studies. I. A scanning microphotometer for automatically measuring and recording certain wood characteristics. Technical Association of the Pulp and Paper Industry 47(7):419–427.

Grissino-Mayer, H.D. 1995. An updated list of species used in tree-ring research. Tree-Ring Bulletin 53 (in press).

Grissino-Mayer, H.D., R.L. Holmes, and H.C. Fritts. 1992. International Tree-Ring Data Bank Program Library User's Manual. Tucson, Arizona, Laboratory of Tree-Ring Research, University of Arizona.

Grose, T.L.T., Saucedo, G.J., and D.L. Wagner. 1990. Cascade–Basin and Range transition east of Lassen Peak. EOS, Transactions of the American Geophysi-

cal Union 71(43):1613.

Guay, R., R. Gagnon, and H. Morin. 1992a. MacDENDRO, a new automatic and interactive tree ring measurement system based on image processing. Pp. 128–131 in Tree Rings and Environment: Proceedings of the International Dendrochronological Symposium, Lundqua Report 34.

Guay, R., R. Gagnon, and H. Morin. 1992b. A new automatic and interactive tree ring measurement system based on a line scan camera. The Forestry Chronicle 68(1):138–141.

Hack, J.T. 1989. Geomorphology of the Appalachian Highlands. Pp. 459–470 in The Geology of North America, Volume F-2, the Appalachian-Ouchita Orogen in the United States, R.D. Hatcher, W.A. Thomas, and G.W. Viele, editors. Boulder, Colorado: The Geological Society of America.

Hansen, J. and S. Lebedeff. 1988. Global surface air temperatures: Update through 1987. Geophysical Research Letters, 15:323–326.

Haston, L. and J. Michaelsen. 1994. Long-term central coastal California precipitation variability and relationships to El Niño–Southern Oscillation. Journal of Climate 7:1373–1387.

Hillis, W.E. 1968. Chemical aspects of heartwood formation. Wood Science Technology 2:241–259.

Hillis, W.E. 1971. Distribution, properties and formation of some wood extractives. Wood Science Technology 5:272–289.

Holmes, R.L. 1983. Computer-assisted quality control in tree-ring dating and measurement. Tree-Ring Bulletin 43:69–78.

Holmes, R.L. 1994. Dendrochronology Program Library User's Manual. Tucson, Arizona: Laboratory of Tree-Ring Research, University of Arizona.

Holmes, R.L., R.K. Adams, and H.C. Fritts. 1986. Tree-Ring Chronologies of Western North America: California, Eastern Oregon, and Northern Great Basin With Procedures Used in the Chronology Development Work Including Users Manuals for Computer Programs COFECHA and ARSTAN. Tucson, Arizona: Laboratory of Tree-Ring Research, The University of Arizona.

Hughes, M.K. and L.J. Graumlich. In press. Multimillennial dendroclimatic records from the western United States. In NATO Advanced Research Workshop on 'Climatic Variations and Forcing Mechanisms of the Last 2000 Years', October 3-7, 1994, R.S. Bradley, P.D. Jones, and J. Jouzel, editors.

Hughes, M.K., F.H. Schweingruber, D. Cartwright, and P.M. Kelly. 1984. July–August temperature at Edinburgh between 1721 and 1975 from tree-ring density and width data. Nature 308:341–344.

Inoué, S. 1986. Video Microscopy. New York, Plenum Press.

Inoué, S. 1989. Video enhancement and image processing in light microscopy. Part 1: Video microscopy. American Laboratory 21(4):52–60.

Inoué, S. and T. Inoué, S. 1989. Video enhancement and image processing in light microscopy. Part 2: Digital image processing. American Laboratory 21(4):62–70.

Jacoby, G.C., E.R. Cook, and L.D. Ulan. 1985. Reconstructed summer degree days in central Alaska and northwestern Canada since 1524. Quaternary Research 23:18-26.

Jacoby, G.C., I.S. Ivanciu, and L.D. Ulan. 1988. A 263-year record of summer temperature for northern Quebec reconstructed from tree-ring data and evidence of a major climatic shift in the early 1800's. Palaeogeography, Palaeoclimatology, Palaeoecology 64:69–78.

Jacoby, G.C., P.R. Sheppard, and K.E. Sieh. 1988. Irregular recurrence of large earthquakes along the San Andreas Fault: Evidence from trees. Science 241:196–199.

Jacoby, G.C. and L.D. Ulan. 1983. Tree ring indications of uplift at Icy Cape, Alaska, related to 1899 earthquakes. Journal of Geophysical Research 88(B11):9305–9313.

Jagels, R. and F. Telewski. 1990. Computer-aided image analysis of tree rings. Pp. 76–93 in Methods of Dendrochronology: Applications in the Environmental Sciences, E.R. Cook and L.A. Kairiukstis, editors. Boston, Kluwer Academic Publishers.

Johnson, A.H., E.R. Cook, and T.G. Siccama. 1988. Climate and red spruce growth and decline in the northern Appalachians. Proceedings of the National Academy of Science 85:5369–5373.

Karl, T.R., C.N. Williams Jr., and F.T. Quinlan. 1990. United States Historical Climatology Network (HCN) Serial Temperature and Precipitation Data. Environmental Sciences Division Publication No. 3404. Oak Ridge, Tennessee: Carbon Dioxide Information Analysis Center, Oak Ridge National Laboratory.

Kilbourne, R.T. and C.T. Anderson. 1981. Volcanic history and "active" volcanism in California. California Geology 34:159–168.

Kreber, B. and A. Byrne. 1994. Discoloration of hem-fir wood: A review of the mechanisms. Forest Products Journal 44:35–42.

LaMarche, V.C. 1974. Paleoclimatic inferences from long tree-ring records. Science 183:1043-1048.

LaMarche, V.C. and R.E. Wallace. 1972. Evaluation of effects on trees of past

movements on the San Andreas Fault, northern California. Geological Society of America Bulletin 83(9):2665–2676.

Leavitt, S.W. and S.R. Danzer. 1993. Method for batch processing small wood samples to holocellulose for stable-Carbon isotope analysis. Analytical Chemistry 65:87–89.

Lingrey, S.H. 1982. Structural Geology and Tectonic Evolution of the Northeastern Rincon Mountains, Cochise and Pima Counties, Arizona. Ph.D. Dissertation, The University of Arizona, Tucson.

Lowe, C.H. and D.E. Brown. 1973. The Natural Vegetation of Arizona. Phoenix: Arizona Resources Information Systems.

Mazepa, V. 1990. Spectral approach and narrow band filtering for assessment of cyclic components and ecological prognoses. Pp. 302–308 in Methods of Dendrochronology: Applications in the Environmental Sciences, E.R. Cook and L.A. Kairiukstis, editors. Boston: Kluwer Academic Publishers.

McMillin, C.W. 1982. Application of automatic image analysis to wood science. Wood Science 14:97–105.

Meisling, K.E. and K.E. Sieh. 1980. Disturbance of trees by the 1857 Fort Tejon earthquake, California. Journal of Geophysical Research 85(B6):3225–3238.

Meko, D. and D.A. Graybill. 1995. Tree-ring reconstruction of upper Gila River discharge. Water Resources Bulletin 31:605–616.

Michaelsen, J. 1987. Cross-validation in statistical climate models. Journal of Climate and Applied Meteorology 26:1589–1600.

Miller, R.G. 1981. Simultaneous Statistical Inference. New York: Springer-Verlag.

Montgomery, D.C. and E.A. Peck. 1992. Introduction to Linear Regression Analysis, 2nd Edition. New York: Wiley.

Moschler, W.W. and P.M. Winistorfer. 1990. Direct scanning densitometry: An effect of sample heterogeneity and aperture area. Wood and Fiber Science 22:31–38.

Munro, M.A.R., M.K. Hughes, P.M. Brown, and E.M.R. Garcia. 1995. Image analysis of tracheid dimensions for dendrochronological use. In Proceedings, International Conference on Tree Rings, Environment and Humanity, J.S. Dean, D.M. Meko, and T.W. Swetnam, editors. (in press)

Mutch, L.S. 1994. Growth Responses of Giant Sequoia to Fire and Climate in Sequoia and Kings Canyon National Parks. MS Thesis, The University of Arizona, Tucson.

Mutton, D.B. 1962. Wood resins. Pp. 331–363 in Wood Extractives and Their Significance to the Pulp and Paper Industries, W.E. Hillis, editor. New York: Academic Press.

Norton, D.A., K.R. Briffa, and M.J. Salinger. 1989. Reconstruction of New Zealand summer temperatures to 1730 AD using dendroclimatic techniques. International Journal of Climatology 9:633-644.

Oosting, H.J. and W.D. Billings. 1951. A comparison of virgin spruce-fir forests in the northern and southern Appalachian system. Ecology 32:84–103.

Page, R. 1970. Dating episodes of faulting from tree rings: effects of the 1958 rupture of the Fairweather fault on tree growth. Geological Society of America Bulletin 81:3085–3094.

Page, W.D., M.A, Hemphill-Haley, and I.G. Wong. 1987. Exaggerated fault scarps in the Modoc Plateau, northeastern California. Geological Society of America Abstracts With Programs 19(7):797.

Palmer, W.C. 1965. Meteorological Drought. U.S. Department of Commerce

Research Paper No. 45. Washington DC: Office of Climatology.

Park, W.K. 1990. Development of anatomical tree-ring chronologies from southern Arizona conifers using image analysis. Ph.D. Dissertation, The University of Arizona, Tucson.

Park, W.K. and F.W. Telewski. 1992. Anatomical parameters for dendrochronology: An image analysis of ponderosa pine from southeastern Arizona, USA. Pp. 301–320 in Proceedings, 2nd Pacific Regional Wood Anatomy Conference, Rojo, J.P., Aday, J.U., Barile, E.R., Araral, R.K., and America, W.M. editors. Laguna, Philippines: Forest Products Research Development Institute.

Park, W.K. and F.W. Telewski. 1993. Measuring maximum latewood density by image analysis at the cellular level. Wood and Fiber Science 25(4):326–332.

Park, W.K., F.W. Telewski, and J.M. Burns. 1992. Some advances in sample preparation techniques for X-ray densitometry and image analysis of increment cores. Pp. 374–385 in Proceedings, 2nd Pacific Regional Wood Anatomy Conference, J.P. Rojo, J.U. Aday, E.R. Barile, R.K. Araral, and W.M. America, editors. Laguna, Philippines: Forest Products Research Development Institute.

Parker, M.L. 1976. Improving tree-ring dating in northern Canada by X-ray densitometry. Syesis 9:163–172.

Parker, M.L. 1987. X-ray densitometry and image analysis as methods in dendrochronology in Canada and the United States. Pp. 57–68 in Methods in Dendrochronology–I, Proceedings of the Task Force Meeting on Methodology of Dendrochronology: East/West Approaches, L. Kairiukstis, Z. Bednarz, and E. Feliksik, editors. Warsaw: Polish Academy of Sciences–Systems Research Institute.

Parker, M.L. and W.E.S. Henoch. 1971. The use of Englemann spruce latewood density for dendrochronological purposes. Canadian Journal of Forest Research 1:90–98.

Parker, M.L. and K.R. Meleskie. 1970. Preparation of X-ray negatives of tree-ring specimens for dendrochronological analysis. Tree-Ring Bulletin 30:11–22.

Richardson, J.H. 1991. Handbook for the Light Microscope–A User's Guide. Park Ridge, New Jersey: Noyes Publications.

Rind, D. and J. Overpeck. 1993. Hypothesized causes of decade-to-century-scale climate variability: climate model results. Quaternary Science Reviews 12:357–374.

Robinson, W.J. and R. Evans. 1980. A microcomputer-based tree-ring measuring system. Tree-Ring Bulletin 40:59–64.

Rochow, T.G. and E.G. Rochow. 1978 An Introduction to Microscopy by Means of Light, Electrons, X-rays, or Ultrasound. New York: Plenum Press.

Rohlf, F.J. and R.R. Sokal. 1981. Statistical Tables. San Francisco: W.H. Freeman and Company.

Rourke, R.V., J.A. Ferwerda, and K.J. LaFlamme. 1978. The Soils of Maine. University of Maine at Orono Miscellaneous Report 203.

Rundel, P.W., D.J. Parsons, and D.T. Gordon. 1977. Montane and subalpine vegetation of the Sierra Nevada and Cascade Ranges. Pp. 559–599 in Terrestrial Vegetation of California, M.G. Barbour and J. Major, editors. New York: Wiley.

Russ, J.C. 1990. Computer Assisted Microscopy: The Measurement and Analysis of Images. Raleigh: North Carolina State University Engineering Extension Education.

Ruzhich, V.V., V.A. San'kov, and Y.I. Dneprovskii. 1982. The dendrochronological dating of seismogenic ruptures in the Stanovoi Highland. Soviet Geology and Geophysics 23:57–63.

Saß, U. and D. Eckstein. 1992. The annual vessel area of beech as an ecological indicator. Pp. 281–285 in Tree Rings and Environment: Proceedings of the International Dendrochronological Symposium, Lundqua Report 34.

Saß, U. and D. Eckstein. 1994. Preparation of large thin sections and surfaces of wood for automatic image analysis. Holzforschung 48:117–118.

Saß, U. and D. Eckstein. 1995. The variability of vessel size in beech (*Fagus sylvatica* L.) and its ecophysiological interpretation. TREES 9:247–252.

Saucedo, G.J., D.L. Wagner, and T.L.T. Grose. 1990. Age and distribution of volcanism–Susanville/Eagle Lake area, northeastern California. EOS, Transactions of the American Geophysical Union 71(43):1613.

Scarborough, R.B. and H.W. Pierce. 1978. Late Cenozoic basins of Arizona. Pp. 253–259 of New Mexico Geological Society Guidebook, 29th Field Conference, J.F. Callender, J.C. Wilt, and R.E. Clemons, editors. Albuquerque: New Mexico Geological Society, Inc.

Schulman, E. 1942. Dendrochronology in pines of Arkansas. Ecology 23:309–318.

Schweingruber, F.H. 1990. Radiodensitometry. Pp. 55–63 in Methods of Dendrochronology: Applications in the Environmental Sciences, E.R. Cook, and L.A. Kairiukstis, editors. Boston: Kluwer Academic Publishers.

Schweingruber, F.H., L. Kairiukstis, and Shiyatov. 1990. Sample selection. Pp. 23–35 in Methods of Dendrochronology: Applications in the Environmental Sciences, E.R. Cook and L.A. Kairiukstis, editors. Boston: Kluwer Academic Publishers.

Sellers, W.D. 1960. Arizona Climate. Tucson, Arizona: Institute of Atmospheric Physics, The University of Arizona.

Shafiqullah, M., P.E. Damon, D.J. Lynch, P.H. Kuck, and W.A. Rehrig. 1978. Mid-Tertiary magmatism in southeastern Arizona. Pp. 231–242 of New Mexico Geological Society Guidebook, 29th Field Conference, J.F. Callender, J.C. Wilt, and R.E. Clemons, editors. Albuquerque: New Mexico Geological Society, Inc.

Sheppard, P.R. 1991. Identifying low-frequency tree-ring variation. Tree-Ring Bulletin 51:29–38.

Sheppard, P.R. and L.J. Graumlich. 1996. A reflected-light video imaging system for tree-ring analysis of conifers. In Proceedings, International Conference on Tree Rings, Environment and Humanity, J.S. Dean, D.M. Meko, and T.W. Swetnam, editors. (in press)

Sheppard, P.R., L.J. Graumlich, and L.E. Conkey. 1996. Dendroclimatological analysis of red spruce from Elephant Mt., Maine, using video imaging techniques. The Holocene (in press).

Sheppard, P.R. and G.C. Jacoby. 1989. Application of tree-ring analysis to paleoseismology: Two case studies. Geology 17:226–229.

Sheppard, P.R. and L.O. White. 1995. Tree-ring responses to the 1978 earthquake at Stephens Pass, northeastern California. Geology 23:109–112.

Shigo, A.L. 1985. Wounded forests, starving trees. Journal of Forestry 83:668–673.

Shiyatov, S., V. Mazepa, and E.R. Cook. 1990. Correcting for trend in variance due to changing sample size. Pp. 133–137 in Methods of Dendrochronology: Applications in the Environmental Sciences, E.R. Cook and L.A. Kairiukstis, editors. Boston: Kluwer Academic Publishers.

Shroder, J.F. and D.R. Butler. 1987. Tree-ring analysis in the earth sciences. Pp. 186–212 in Proceedings of the International Symposium on Ecological Aspects of Tree-Ring Analysis, G.C. Jacoby and J.W. Hornbeck, compilers. Palisades, New York: Lamont-Doherty Geological Observatory.

Smith, J.H.G. 1977. Tree-ring analyses can be improved by measurement of component widths and densities. The Forestry Chronicle 53(2):91–95

Smith, W. 1986. The effects of eastern north Pacific tropical cyclones on the southwestern United States. National Oceanic and Atmospheric Administration Technical Memorandum NWS WR-197. Salt Lake City, Utah: U.S. Department of Commerce.

Soil Survey Staff. 1995. Classification of Soils Series of the United States and the Virgin Islands. Washington, DC: Natural resources Conservation Service.

Sokal, R.R. and F.J. Rohlf. 1981. Biometry. San Francisco: W.H. Freeman and Company.

Stahle, D.W., R.B. VanArsdale, and M.K. Cleaveland. 1992. Tectonic signal in baldcypress trees at Reelfoot Lake, Tennessee. Seismological Research Letters 63:439–447.

Stokes, M.A. and T.L. Smiley. 1968. An Introduction to Tree-Ring Dating. Chicago: The University of Chicago Press.

Swetnam, T.W. and J.L. Betancourt. 1990. Fire–southern oscillation relations in the Southwestern United States. Science 249:1017–1020.

Swetnam, T.W., M.A. Thompson, and E.K. Sutherland. 1985. Using Dendrochronology to Measure Radial Growth of Defoliated Trees. USDA Forest Service Agriculture Handbook No. 639.

Telewski, F.W., J.M. Burns, and L. Ulan. 1987. A thin-section technique for x-ray

densitometric analysis of narrow tree-ring series. Pp. 651–657 in Proceedings, International Symposium on Ecological Aspects of Tree-Ring Analysis, G.C. Jacoby and J.W. Hornbeck, compilers. Palisades, New York: Lamont-Doherty Geological Observatory.

Telewski, F.W. and G.C. Jacoby. 1987. Current status of X-ray densitometry. Pp. 630–646 in Proceedings, International Symposium on Ecological Aspects of Tree-Ring Analysis, G.C. Jacoby and J.W. Hornbeck, J.W., compilers. Palisades, New York: Lamont-Doherty Geological Observatory.

Thetford, R.D., R.D. D'Arrigo, and G.C. Jacoby. 1991. An image analysis system for determining densitometric and ring-width time series. Canadian Journal of Forest Research 21:1544–1549.

United States Forest Service. No date. Soil Survey of Shasta-Trinity Forest Area, California.

Van West, C.R. 1990. Modeling Prehistoric Climatic Variability and Agricultural Production in Southwestern Colorado: A GIS Approach. Ph.D. Dissertation, Washington State University, Pullman.

Vollenweider, P., I. Dustin, R.M. Hofer, P. Vittoz, and P. Hainard. 1994. A study of the cambial zone and conductive phloem of common beech (*Fagus sylvatica* L.) using an image analysis method. I. Influence of tree age on the structure. Trees 9:106–113.

Wallace, R.E. and V.C. LaMarche. 1979. Trees as indicators of past movements on the San Andreas Fault. Earthquake Information Bulletin 2(4):127–131.

Webb, R.H. and J.L. Betancourt. 1992. Climatic variability and flood frequency of the Santa Cruz River, Pima County, Arizona. U.S. Geological Survey Water-Supply Paper 2379. Washington, DC: U.S. Government Printing Office.

Weisberg, S. 1980. Applied Linear Regression. New York: John Wiley and Sons.

Wilcox, M.D. 1975. Wood brightness variation in clones of loblolly pine. Silvae Genetica 24(2-3):54-59.

Yamaguchi, D.K., L. Filion, and M. Savage. 1993. Relationship of temperature and light ring formation at subarctic treeline and implications for climate reconstruction. Quaternary Research 39:256–262.

Yanosky, T.M. and C.J. Robinove. 1986. Digital image measurement of the area and anatomical structure of tree rings. Canadian Journal of Botany 64(12):2896–2902.

Yanosky, T.M., C.J. Robinove, and R.G. Clark. 1987. Progress in the image analysis of tree rings. Pp. 658–665 in Proceedings, International Symposium on Ecological Aspects of Tree-Ring Analysis, G.C. Jacoby and J.W. Hornbeck, compilers. Palisades, New York: Lamont-Doherty Geological Observatory.